A STUDY ON CATALYTIC DIMETHYL ETHER PRODUCTION FROM SYNTHESIS GAS WITH CO_2

by

Necdet Semih Altınsoy

B.S., Chemical Engineering, Boğaziçi University, 2018

B.S., Chemistry, Boğaziçi University, 2018

Submitted to the Institute for Graduate Studies in
Science and Engineering in partial fulfillment of
the requirements for the degree of
Master of Science

Graduate Program in Chemical Engineering

Boğaziçi University

2020

ACKNOWLEDGEMENTS

I would like to express my sincere thankfulness to my thesis supervisor Prof. Dr. Ahmet Kerim Avcı for endless support, patience and trust in me. Working with him was a privilege and I consider myself fortunate.

I would like to express my sincere gratefulness to my thesis co-supervisor Prof. Dr. Zeynep İlsen Önsan for suggestions, support and trust in me. Working with her was a privilege and I consider myself fortunate.

I would like to express my thankfulness to my thesis committee, Prof. Dr. Ahmet Erhan Aksoylu, Prof. Dr. Hüsnü Atakül, for devoting their time to read, listen and comment on my study.

I would like to express my thankfulness to Prof. Dr. Ahmet Erhan Aksoylu for sharing his wisdom.

I would like to express my thankfulness to professors of lectures that I took during both my graduate and undergraduate study.

I would like to thank my lab mates including former members, Ceren Hatipoğlu, Furkan Öztürk, Hasan Köybaşı, Mert Özden, Özge Selçuk, Selin Baç Bilgi, Sinan Koç, Uğurcan Tozar, who were beside me during this study.

I would like to thank my colleagues, Serhat Erşahin, Cihat Öztepe, Gülten Çelebi, İlke Kaykanat, Enes Emre Taş, Ali Uzun, Sercan Altundemir, Pınar Özdemir, Merve Eropak, Olcay Türkmen, Melek Selcen Başar, Burcu Acar.

I would like to appreciate the kindness of the departmental staff Dilek Kırkoç, Melike Gürbüz, Yakup Bal, Şükrü Ordu and Belgin Balkan.

I would like to thank Murat Düzgünoğlu, not only a former departmental staff but also a close friend of mine.

I would like to thank my family for their support in everything I encountered in my life and for bringing me up.

This study was supported by Bogazici University Research Fund, Grant Number: BAP-16463.

ABSTRACT

A STUDY ON CATALYTIC DIMETHYL ETHER PRODUCTION FROM SYNTHESIS GAS WITH CO_2

Increasing concerns on the emissions of hazardous species have boosted efforts towards development of cleaner alternatives of the conventional, crude-oils based fuels. In this respect, dimethyl ether (DME) is envisioned as a promising replacement of the present fuels due its numerous benefits such as non-toxicity, SO_2 and soot free combustion and compatibility with the existing fuel distribution and processing infrastructures. DME synthesis involves conversion of synthesis gas (H_2+CO+CO_2) on methanol synthesis and dehydration catalysts. If catalysts are present in the same reactor, used method is called direct DME synthesis, otherwise is called indirect DME synthesis. The present study involves the direct route, i.e. the physical mixture of Cu-ZnO/γ-Al_2O_3 and γ-Al_2O_3, catalysts for methanol synthesis and dehydration, respectively. Synthesis gas (syngas) is formulated either as CO+H_2 or CO_2+H_2, with the latter being much less studied and technically more difficult. Catalyst configuration, GHSV and pressure tests were conducted when the carbon source in syngas was CO. Replacement of CO with CO_2 necessitated a more active dehydration catalyst, which was obtained by impregnating PTA on γ-Al_2O_3. Relative amounts of the catalysts and molar inlet H_2/CO_2 ratio were also studied as additional parameters. Moreover, sorption assisted CO_2-to-DME conversion was also investigated. For the mixed configuration of catalysts and sorbent (Zeolite 3A), 30 wt.% PTA impregnation on γ-Al_2O_3 and 3 g sorbent addition were found as the optimum case at 225 ^{0}C, 30 bar, H_2/CO_2 = 3, dehydration to synthesis catalysts ratio = 2, GHSV = $\sim$ 1750 h^{-1}. Sorbent addition led to a notable increase in CO_2 conversion and DME yield without sacrificing from the exit DME molar flow rate. Sorption capacity recovery of the sorbent upon regeneration was also investigated.

ÖZET

CO_2 İÇEREN SENTEZ GAZINDAN DİMETİL ETHER ÜRETİMİ

Zararlı maddelerin emisyonlarına karşı artan kaygı geleneksel fosil yakıtlara alternatif temiz yakıt üretimi için olan çalışmaları arttırmaktadır. Bu bağlamda, dimetil ether (DME)'in toksik olmaması, yanması sonucu SO_2 ve is üretmemesi ve mevcut yakıt dağıtım ve işleme altyapısıyla uyumlu olmasından DME güncel yakıtların yerini almak için umut vaat etmektedir. DME sentezi sentez gazının (H_2+CO+CO_2) metanol sentez ve dehidrasyon katalizörleri üzerinde dönüşümünü içermektedir. Katalizörler aynı reaktörde mevcutsa kullanılan metoda direkt DME sentez metodu denir diğer türlü metoda indirekt DME sentez metodu denmektedir. Mevcut çalışma sırasıyla metanol sentez ve dehidrasyon katalizörleri olan Cu-ZnO/γ-Al_2O_3 ve γ-Al_2O_3 fiziksel olarak karıştırıldığı direkt metodu içermektedir. Sentez gazı CO+H_2 ya da CO_2+H_2 olarak hazırlanmaktadır ve ikinci formülasyon teknik olarak daha zor olmakla beraber daha az çalışılmıştır. Katalizör konfigürasyon, GHSV ve basınç testleri sentez gazındaki karbon kaynağı CO iken yapılmıştır. CO'in yerine CO_2'in kullanılması daha aktif dehidrasyon katalizörü olan PTA emdirilmiş γ-Al_2O_3'nın kullanılmasını gerektirmiştir. Katalizörlerin görece miktarları, giriş molar H_2/CO_2 oranıyla beraber ek parametreler olarak çalışılmıştır. Sorban destekli CO_2'tan DME sentezi ayrıca incelenmiştir. Katalizörler ve sorbanın (Zeolite 3A) karışık olduğu durum için 225 ^{0}C'de ve 30 bar'da, $H_2/CO_2 = 3$, dehidrasyon katalizörüne sentez katalizörü oranı = 2, GHSV = $\sim$ 1750 h^{-1} iken ağırlıkça %30 PTA emdirilmiş γ-Al_2O_3 ve 3 g sorban ilavesi optimum durum olarak tespit edilmiştir. Sorban ilavesi çıkış DME molar akış miktarından feragat etmeden CO_2 dönüşümünü ve DME verimini dikkate değer miktarda arttırmak için önemli bulunmuştur. Ayrıca, sorbanın yenilemeden sonra kapasitesinin geri dönüşümü incelenmiştir.

TABLE OF CONTENTS

ACKNOWLEDGEMENTS iii
ABSTRACT v
ÖZET vi
LIST OF FIGURES ix
LIST OF TABLES xiii
LIST OF SYMBOLS xiv
LIST OF ACRONYMS/ABBREVIATIONS xv
1. INTRODUCTION 1
2. LITERATURE SURVEY 4
2.1. Importance of DME 4
2.2. DME Synthesis Methods 6
2.2.1. Indirect DME Synthesis 7
2.2.1.1. Thermodynamic Analyses 7
2.2.2. Direct DME Synthesis 8
2.2.2.1. Thermodynamic Analyses 8
2.2.2.2. Operating Conditions 9
2.3. Catalysts for DME Synthesis 11
2.3.1. Methanol Synthesis Catalysts 11
2.3.2. Methanol Dehydration Catalysts 16
2.3.3. Bifunctional and Hybrid Catalysts 23
2.4. Sorption Enhanced DME Synthesis 29
3. EXPERIMENTAL WORK 31
3.1. Materials 31
3.1.1. Catalysts, Active Metal Precursors and Sorbent 31
3.1.2. Gases 31
3.2. Pre-reaction 31
3.2.1. Catalyst Preparation 32
3.2.2. Catalyst Loading and Reduction 34

3.2.3. Mixture of Feed Streams and Pressurization 37
3.3. Reaction System 37
3.4. Analysis Systems 42
3.4.1. Gas Chromatography with Thermal Conductivity Detector . . . 42
3.4.2. Gas Chromatography-Mass Spectrometer 43
3.5. Complete Procedure as Flowchart 46
3.6. Definitions 48
4. RESULTS AND DISCUSSION 51
4.1. CO as Carbon Source 54
4.1.1. Catalyst Configurations 55
4.1.2. Reactor Pressure 58
4.1.3. Reactor GHSV 59
4.2. CO_2 as Carbon Source 60
4.2.1. H_2/CO_2 Ratio in the Feed Stream 60
4.2.2. Dehydration Catalysts and Dehydration Catalyst to CZA ratio . 61
4.3. Sorption Enhanced DME production from CO_2 63
5. CONCLUSION 68
5.1. Conclusions from CO as Carbon Source 68
5.2. Conclusions from CO_2 as Carbon Source 68
5.3. Conclusions from Sorbent Addition to The Reactor 69
5.4. Recommendations 69
REFERENCES 71
APPENDIX A: CHROMATOGRAPH CALIBRATIONS 79
A.1. Gas Chromatograph Calibration 79
A.2. Gas Chromatograph-Mass Spectrometer Calibration 82
APPENDIX B: MASS FLOW CONTROLLER CALIBRATIONS 84

LIST OF FIGURES

Figure 1.1. DME as chemical intermediate. 1

Figure 1.2. Synthesis gas sources and DME synthesis methods. 2

Figure 1.3. Proposed CO_2 recycle for DME synthesis. 3

Figure 2.1. Process flow sheet for indirect DME synthesis. 7

Figure 2.2. Process flow sheet for direct DME synthesis. 8

Figure 3.1. Crushed and sieved catalysts before loading to the reactor. 33

Figure 3.2. Loaded reactor installed into the system. 35

Figure 3.3. Scheme of reaction and analysis systems. 39

Figure 3.4. Appearance of BTRS-Jr PC. 40

Figure 3.5. MFCs inside the BTRS. 40

Figure 3.6. External MFC. 41

Figure 3.7. Back pressure regulator of BTRS. 41

Figure 3.8. Shimadzu GC-2014 System. 42

Figure 3.9. Shimadzu GCMS-QP2010 Ultra. 44

Figure 3.10. Flowchart Depending on Carbon Source and Presence of Sorbent. 47

Figure 4.1. Effect of Temperature on DME Selectivity at Different Pressure Levels When H_2/CO_2 Ratio is 3. 52

Figure 4.2. Effect of Temperature on CO Selectivity at Different Pressure Levels When H_2/CO_2 Ratio is 3. 52

Figure 4.3. Effect of Temperature on CO_2 Conversion at Different Pressure Levels When H_2/CO_2 Ratio is 3. 53

Figure 4.4. Effect of Pressure on Equilibrium CO_2 Conversion and DME Yield at 225 ^{0}C When H_2/CO_2 Ratio is 3. 53

Figure 4.5. Effect of Temperature and Pressure on CO_2 Conversion Gain When H_2/CO_2 Ratio is 3. 55

Figure 4.6. Effect of Catalyst Configuration on CO Conversion. 56

Figure 4.7. Effect of Catalyst Configuration on DME Yield. 57

Figure 4.8. Effect of Catalyst Configuration on CO_2 Yield. 57

Figure 4.9. Effect of Pressure on CO Conversion and DME Yield. 58

Figure 4.10. Effect of GHSV on CO Conversion and DME Yield. 59

Figure 4.11. Effect of H_2/CO_2 Ratio on CO_2 Conversion. 60

Figure 4.12. Effect of PTA Impregnation on DME Yield (H_2/CO_2 = 10, mass of dehydration catalyst = 0.75 g). 62

Figure 4.13. Effect of PTA Impregnation Amount on CO_2 Conversion and DME Yield. 62

Figure 4.14. Effect of 30 wt.% PTA Impregnated γ-Al_2O_3 to CZA Ratio on CO_2 Conversion and DME Yield. 63

Figure 4.15. Effect of Sorbent Amount on CO_2 Conversion. 66

Figure 4.16. Effect of Sorbent Amount on DME Yield. 66

Figure 4.17. Regenerated Sorbent-DME Yield Relation for 3 g Sorbent Addition. 67

Figure 4.18. Sorption Recovery Percentage-Regeneration Times Relation for 3 g Sorbent Addition. 67

Figure A.1. Shimadzu GC-2014 H_2 Calibration. 79

Figure A.2. Shimadzu GC-2014 CO Calibration. 80

Figure A.3. Shimadzu GC-2014 CO_2 Calibration. 80

Figure A.4. Shimadzu GC-2014 N_2 Calibration. 81

Figure A.5. Shimadzu GC-2014 CH_4 Calibration. 81

Figure A.6. Shimadzu GCMS Ultra QP2100 Ultra DME Calibration for CO as Carbon Source. 82

Figure A.7. Shimadzu GCMS Ultra QP2100 Ultra DME Calibration for CO_2 as Carbon Source. 83

Figure B.1. H_2 MFC Calibration. 84

Figure B.2. CO MFC Calibration. 85

Figure B.3. CO_2 MFC Calibration. 86

Figure B.4. N_2 MFC Calibration. 87

LIST OF TABLES

Table 2.1. Life-cycle analysis for DME and diesel in light-duty vehicles. . . . 4

Table 2.2. Properties of DME and diesel fuel. 5

Table 2.3. For indirect DME synthesis method thermodynamic analyses at 225 ^{0}C and 30 bar while 20% N_2 is present. 8

Table 2.4. For direct DME synthesis method thermodynamic analyses at 225 ^{0}C and 30 bar while 20% N_2 is present. 9

Table 2.5. Summary table of bifunctional and hybrid catalysts. 28

Table 3.1. Catalysts, Active Metal Precursors and Sorbent. 31

Table 3.2. Reaction, Calibration and Carrier Gases. 32

Table 3.3. Flow rates used in experiments during pressurization and reaction. 36

Table 3.4. Analysis Method of GC. 43

Table 3.5. Analysis Method of GCMS for CO as Carbon Source. 45

Table 3.6. Analysis Method of GCMS for CO_2 as Carbon Source. 46

LIST OF SYMBOLS

$Q_{i,in}$	Volumetric flow rate of i component in the feed stream
$Q_{i,out}$	Volumetric flow rate of i component in the exit stream
$Q_{i,out,max}$	Maximum possible volumetric flow rate of i component in the exit stream
Q_{in}	Volumetric flow rate of feed stream
$Q_{in,h^{-1}}$	Volumetric flow rate of feed stream per hour
Q_{out}	Volumetric flow rate of exit stream
SR_i	Sorption recovery percentage of i^{th} cycle
$x_{i,in}$	Fraction of i component in the feed stream
$x_{i,out}$	Fraction of i component in the exit stream
X_{CO_x}	Conversion of CO_x
Y_i	Yield of component i
$Y_{DME,i}$	Yield of DME for i^{th} cycle
$\rho_{CZA,45\text{-}60}$	Density, in g ml^{-1}, of CZA having 45-60 mesh size

LIST OF ACRONYMS/ABBREVIATIONS

3-D	Three dimensional
AS-40	An anionic surfactant
BPR	Back pressure regulator
BTRS	Benchtop reaction system
CI	Compression ignition
CP	Co-precipitation
CPG	CO_2 Conversion Percentage Gain
C-SAC	Conventional steam-assisted method
CZA	$Cu/ZnO/Al_2O_3$
DME	Dimethyl ether
DP	Deposition precipitation
EGR	Exhaust gas recirculation
FER	Ferrierite type zeolite
FER10	Ferrierite type zeolite having Si/Al ratio of 10
GC	Gas Chromatography
GCMS	Gas Chromatography Mass Spectrometry
GHSV	Gas hourly space velocity
$GHSV_{CZA}$	Gas hourly space velocity calculated based on CZA
HSY	High silica Y type zeolite
IM	Impregnation
KFI	Zeolite type having KFI type framework
LPG	Liquid petroleum gas
MCM-41	Mesoporous material having hierarchical structure
MFC	Mass flow controller
MFI	A zeolite structure type
PTA	Phosphotungstic acid hydrate
PTFE	Politetrafloroetilen
Rho	A zeolite type

RUB-13	A zeolite type
SAPO-11	A zeolite type
SBA-15	A mesoporous silica sieve
SDA	Structure directing agent
SDY	Steam de-aluminate H-Y zeolite
SSZ-13	A zeolite type
STY	Space time yield
SIRAL20	Amorphous silica-alumina catalyst containing 20 wt.% silica
TCD	Thermal conductivity detector
TOS	Time on stream
WHSV	Weight hourly space velocity
Y-type	A zeolite type
ZCZ	$Cu/ZnO/ZrO_2$
ZSM-5	A zeolite type

1. INTRODUCTION

Sustainable energy production has become an important subject to resolve issues related to the environmental pollution, global warming and energy security. In this respect, alternative fuels and technologies that allow for more efficient usage of energy have drawn increasing attention. For successful implementation of the fuel, criteria different than allowing sustainable energy production are also present. Fuels that can be stored with ease, that are non-toxic and having high energy density should be developed and produced abundantly. Dimethyl ether could be this type of alternative future fuel since it is a clean compression ignition fuel having no SO_2 and less CO formation. Moreover, combustion of DME does not produce soot. In terms of storage, DME is similar to LPG because it can be liquefied with increasing pressure at room temperature [1]. Compression ignition of DME is not its single usage, DME can be used as fuel for power generation using gas turbines. Other than as a fuel, DME can be used as aerosol propellant and solvent. Other important usage of DME can be as a chemical intermediate for synthesis of chemicals as shown in Figure 1.1 such as acetic acid, methyl acetate, dimethoxyethane [2, 3].

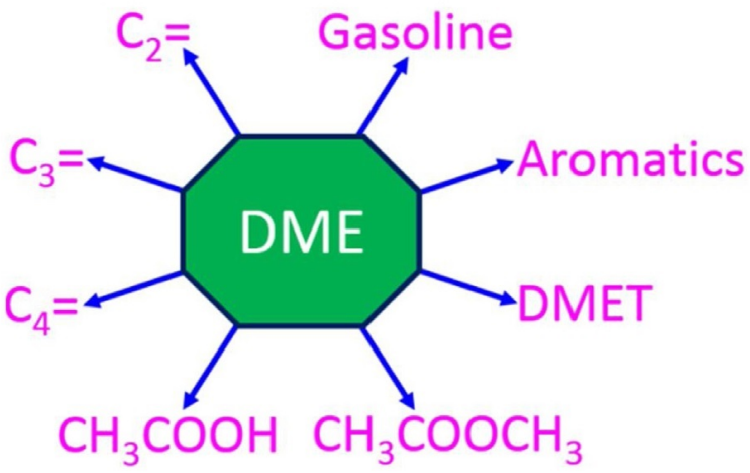

Figure 1.1. DME as chemical intermediate [2].

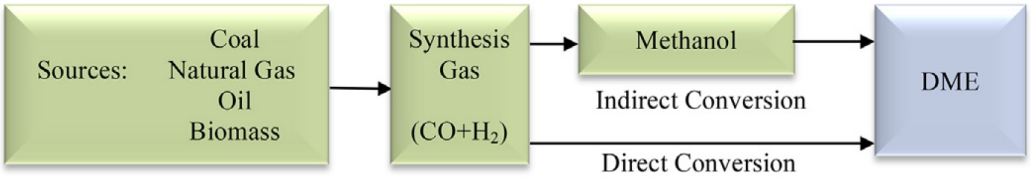

Figure 1.2. Synthesis gas sources and DME synthesis methods [4].

As seen in Figure 1.2, DME synthesis can be investigated as two parts, which are synthesis of methanol and its dehydration to DME. The feed to methanol synthesis is synthesis gas, which is composed of a mixture of CO, CO_2 and H_2, whose relative amounts depend on the hydrocarbon source (e.g. natural gas, coal, biomass) and the process (e.g. autothermal reforming, gasification, partial oxidation) of making syngas.

Two different methods to synthesize DME is present according to reactions that take place in the reactor. If methanol synthesis and dehydration reactions take place in the same reactor on the physical mixture of respective catalysts, that method is referred as direct DME synthesis method. Direct DME synthesis allows higher single pass CO conversion compared to the indirect DME synthesis, in which the synthesis and dehydration reactions take place in two separate reactors.

Synthesizing DME from syngas containing CO_2 together with CO and H_2 or from CO_2-H_2 mixtures where CO_2 is the single carbon source are appealing approaches to deal with global warming as described schematically in Figure 1.3.

The present study involves parametric investigation of conversion of syngas to DME. The study is grouped into two parts depending on the carbon source of syngas. In the first part, where syngas is considered as mixture of CO and H_2, the effect of reaction pressure, relative locations of the synthesis and dehydration catalysts and the GHSV are studied. Learnings from the first part are used in the second part where syngas is assumed as a mixture of CO_2 and H_2. Owing to the stable nature of CO_2, hydrogenation to DME necessitates a stronger (i.e. more acidic) dehydration

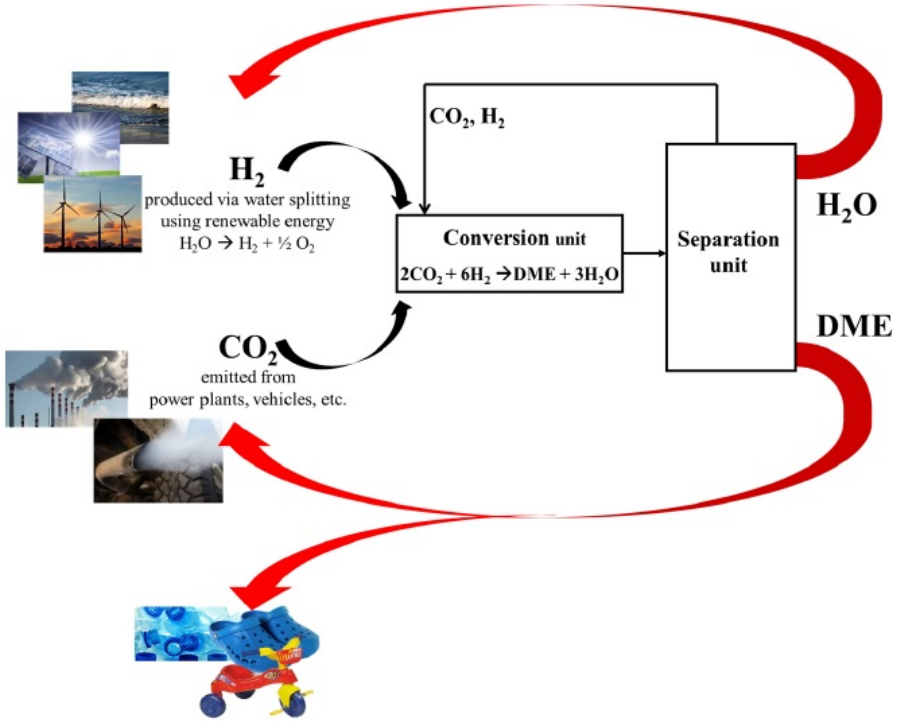

Figure 1.3. Proposed CO_2 recycle for DME synthesis [3].

catalysts. Therefore, the second part of the work is focused on developing active dehydration catalysts. Moreover, in an effort to relax the thermodynamic limitations, CO_2 hydrogenation is studied in the presence of a solid sorbent. The impact of the sorbent was quantified by benchmarking with the respective thermodynamic limits.

2. LITERATURE SURVEY

2.1. Importance of DME

DME has drawn attention to replace conventional diesel as DME is a clean compression ignition fuel having no SO_2 emission, less hydrocarbons and CO emission. Low NO_x can be achieved with EGR application. Hydrocarbons, particulates and CO_2 emission values in light-duty vehicles found by life-cycle analysis of Sweden Petroleum Institute is shown in Table 2.1. Moreover, combustion of DME does not produce soot. Easy vaporization and absence of C-C bond help soot free operation as DME has high cetane number, demonstrating combustion delay after fuel injection. Higher cetane number means less delay between injection and combustion of fuel. These reasons lead to easy auto-ignition. DME is helpful to reduce local air pollution since combustion of DME produces less particulate matter. Oxygen content of DME is important for the reduction of particulate matter after combustion. Oxygen content is also effective on high cetane number and low autoignition temperature. Further comparison of physical properties of DME and diesel is shown in Table 2.2 [1, 5–8].

Table 2.1. Life-cycle analysis for DME and diesel in light-duty vehicles [8].

	DME	**Diesel**
Hydrocarbons (mg/MJ)	21	54
Particulates (mg/MJ)	3.3	26
CO_2 (mg/MJ)	6700	7500
NO_x (mg/MJ)	325	281

Table 2.2. Properties of DME and diesel fuel [5].

Fuel property	**Unit**	**DME**	**Diesel**
Chemical structure		CH3-O-CH3	-
Molar mass	g/mol	46	170
Carbon content	mass%	52.2	86
Hydrogen content	mass%	13	14
Oxygen content	mass%	34.8	0
Carbon-to-hydrogen ratio		0.337	0.516
Critical temperature	K	400	708
Critical pressure	MPa	5.37	3
Critical densitiy	Kg/m^3	259	
Liquid density	Kg/m^3	667	831
Cetane number		>55	40-50
Auto-ignition temperature	K	508	523
Stoichiometric air/fuel mass ratio		9	14.6
Boiling point at 1 atm	K	248.1	450-643
Lower heating value	MJ/kg	27.6	42.5
Modulus of elasticity	N/m^2	6.37E+8	14.86E+8
Kinematic viscosity of liquid	cSt	<0.1	3
Surface tension	N/m	1.2E-2	2.7E-2
Vapor pressure	kPa	530	<< 10

DME is a non-carcinogenic, non-teratogenic, non-mutagenic, non-toxic and colourless gas with ether like odor at room temperature. DME does not exist as natural. Vapour pressure of DME is between propane and butane, which are main ingredients of LPG. Higher vapor pressure of DME than diesel allows to use lower pressure injection system. DME can be liquefied with increasing pressure at room temperature. Because of these, storage of DME is similar to LPG, which can allow the use of the same infrastructure as LPG with some modifications [1,5,6,9–11]. On the other hand, volumetric energy density of diesel is greater than DME, storage tank required for DME should

be twice the size of storage tank required for diesel [1].

As drawbacks of DME usage in CI engines, lower fuel lubricity, lower viscosity, lower density and higher compressibility, higher vapor pressure than diesel can be shown. To overcome these drawbacks, some improvements have to be done in fuel injection system. Another drawback of DME usage is combustion of DME produces formaldehyde, acetaldehyde and formic acid [5, 6].

DME can also be used as fuel for power generation using gas turbines. Other than as a fuel, DME can be used as aerosol propellant and solvent. Other important usage of DME can be as a chemical intermediate for synthesis of chemicals as shown in Figure 1.1 such as acetic acid, methyl acetate, dimethoxyethane [2, 3].

2.2. DME Synthesis Methods

DME synthesis can be investigated considering three reactions, which are methanol synthesis, methanol dehydration and water-gas shift reaction. These reactions are shown respectively in equations 2.1, 2.2 and 2.3. For CO_2 hydrogenation, a seperate equation does not have to be written. Using reactions 2.1 and reverse of 2.3, a reaction for CO_2 hydrogenation can be obtained. Reactions 2.1 and 2.3 take place on the same metallic catalyst while reaction 2.2 takes place on a catalyst with acidic function. Location of these two catalysts whether in the same reactor or not determines the preferred method (i.e. indirect or direct) for DME synthesis [3, 12].

$$CO + 2H_2 \rightleftharpoons CH_3OH \qquad \Delta H_{298K} = -90.6 \, \frac{kJ}{mol} \tag{2.1}$$

$$2CH_3OH \rightleftharpoons CH_3OCH_3 + H_2O \qquad \Delta H_{298K} = -23.4 \, \frac{kJ}{mol} \tag{2.2}$$

$$CO + H_2O \rightleftharpoons CO_2 + H_2 \qquad \Delta H_{298K} = -41.2 \, \frac{kJ}{mol} \tag{2.3}$$

2.2.1. Indirect DME Synthesis

Indirect DME synthesis method utilizes two consecutive reactors in which methanol synthesis from synthesis gas and methanol dehydration to DME take place respectively. Example scheme can be seen in Figure 2.1. As feed gases, CO_2 and H_2 are selected in the process shown in Figure 2.1. Nevertheless, CO_2 can be replaced with CO as well.

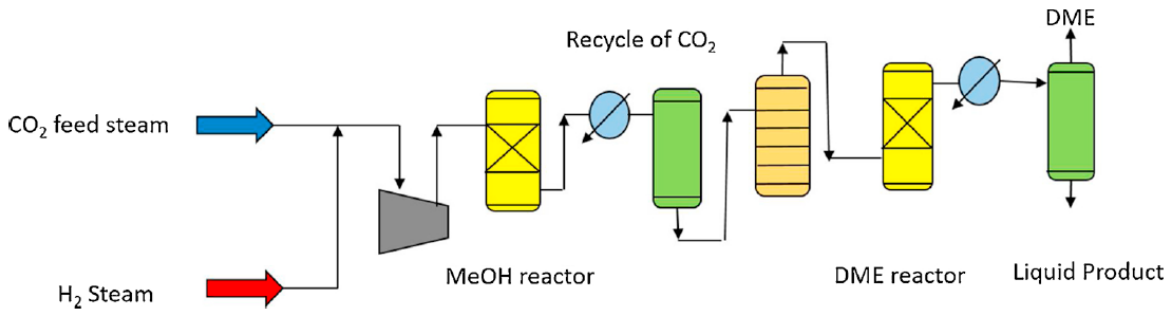

Figure 2.1. Process flow sheet for indirect DME synthesis [13].

2.2.1.1. Thermodynamic Analyses. In order to show the difference between indirect and direct (Section 2.2.2) methods clearly, a preliminary thermodynamic analysis is conducted via the Gibbs Free Energy minimization technique using Chemcad platform [3, 12, 14]. With thermodynamic analysis, achievable conversion of carbon containing gas in the feed gas can be determined. Thermodynamic analysis for indirect method is conducted assuming dehydration to DME is not taking place, only hydrogenation of CO or CO_2 taking place depending on the feed gas. As feed gases, stoichiometric amount of reactants are used for DME synthesis. For CO containing feed gas and CO_2 containing feed gas, achievable conversion values are shown in Table 2.3, separately. Comparison of these figures with the figures of available other method, direct DME synthesis, for the same feed and reaction conditions is made in Section 2.2.2.1. Conversion difference between the two feed gases, CO containing and CO_2 containing, comes from the reverse water-gas shift reaction. Formation of water as a result of reverse water-gas shift reaction limits the CO_2 conversion since water-gas shift reaction is an equilibrium reaction.

Table 2.3. For indirect DME synthesis method thermodynamic analyses at 225 ^{0}C and 30 bar while 20% N_2 is present.

	CO as feed gas	**CO_2 as feed gas**
Conversion of carbon containing feed gas (%)	47.5	20.1

2.2.2. Direct DME Synthesis

Direct DME synthesis method, schematically presented in Figure 2.2, involves a single reactor in which methanol synthesis and methanol dehydration catalysts are loaded in mixed form. When CO and H_2 are selected as feed gases, simultaneously taking place water-gas shift reaction helps to remove H_2O formed by increasing CO_2 as a result of methanol dehydration reaction. Higher CO conversion values are in reach with direct DME synthesis method by observing increase in DME yield because of water usage in the reaction and by observing increase in CO_2 formation.

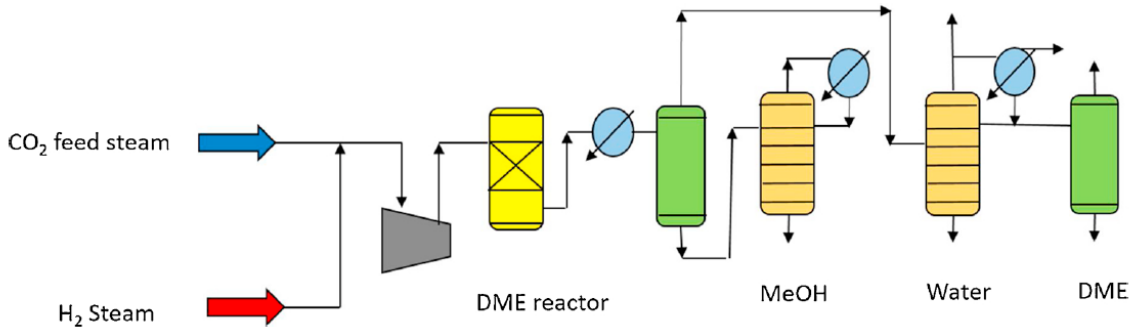

Figure 2.2. Process flow sheet for direct DME synthesis [13].

2.2.2.1. Thermodynamic Analyses. For thermodynamic analysis of direct DME synthesis method, methanol dehydration is included to observe the effect of reactor intensification. For direct synthesis method, achievable conversion of carbon source in the syngas and DME yield are shown in Table 2.4. When CO is used as carbon source, direct DME synthesis method offers conversion increase compared to indirect DME

synthesis method with *in-situ* conversion of methanol to DME, relaxation of thermodynamic limit of methanol synthesis, and with *in-situ* conversion of water formed as a result of dehydration of methanol to H_2 through water-gas shift reaction. Increase in CO_2 conversion between two methods is not that much drastic as in the case of CO feeding. Formation of water both as a result of reverse water-gas shift reaction and methanol dehydration limits the conversion of CO_2. Increase in the conversion can be explained with a decrease in the methanol and CO concentration. Effect of intensification obtained with usage of a single reactor is not that significant when CO_2 is present as carbon source compared to CO. In this respect, *in-situ* removal of H_2O can be envisioned as a promising solution to elevate CO_2 conversion and DME yield [15].

Table 2.4. For direct DME synthesis method thermodynamic analyses at 225 ^{0}C and 30 bar while 20% N_2 is present.

	CO as feed gas	**CO_2 as feed gas**
Conversion of carbon containing feedgas(%)	96.7	28.5
DME yield(%)	66.2	21.0

2.2.2.2. Operating Conditions. This subsubsection includes important operating conditions to consider. These operating conditions include compositions of gases in feed gas, GHSV through the reactor, pressure inside the reactor, temperature of the reactor, reduction conditions for the methanol synthesis catalyst, ratio of the methanol synthesis catalyst to the dehydration catalyst and relative configuration of catalysts inside the reactor.

For CO or CO_2 as only carbon source in feed stream, different H_2/CO_x ratios are used. In general, the pertinent stoichiometric values (i.e. H_2/CO=2 and H_2/CO_2=3) are selected. Other than single carbon source cases, both CO and CO_2 can co-exist within syngas. In this case, a variety of CO_2/CO ratios can be used. Single carbon source case is covered in this thesis. For CO as only carbon source case, H_2/CO ratio 2 gives higher CO conversion than lower ratios. Higher ratios reduces desired DME production rate [4, 16]. For CO_2 as only carbon source case, H_2/CO_2 ratio

3 is selected in various articles as H_2/CO_2 ratio 3 is stoichiometric ratio for CO_2 hydrogenation [17–19].

Considering GHSV dependance of methanol synthesis catalyst, loading amount of methanol synthesis catalyst and reactant flow rate through the reactor are important. When CO is selected as only carbon source, methanol synthesis catalyst to methanol dehydration catalyst ratio 1 is used. When 1 g of each catalysts is loaded, 30 Nml min^{-1} reactant flow is passed over the catalyst. This value corresponds to about 1500 h^{-1} for methanol synthesis which is below the maximum recommended value in the handbook of the HiFUEL R120 methanol synthesis catalyst [16].

According to the Le Chatelier's Principle, for methanol synthesis reaction, increasing the pressure favors the formation of methanol. Majority of articles used pressures between 20-50 bar to increase the conversion of carbon containing feed gas [17–19]. In order to increase thermodynamic limit both as yield and conversion lower temperatures are preferred while higher temperature favors reactions kinetically. Higher limit of the temperature is usually limited by the onset of sintering of the Cu-based methanol synthesis catalysts. Therefore, temperature is ranged between 220-300 ^{0}C [20–23].

For different carbon sources available in the feed stream, mass ratio of methanol synthesis catalyst to methanol dehydration catalyst changes. When CO is only carbon source in the feed stream, the ratio is usually selected as 1. For CO_2 as only carbon source in feed stream, more reactive surface is required for dehydration of methanol. Increasing the dehydration catalyst amount to twice of the synthesis catalyst is beneficial especially when the methanol concentration is low inside the reactor during hydrogenation of the CO_2 [20].

Configuration of the two catalysts inside the reactor is important when water-gas shift reaction is considered. When CO is the only carbon source inside the feed, water-gas shift reaction is important for the removal of water formed as a result of methanol dehydration reaction. Water-gas shift reaction takes place on methanol synthesis cat-

alyst so mixing of these two catalyst is required especially for CO hydrogenation. For CO_2 hydrogenation, mixing is also important considering the formed H_2O as a result of reverse water-gas shift reaction. H_2O formed as a result of reverse water-gas shift reaction can reduce the dehydration of methanol if reverse water-gas shift reaction reaches equilibrium before dehydration of methanol reaction starts [24].

2.3. Catalysts for DME Synthesis

DME synthesis being independent of the method used for synthesis can be investigated as two parts consisting of different reactions, methanol synthesis and methanol dehydration. For methanol synthesis part, the same catalyst can be used being independent of the carbon source of the feed stream, CO or CO_2. In contrast with the metallic nature of the synthesis catalyst, methanol dehydration catalysts should have acidic properties. Depending on the carbon source in feed stream, acidity of the dehydration catalyst becomes important. Methanol synthesis and dehydration catalysts are usually physically mixed together before they were loaded to the reactor. Other than physically mixing together those two catalysts, another option available is to prepare a single grain on which those two functions are available. In this case, the catalyst is called as a hybrid catalyst. A concise review of the methanol synthesis and dehydration catalysts is provided in the following sections.

2.3.1. Methanol Synthesis Catalysts

Arena *et al.* [25] prepared Cu–ZnO/ZrO_2 catalysts which have constant 44 wt.% ZrO_2 loading with varying CuO and ZnO loadings between 0-56 wt.% for hydrogenation of CO_2 to methanol. For the preparation of the catalyst, reverse co-precipitation method was used. An aqueous solution containing $Cu(NO_3)_2$, $Zn(NO_3)_2$, $ZrO(NO_3)_2$ was added to 0.1 M $NaHCO_3$ solution keeping pH of the solution in the range 7.0 - 7.5 with continuous addition of 0.1 M $NaHCO_3$ solution. Precipitate was aged, filtered, washed, dried and calcined. Calcination was conducted under air at 623 K for 4 h. Method applied, reverse co-precipitation with ultrasound irradiation, provided

improvement in the surface area exposure and dispersion. Strong promoting effect of ZnO was proven on the surface area, dispersion and reducibility of the catalyst. Commercial Cu–ZnO/Al_2O_3 was used for comparison. Negative effect of water on the rate of methanol formation was related with the reference Cu–ZnO/Al_2O_3 catalyst. Reaction conditions were 473-513 K, 10 - 30 bar, $H_2/CO_2/N_2$ = 9:3:1 and GHSV = 4400 - 8800 $NLh^{-1}kg_{cat}^{-1}$. At higher GHSV, both methanol selectivity and conversion of the reference catalyst was low compared to Cu–ZnO/Al_2O_3. According to STY for methanol, Zn/Cu ratio of 0.3 - 0.5 displayed maximum performance both at low GHSV and high GHSV. At low GHSV, 30 bar, selectivity to methanol was about 70% at 473 K and decreased to about 50% for all supports and Zn/Cu ratios. At low GHSV, 30 bar, CO_2 conversion was about 7% at 473 K and increased to about 17% for all supports and Zn/Cu ratios. During the stability test conducted for 18 h at 473 K, 10 bar and low GHSV, selectivity and conversion values of reference and Cu(9)ZnO(3)/ZrO_2(6) catalysts remained unchanged.

Pérez-Ramirez *et al.* [26] studied CO_2 hydrogenation to methanol using Indium Oxide as catalyst and comparing Indium Oxide catalyst to conventional Cu-ZnO-Al_2O_3 catalyst as benchmark. Solution of $In(OH)_3.xH_2O$ dissolved in a 1:3 mixture of deionized water and alcohol was used for impregnation of supports. Supported In_2O_3 catalysts containing 9 wt.% In were prepared in powder or extrudate forms evaporating solvent from impregnated supports and drying, calcining them. Calcination was conducted at 573 K for 3 h under static air. Activation condition for In_2O_3 catalysts was 573 K and 5 bar for 1 h under Ar atmosphere. Reaction conditions were 473-573 K, 50 bar, H_2/CO_2=4:1 and GHSV=16000 h^{-1}. Explanation given for the usage of high GHSV was to diminish compared to slower reverse water-gas shift reaction. Reverse water-gas shift reaction requires much higher GHSVs to diminish on Cu-ZnO-Al_2O_3 compared to In_2O_3. 47% selectivity was the highest obtained with Cu-ZnO-Al_2O_3 catalyst at 473 K. On the contrary, In_2O_3 showed 100% selectivity on the given temperature range. On In_2O_3 catalyst STY for methanol was $\sim$ 0.33 g_{MeOH} h^{-1} g_{cat}^{-1} while on Cu–ZnO/Al_2O_3 catalyst $\sim$ 0.13 g_{MeOH} h^{-1} g_{cat}^{-1} at 573 K. Supported In_2O_3 catalyst was stable for 1000 h on stream while Cu-ZnO-Al_2O_3 lost 44% in 100 h.

Jingfa *et al.* [27] prepared $Cu/ZnO/Al_2O_3$ catalysts having the same copper, zinc, aluminun ratio, 45:45:10, with three different methods to test their activity for methanol synthesis from CO_2 hydrogenation. Methods used were conventional oxalate coprecipitation, oxalate gel-coprecipitation, conventional carbonate coprecipitation. For conventional oxalate coprecipitation, 1 M aqueous oxalic acid solution 20% excess was added on 0.1 M copper nitrate, zinc nitrate and aluminum nitrate aqueous solution. Precipitates dried at 110 ^{0}C. Volume shrinkage was not observed during drying process. For oxalate gel-coprecipitation, nitrate solutions were dissolved in ethanol instead of aqua being different than conventional oxalate precipitation. Upon drying, volume shrinkage to fifth of initial volume was observed. For conventional carbonate precipitation, 0.1 M carbonate solution and 0.1 M nitrate solution were simultaneously added into 100 ml deionized water at 80 ^{0}C with vigorous stirring. During mixing, pH of the solution was kept between 6.5-7.0. Precipitates were aged for 30 min at 50 ^{0}C, filtered and washed with hot deionized water, later dried at 110 ^{0}C overnight. Calcination procedure was 150 ^{0}C for 1 h, 200 ^{0}C for 1 h, 250 ^{0}C for 1 h, 300 ^{0}C for 1 h and 360 ^{0}C for 4 h. For reduction, reactor was heated to 240 ^{0}C with 2 ^{0}C min^{-1} ramp. Reduction duration was 10 h under 40 ml min^{-1} containing 5% H_2 and 95% Ar. CO_2/H_2 ratio in reactant gas was 1:3. Temperature and pressure range was 180 ^{0}C - 300 ^{0}C and 5 - 40 bar, respectively. GHSVs used were 3600 and 10000 h^{-1}. According to the data provided, catalysts prepared by oxalic acid precipitation methods showed higher CO_2 conversion both at lower and higher GHSVs compared to the catalyst prepared using carbonate precipitation. Reaction conditions for the given data was 240 ^{0}C, 20 bar. Highest methanol yield was obtained with the catalyst prepared using oxalate gel-coprecipitation method. Even at the highest GHSV, catalyst prepared with oxalate gel-coprecipitation method retained CO_2 conversion and methanol selectivity. Retaining high conversion level and methanol selectivity at high GHSV led to high methanol yield.

Ning *et al.* [28] studied effect of preparation method on the element distribution of $Cu/ZnO/Al_2O_3$ catalyst. Oxalate gel-coprecipitation method and conventional ammonium bicarbonate coprecipitation procedures were compared. Catalysts prepared

with these methods were named as U8 and C9, respectively. CuO and ZnO mass ratios were 60:40 in catalysts prepared with both methods. For oxalate gel-coprecipitation method, oxalic acid solution was added upon solution of copper nitrate, zinc nitrate and aluminum nitrate dissolved in ethanol. Precipitates were aged for 30 min and solvent were evaporated at 323 K. 383 K was the over night drying temperature. Calcination was applied at 423 K for 1 h, 473 K for 1 h, 523 K for 1 h, 573 K for 1 h and 633 K for 4 h under air atmosphere. 300 bar pressure were applied for pelletizing and pellets were crashed into 40-60 mesh size. Cu and Zn were mixed homogeneously in U8 catalyst prepared using oxalate gel-coprecipitation method. Cu aggregates more on the surface of C9 catalyst prepared with conventional ammonium bicarbonate coprecipitation method. Aggregation of Cu on the surface makes reduction of C9 catalyst easier. On the contrary, U8 has more close to isomorphous distribution of Cu and Zn. Reaction conditions were 513 K, 10 bar, 3600 ml $gcat^{-1}$ h^{-1}. Methanol peak area read using gas chromatograph was presented as performance criteria fot the catalysts and methanol peak areas for U8 were higher than C9. Higher activity of U8 were related with Cu-Zn species since ZnO helped reverse spill over of H_2, related with the acceleration of methanol synthesis.

Liu *et al.* [29] prepared Cu/ZrO_2 catalysts using different methods for CO_2 hydrogenation for methanol synthesis. Three different methods used were deposition-precipitation(DP), impregnation(IM) and co-precipitation(CP). For IM and DP catalysts, zirconia aerogel prepared with supercritical fluid drying method having higher specific surface area and larger pore volume were used. Effect of catalyst composition and catalyst preparation method were investigated. For the selected catalyst composition and catalyst preparation method, effect calcination temperature were also investigated. To prepare zirconia aerogel, 0.17 M $ZrOCl_2.8H_2O$ solution and 0.2 M ammonia solution were added to a beaker containing 100 ml deionized water keeping the pH of the solution between 6.5-10.0. Precipitate was filtered and washed with first deionized water, later with ethanol. For supercritical fluid drying of the precipitate, ethanol and high pressure autoclave were used. Supercritical drying conditions were 260 ^{0}C, 76 bar and 15-20 min. CP catalysts were prepared mixing 0.1 M NaOH solu-

tion with a solution containing 0.17 M $ZrOCl_2$ and $Cu(NO_3)_2$ at constant pH of 7.0. IM catalysts were prepared by impregnating zirconia aerogel with 0.1 M $Cu(NO_3)_2$. After impregnation, drying and calcination were applied. DP catalysts were prepared using zirconia aerogel and precipitate of 0.1 M NaOH solution and 0.1 M $Cu(NO_3)_2$ solution at constant pH of 7.0. Standard calcination temperature was 350 ^{0}C and for the selected catalysts showing better catalytic activity with selected preparation method and composition, calcination temperature 450, 550 and 650 ^{0}C were also tried. Catalysts prepared with DP method showed larger specific surface area, more uniform and smaller particle size. Reaction conditions were 220-240 ^{0}C, 20 bar, 5400 h^{-1} and H_2/CO_2=3. Highest methanol yield, $\sim$ 0.36 g g_{cat}^{-1} h^{-1}, was obtained in a reaction at 240 ^{0}C with 30-40% copper oxide containing catalyst prepared with DP method calcined at 350 ^{0}C.

Tsang *et al.* [30] studied methanol synthesis from CO_2 hydrogenation over Pd@Zn core-shell catalysts at low pressure 20 bar. Pd based catalyst was preferred because Pd was more active compared to Cu and Pd was more durable against sintering. Reason behind selection of core and shell structure was to suppress RWGS reaction. To prepare ZnO-CdSe support, CdSe and ZnO were grown sequentially. CdSe were synthetized using solutions of Na_2SeSO_3 and $Cd(NO_3)_2$. Na_2SeSO_3 were prepared using Se powder and Na_2SO_3. $Cd(NO_3)_2$ and sodium citrate containing solution were mixed with Na_2SeSO_3 to prepare CdSe particles. Zinc nitrate and NaOH were dissolved in deionized water and CdSe particles dispersed in ethanol were added to the prepared zinc solution. Ethylenediamine was also added to the mixture. After stirring white crystalline product were formed and collected with centrifuge. Product was washed with water and ethanol. Later, prodect was dried in oven at 60 ^{0}C for 12 h. Prepared support was impregnated immersing support into $Pd(NO_3)_2$ in ethanol solution. Solution were dried at 50 ^{0}C. Calcination was in air at 450-500 ^{0}C for 2 h. Reduction were conducted under 20 ml min^{-1} H_2 flow at 280 ^{0}C for 2 h. Reactor outer diameter was 12.7 mm. H_2/CO_2 ratio was 2.8:1 in the feed stream and feed gas flow rate was 30 ml min^{-1} over 0.1 g catalyst. Pd impregnation was 5 wt.%. Studied catalyst shows higher methanol yield at low temperature and pressure compared to industrial Cu based cata-

lysts. Pd@Zn surfaces show high ability to activate H_2 because of higher H adsorption energies and they stabilizes HCOO species more than COOH species allowing to suppress RWGS reaction. At 20 bar and 270 ^{0}C, 6.1 $g_{methanol}$ $g_{active\ metal}^{-1}$ h^{-1} with 70% selectivity was obtained with the studied core and shell catalyst containing 26.4 wt.% CdSe while commercial Cu based catalysts gave below 5% selectivity and close to zero yield.

2.3.2. Methanol Dehydration Catalysts

Goodman *et al.* [31] studied dehydration of methanol to DME over different solid acid catalysts, γ-Al_2O_3, H-ZSM-5, amorphous silica-alumina and titania modified zirconia. Activity for the reaction was observed together with the DME selectivity on all catalysts. Aqueous ammonia or sodium hydroxide was slowly added on to aqueous ethanol solution of $TiCl_4$ and $ZrCl_4$ until pH of the solution reach to $\sim$ 8.0 to prepare 50 mol% TiO_2/ZrO_2. Obtained precipitate was filtered and washed until chlorine ion was detected. Precipitate was dried at 110 ^{0}C and calcined at 550 ^{0}C for 3.5 h. Pure TiO_2 and ZrO_2 were obtained using the same procedure. 1.0 wt.% TiO_2/Al_2O_3 was prepared using the same procedure, as well. According to precipitant, NH_4^+ or Na^+ was added before to the name of the catalyst. Amorphous silica-alumina, γ-Al_2O_3 and ZSM-5 were supplied prepared. Sample was activated under 40 ml/min air flow at 550 ^{0}C for 1 h. Under 60 ml/min He flow, sample was lowered to the reaction temperature. At 116 Torr methanol partial pressure, conversion increased from 6.3% to more than 90% at 250 ^{0}C over γ-Al_2O_3. DME and water were the only reaction products. 23 Torr water addition to the reaction medium increased activation energy for the DME formation from 25 kcal mol^{-1} to 37 kcal mol^{-1} over γ-Al_2O_3. Competitive adsorption of water with methanol reduces conversion level that can be achieved. Upon 113 Torr H_2O addition, conversion achieved was 39% under 81.4 Torr methanol partial pressure at 250 ^{0}C. NH_4^+-TiO_2/Al_2O_3 showed similar behavior to γ-Al_2O_3. Na^+-TiO_2/Al_2O_3 had lower activity and coke formation since Na^+ blocks strong acid sites. Reduced coke formation was important for the life time of the catalyst. Activity and stability of the catalyst can be tuned by amount of Na^+ present. 50 mol% TiO_2/ZrO_2 showed

higher catalytic activity from the pure constituents because of the acid base harmony of the constituents, however, activity of 50 mol% TiO_2/ZrO_2 is less than γ-Al_2O_3. H-ZSM-5(50) containing both lewis acid and bronsted acid sites was affected from water addition, however, H-ZSM-5(150) containing bronsted acid sites, because of less Al amount, was not affected from water partial pressure increase. Using H-ZSM-5(50), 78% methanol conversion and 100% DME selectivity was obtained at 190 ^{0}C. H-ZSM-5(50) catalyst showed the highest catalytic activity while obtained DME selectivity was 20% at 280 ^{0}C. Increasing temperature was not found good for selectivity of DME when H-ZSM-5(50) was used as catalyst. Increasing acidity on amorphous silica-alumina with increasing silica content decreases rate of methanol dehydration. Compared to other tested catalysts amorphous silica-alumina catalyst containing 20 wt.% silica (SIRAL20) showed the highest yield at 280 ^{0}C while having wider temperature tolerance range.

Shen *et al.* [32] studied nature, strength and number of surface acid sites of H-ZSM-5, steam de-aluminated H-Y zeolite (SDY), γ-Al_2O_3, $Ti(SO_4)_2/\gamma$-Al_2O_3 catalysts for the dehydration of methanol to DME. Microcalorimetric adsorption of ammonia, infrared spectroscopy and isopropanol decomposition were the used methods. NH_4-ZSM-5 having SiO_2/γ-Al_2O_3 ratio of 25 was calcined at 823 K for 3 h to prepare H-ZSM-5. NaY zeolite was ammonium exchanged and, later, steam treated at 873 K for 5 h to prepare SDY. 5 wt.% $Ti(SO_4)_2$ was impregnated on γ-Al_2O_3. Impregnated γ-Al_2O_3 was dried at 383 K overnight and calcined at 723 K for 1.5 h. GHSV was 3400 ml g_{cat}^{-1} h^{-1} and feed compositon was 21:79 methanol to N_2. H-ZSM-5 and SDY contained high number of Brϕnsted acid sites. High number of Brϕnsted acid sites was not preferable at high temperature since hydrocarbons and coke were produced above 513 K. Above 553 K, coke formation on H-ZSM-5 and SDY was serious. H-ZSM-5 showed high activity as low as 423 K. At 443 K, activity was maximum and activity decreased thermodynamically with temperature increase. Strong acid sites can be selectively poisoned for usage of H-ZSM-5 at higher temperatures. Steam de-alumination produced extra framework of aluminum, which helped to increase surface Lewis acidity of SDY. Activity of the SDY, which was deactivated by coke formation, can be regenerated by burning off the coke formed. Below 573 K, conversion of methanol was

less on γ-Al_2O_3 eventhough DME selectivity was high. Low activity of γ-Al_2O_3 in temperature range of 493-553 K required modification especially for using γ-Al_2O_3 as acidic catalyst in direct DME synthesis at lower temperatures. $Ti(SO_4)_2$ modification of γ-Al_2O_3 improved Brϕnsted surface acidity so reaction activity for methanol dehydration to DME. Hydrocarbon by-product and coke formation was not observed on $Ti(SO_4)_2/\gamma$-Al_2O_3 in temperature range of 513-593 K. At 513 K, thermodynamically limited conversion, $\sim$ 85%, was obtained using $Ti(SO_4)_2/\gamma$-Al_2O_3. Order of catalyst activities was found as H-ZSM-5>SDY>$Ti(SO_4)_2/\gamma$-Al_2O_3>γ-Al_2O_3.

Hwang *et al.* [33] studied methanol dehydration to DME over H-ZSM-5, NaH-ZSM-5 and compared them to γ-Al_2O_3. Commercial γ-Al_2O_3 and ZSM-5 were provided. Hydrogen form H-ZSM-5 was obtained by calcining at 823 K for 10 h under flowing air with 10 K min^{-1} ramp. NaH-ZSM-5 was obtained treating H-ZSM-5 with 1M $NaNO_3$, washing three times with de-ioned water, drying at 393 K for 2 h and calcining at 823 K for 10 h under flowing air with 10 K min^{-1} ramp. Activation conditions for catalyst was pure N_2 flow at 773 K for 4 h. Reaction conditions were WHSV=4 h^{-1}, 523 K. Conversion on H-ZSM-5 decreased slightly through the 500 min reaction time while conversion on γ-Al_2O_3 decreased initially and continued stable. DME selectivity on γ-Al_2O_3 decreased slightly through the 500 min reaction time while DME selectivity on H-ZSM-5 decreased more. At $\sim$ 575 K, methanol conversion reaches thermodynamic limit on γ-Al_2O_3 while at $\sim$ 500 K, methanol converison reaches thermodynamic limit on H-ZSM-5. Increasing Si/Al ratio was useful to increase DME selectivity even though catalytic activity was decreased. H-ZSM-5(50) and H-ZSM-5(140), where numbers in paranthesis denote SiO_2/Al_2O_3 ratio, showed similar catalytic activity together with DME selectivity of >99. Catalytic activity of H-ZSM-5 and NaH-ZSM-5 was higher than γ-Al_2O_3. Order of catalyst activities was found as H-ZSM-5(30)>NaH-ZSM-5(30)>γ-Al_2O_3. DME selectivity of Na^+ ion-exchanged H-ZSM-5(NaH-ZSM-5) was higher than H-ZSM-5 because of removed strong acid sites.

Catizzone *et al.* [34] studied effect of water on methanol dehydration to DME over Ferrierite versus γ-Al_2O_3 catalysts. FER-type zeolites having different acidity

levels and Si/Al ratios of 10, 25, 45 were prepared. Structure directing agent(SDA) for FER10, FER-type zeolite having Si/Al ratio of 10, was pyrrolidine. SDA for FER25 was pyridine and synthesis gel having Si/Al ratio of 30 was used to prepare FER25. SDA for FER45 was pyridine and synthesis gel having Si/Al ratio of 60 was used to prepare FER45. Hydrothermal crystallization duration was 90 h. Solid was recovered with filtration and washed with distilled water several times. Calcination was done under air flow at 550 ^{0}C. Commercial γ-Al_2O_3 was provided. Temperature range used for reaction was 140-240 ^{0}C. WHSV for reaction was 2.7 g_{MeOH} h^{-1} g_{cat}^{-1}. Different ratios of water/methanol were investigated without changing the methanol WHSV. Most effective FER-type zeolite was also tested at 280 ^{0}C for 60 h to investigate effect of water on coke deposition. Order of catalytic activity for methanol conversion was FER10>FER25>FER45>γ-Al_2O_3. Above 200 ^{0}C, catalytic activity of γ-Al_2O_3 was higher than FER45. Catalytic activity of γ-Al_2O_3 reduced more compared to tested FER-type zeolites upon water addition to reactant stream. At 200 ^{0}C, methanol conversion over γ-Al_2O_3 decreased from 30% to 13% with water addition to stream equal to 0.1 times the methanol fed to the reactor. Above 200 ^{0}C, zeolites showed negligible deactivation upon water addition to reactant stream. Water addition also reduced amount of coke formed on zeolite catalysts together with intial coke formation rate. Selectivity of FER10 decreased from 0.97 to 0.92 upon temperature increase from 180 ^{0}C to 240 ^{0}C. For FER25 and FER45 decrease was from 1.0 to 0.97.

Ojeda *et al.* [35] studied methanol dehydration to DME over niobium (V) oxalate impregnated using method of incipient wetness TiO_2 catalysts with different loadings. Before impregnation, TiO_2 was treated at 823 K for 4 h under air. Impregnation was done at room temperature using aqueous solutions of niobium (V) oxalate. With increasing Nb loading, number of Lewis acid sites decreased and acid site strength increased. Impregnated solids were dried at 393 K overnight while calcination was done at 773 K for 4 h under ambient air. Prepared catalyst with different Nb loadings were denoted as xNb/TiO_2, where x was the Nb atoms present at nm^{-2}. Reaction conditions were 573 K, 6.1 kPa methanol partial pressure, 13.9 mmol h^{-1} g_{cat}^{-1}. SiC was used as inert filler while loading to the reactor. Methanol conversion rate and

selectivity to DME of TiO_2 support were 0.32 mmol h^{-1} g_{cat}^{-1} and 83%, respectively. At highest Nb loading, 9.0Nb/TiO_2, methanol conversion rate and selectivity to DME increased to $\sim$ 0.9 mmol h^{-1} g_{cat}^{-1} and 93%, respectively. At highest Nb loading, Brϕnsted acid were also present. Catalytic activity of NbO_x/TiO_2 catalysts prepared showed increasing trend with the strength of acid sites present.

Tatsumi *et al.* [36] studied dehydration of methanol to DME over zeolites Rho, KFI $\leq$ 200 ^{0}C and compared results of Rho and KFI with γ-Al_2O_3, SSZ-13, RUB-13 and ZSM-5. For synthesis of zeolites, gels with the Si/Al ratio of 5.0 were used. Rho zeolite synthesized without using SDA. $Al(OH)_3$ was dissolved refluxing at 100 ^{0}C in aqueous NaOH solution and was cooled to room temperature in a Teflon beaker. Aqueous solution of CsOH. H_2O was addded to the cooled solution and with slow addition of colloidal silica AS-40 under vigorous stirring, homogeneous synthesis gel was obtained. Composition of the gel was $1.8Na_2O$:$0.3CsO$:$1.0Al_2O_3$:$10SiO_2$:$100H_2O$. Gel was homogenized for 2 h with stirring and transferred to a polypropylene bottle. Hydrothermal crystallization was 10 day long without agitation at 80 ^{0}C in a pre-heated oven. Solid product was obtained with vacuum filtration, later, washed and dried at 70 ^{0}C. Other Rho type zeolites having Si/Al ratio of 10 and 20 were also prepared. To prepare KFI zeolite, $Al(OH)_3$ was dissolved refluxing at 100 ^{0}C in KOH solution. Solution was cooled to room temperature and poured to Teflon beaker. Later, solution was mixed with the $SrCl_2.H_2O$ and 18-crown-6 with stirring. With slow addition of colloidal silica AS-40 under vigorous stirring, homogeneous synthesis gel was obtained. Composition of the gel was $2.3K_2O$:$0.1SrO$:$1.0Al_2O_3$:$10SiO_2$:$220H_2O$:1.0(18-crown-6). 0.5 h extra stirred gel was transferred to a teflon vessel enclosed in steel bomb. Hydrothermal crystallization was 120 h at 150 ^{0}C in a pre-heated oven. Solid product was obtained with vacuum filtration, later, washed and dried at 70 ^{0}C. Organic SDA for preparation of KFI was 18-crown-6. Dried precipitate was calcined at 550 ^{0}C to remove SDA. Catalyst pretreatment was at 500 ^{0}C for 1 h. Reaction conditions were 5-20 kPa methanol partial pressure, 150-200 ^{0}C and WHSV of 1.0-3.8 h^{-1}. Rho zeolite showed $\sim$ 93% methanol conversion with 100% DME selectivity at 200 ^{0}C and at 150 ^{0}C, methanol conversion and DME selectivity were $\sim$ 70% and 100%, respectively. At

150 ^{0}C, Rho zeolite showed more than 10 times catalytic activity of γ-Al_2O_3. WHSV increase in the range given in the reaction condition did not affect activity of Rho type zeolite. At 200 ^{0}C and WHSV of 1.0 h^{-1}, Rho, KFI and SSZ-13 showed thermodynamic level of methanol conversion with 100% selectivity. Zeolite RUB-13 showed catalytic activity lower than γ-Al_2O_3 being related with 2-D framework. Rho type had more solid acid sites than KFI. Below 200 ^{0}C, small-pore zeolites with medium-strong acidity and 3-D channels showed better catalytic activity compared to γ-Al_2O_3. Important features of Rho zeolite affecting catalytic performance were surface area and smaller crystallite size, which were 812 m^2 g^{-1} and 1 μm, respectively. Performance of Rho zeolite was stable in a 3 day run.

Yi *et al.* [37] studied methanol dehydration to DME over nano-sized SAPO-11 zeolite synthesized using seed-induced quasi-solvothermal conversion protocol without a secondary porogen. For preparation of micro-sized and nano-sized gels, the same solution was used. For preparation of used solution, aluminium isopropoxide was hydrolyzed in deionized water for 12 h with stirring and H_3PO_4 was added and homogenized for 4 h. Later, di-n-propylamine was firstly added, tetraethyl orthosilicate was secondly added. Micro-sized SAPO-11 was prepared transferring prepared solution to Teflon-lined stainless steel autoclave and hydrothermally crystallizing at 433 K for 24 h. For preparation of nano-sized SAPO-11, prepared gel was pre-crystallized at 433 K for 24 h. Solvent of the gel evaporated at 333 K and 25 mL ethanol was added with stirring. Residual solvent was evaporated at 333 K for 48 h. Obtained solid was crashed into powder, which was later transferred into crucible, which was placed into Teflon-lined stainless steel autoclave. Between autoclave and crucibel, 20 ml of ethanol was added for quasi solvothermal conditions. Autoclave was left in an oven at 473 K for 24 h. Recovered products with filtration were washed with deionized water, dried at 373 K and calcined at 873 K for 6 h. Activation conditions were 473 K, 2 h and under 20 ml min^{-1} N_2 flow. During reaction, N_2 to methanol ratio was 240. Compositon of SAPO-11 was 1.0 Al_2O_3: 1.0 P_2O_3: 2.0 di-n-propylamine: 0.3 Tetraethyl orthosilicate: 50 H_2O. Advantages of method used to synthesize nano-sized SAPO-11 were promotion of SAPO-11 nucleation, nanoscale proximity between seed structure

and amorphous compound, lower level of Si atom incorporation and smaller crystallization of SAPO-11 when ethanol was modifier. Large particles with 200nm average size formed by aggregation of smaller 20-30 nm sized SAPO-11 nanocrystals had lower acidity, larger surface area and higher inter-crystal mesoporosity than micro-sized SAPO-11 crystals. Performance of nano-sized SAPO-11 was better than micro-sized SAPO-11 and γ-Al_2O_3. Order of catalyst activity per area was nano-SAPO-11 > micro-SAC-SAPO-11 > γ-Al_2O_3. At 500 K, methanol conversions on nano-SAPO-11 and γ-Al_2O_3 were $\sim$ 30% and $\sim$ 15%, respectively while DME selectivities were close to unity.

Li *et al.* [38] studied methanol dehydration to DME over metal ion, which were Al, Ga, Sn, Zr and Fe, doped MCM-41 prepared using hydrothermal synthesis method. Si/Al ratios of 5, 10, 20, 30 and 50 were prepared. Tetraethyl orthosilicate was dissolved in dilute sulfuric acid solution and 10 wt.% cetrimonium bromide was added. $AlCl_3$ and NaOH were added. pH of the solution become 10-11. In Teflon-lined rotating autoclave, solution was crystallized at 110 ^{0}C for 48 h. Cooled product was filtered, washed, dried at 110 ^{0}C and calcined in air at 550 ^{0}C for 6 h. At 90 ^{0}C, calcined sample treated with 1.0 M NH_4Cl solution for 2 h. Filtering, washing, drying repeated and calcination was conducted for 2 h at 550 ^{0}C. Ratio of ingredients, CTAB:TEOS:Al_2O_3:NaOH:H_2O, were 0.16:1:x:0.24:110. For other than Al doping, Si/M ratio was 10 and instead of aluminium chloride, chloride of corresponding metal was used. Activation conditions were 400 ^{0}C, 30 ml min^{-1} N_2, 4 h. Reaction conditions were 300-425 ^{0}C, 1 bar and 0.1 ml min^{-1} liquid methanol flow to be vaporized. Metal ion doped MCM-41 catalysts, M-MCM-41, showed similar structure to MCM-41, which had long-range ordered mesoporous structure. As the reaction temperature was increased, methanol conversion increased even though methanol dehydration is thermodynamically limited, where increasing temperature reduces achievable conversion. Amount of weak acid site increased with increasing amount of Al doping. Highest catalytic performance obtained, which was achieved when Si/Al ratio molar ratio was 10, was 80% conversion and 100% selectivity. Order of catalytic activity, according to metal ion doped and coordination number of doped metal ion, was Al-MCM-41 > Ga-MCM-41 > Zr-MCM-41 > Fe-MCM-41 > Sn-MCM-41=0.

2.3.3. Bifunctional and Hybrid Catalysts

Ruan *et al.* [39] studied effect of zeolite type on single-step DME synthesis from syngas over CuZnAl-zeolite bifunctional catalyst. Bifunctional catalysts used were prepared physically mixing Cu-ZnO-Al_2O_3 and zeolite in 2:1 ratio, respectively. Activation conditions were 5% H_2 flow diluted with N_2, 245 ^{0}C and 10 h. Reaction conditions were H_2/CO ratio of 2, 260 ^{0}C, 50 bar and 1500 ml g_{cat}^{-1} h^{-1}. Zeolite type used for the process affected activity, selectivity and stability of the bifunctional catalyst. CO conversion and DME selectivity were affected by weak and strong acid sites, pore structure and Si/Al distribution. Si:Al ratios given in parentheses; ZSM-5(30), Y(5.1) and Ferrierite(20) showed higher DME yield compared to other zeolites. Maximum CO conversion, DME selectivity and DME yield were 93%, 65.9% and 301.7 g kg_{cat}^{-1} h^{-1}.

Rooney *et al.* [40] studied DME synthesis from synthesis gas admixing different solid acid catalysts; NH_4ZSM-5, HZSM-5 and γ-Al_2O_3; with CZA. For NH_4ZSM-5, Si/Al ratio of both 23 and 80 were used while Si/Al ratio of 80 was used for HZSM-5. Activation conditions were 20 ml min^{-1} 5% H_2 flow diluted with He, 250 ^{0}C and 6 h at atmospheric pressure. Composition of the feed gas composed of H_2:CO:CO_2:Ar was 62:31:4:3. Reaction conditions were 200-260 ^{0}C, 20 bar and 2400 ml g_{cat}^{-1} h^{-1}. Admixed bifunctional CZA/HZSM-5 catalyst having Si/Al ratio of 80 and containing 25 wt.% solid acid catalyst showed high stability. 16.2% of initial catalytic activity was lost over 212 h continuous reaction time. Deactivation was related to the coke formation on methanol synthesis catalyst, which can be removed above sintering temperature. Highest CO conversion obtained was 63.43% at 260 ^{0}C with CZA/NH_4ZSM-5(80) while second highest, not much different, was 59.77% with CZA/HZSM-5(80), which had DME selectivity of $\sim$ 70%.

Huang *et al.* [41] studied synthesis gas conversion to DME over bifunctional catalysts to investigate effect of preparation method and dehydration component. Activation conditions were H_2 flow, 230 ^{0}C and 4 h. Reaction conditions were 290 ^{0}C, 40 bar, 1500 h^{-1}, H_2/CO ratio of 2 with 5% CO_2 compositon in feed flow. Highest catalytic

activity was obtained with CZA/HSY and CZA/HZSM-5, prepared with coprecipitating sedimentation, showing 89% CO conversion and 99% DME selectivity in organic products. Synergistic effect of catalytically active parts of bifunctional catalyst was observed. CO conversion increased dramatically since thermodynamic limit of methanol synthesis was broken.

Bonura *et al.* [42] studied direct synthesis of DME from CO_2 hydrogenation over CuZnZr-zeolite catalysts. Prepared CuZnZr catalysts had Cu loading ratio between 33-60%. Prepared MFI type zeolite catalysts had Si/Al ratio of 15, 25, 50 and 100. Beside physical mixing of methanol synthesis and methanol dehydration catalysts, catalysts were chemically combined by precipitating CuZnZr catalyst in an oxalic acid solution containing zeolite finely dispersed. Physical mixing ratios of methanol synthesis and methanol dehydration catalysts were 1:1 and 9:1. Chemical mixing ratio of methanol synthesis and methanol dehydration catalyst was 9:1. Activation conditions were pure hydrogen flow, atmospheric pressure, 300 ^{0}C and 1 h. Reaction conditions were 180-240 ^{0}C, 30 bar, feed gas H_2:CO_2:N_1 ratio of 9:3:1 and 10000 h^{-1}. CuZnZr catalyst containing 60 wt.% Cu showed highest CO_2 conversion, 18.0%, and methanol yield, 51.1% , which were close to equilibrium values. Si/Al ratio of 25 for zeolite was important when catalytic activity and resistance to deactivation in presence of water were considered. DME synthesis showed lower CO_2 conversion compared to methanol synthesis on the same catalyst due to water accumulation. Prepared bifunctional catalyst with physical mixing of CuZnZr having 60 wt.% Cu and MFI(25) in 9:1 ratio showed 15.4% CO_2 conversion and DME selectivity of 37.6%, both of which were higher than corresponding values for mixing ratio of 1:1. Chemically mixed catalyst showed higher CO_2 conversion, 15.9%, and DME yield, 38.5%. Decreasing GHSV to 2500 h^{-1} showed positive effect both on CO_2 conversion and DME yield on hybrid catalyst. After decreasing GHSV, with increasing pressure to 50 bar, CO_2 conversion increased to 23.6% while DME selectivity increased to 49.3%.

Suh *et al.* [43] studied CO_2 conversion to DME over bifunctional Al_2O_3/Cu/ZnO having Al composition between 30-80 mol% prepared with sequential precipitation and

also investigated Ferrierite type zeolite addition to form dual bed system. Activation conditions were 100 ml flow containing 20% H_2 diluted in N_2, 573 K and 5 h. Reaction conditions were H_2:CO_2:N_2 ratio of 72:24:4, 573 K, 50 bar and 1450 L kg_{cat}^{-1} h^{-1}. Activity and acidity of catalysts having 60-80% Al content was higher than commercial Al_2O_3. Cu dispersion was 6-7% being independent of Cu loading. CO_2 conversion of 25% and DME selectivity of 75% excluding CO selectivity were obtained with prepared bifunctional catalyst Al_2O_3/Cu/ZnO having 80% Al. Dual bed system enabled CO free DME selectivity to increase 82.2% while GHSV was reduced to 355 L kg_{cat}^{-1} h^{-1} due to addition of more catalyst to the system. Fraction of methanol was converted to DME and fraction of DME was converted to methyl acetate over Ferrierite.

Frusteri *et al.* [44] studied one step hydrogenation of CO_2 to DME over four different combination of methanol synthesis catalyst, Cu-ZnO-ZrO_2 (ZCZ), and methanol dehydration catalyst, HZSM-5. Reverse co-precipitation of ZCZ in a solution containing finely dispersed HZSM-5, dual-bed of ZCZ and HZSM-5, pelletization of homogenous mixture of ZCZ and HZSM-5 in powder form, homogeneous physical mixture of ZCZ and HZSM-5 were tested combination methods. Activation conditions were pure hydrogen flow at atmospheric pressure, 573 K and 1 h. Reaction conditions were H_2:CO_2:N_2 ratio of 69:23:8 in feed stream, 443-563 K, 1-50 bar and 4500-36000 NL kg_{cat}^{-1} h^{-1}. Reverse co-precipitation of ZCZ in a solution containing finely dispersed HZSM-5 caused loss of weak-medium acidity of zeolite. Highest DME productivity of 4.4 mmol kg_{zcz}^{-1} s^{-1} was obtained over bifunctional prepared with physical mixing method at 513 K, 30 bar and 9000 NL kg_{cat}^{-1} h^{-1}. At 493 K, 9000 NL kg_{cat}^{-1} h^{-1} and 30 bar; CO_2 conversion was $\sim$ 10% and DME selectivity was $\sim$ 50%. Metal/oxides-acid interface was determined as main factor for CO_2 conversion and DME productivity. Catalytic behavior of Cu-ZnO-ZrO_2/HZSM-5 was highly dependent on the ratio of metal oxides to acid surface sites. 50 wt.% zeolite loading was more effective compared to higher and lower loading ratios.

Liang *et al.* [45] studied one-step CO_2 hydrogenation to DME over mixture of Cu-ZnO based catalysts prepared with concentrations ranging from 0.1 to 1.0 and HZSM-5

to investigate catalyst preparation and reaction conditions. Activation conditions were 20 ml min^{-1} pure H_2 flow, 250 ^{0}C and 10 h. Reaction conditions were H_2:CO_2 ratio of 3, 220-280 ^{0}C, 21-42 bar and 1525 NL kg_{cat}^{-1} h^{-1}. Increasing concentration of precursor resulted in a decrease in Cu surface area and Cu dispersion. At 42 bar and 260 ^{0}C, 30.5% CO_2 conversion and 72.0% DME selectivity were obtained. Prepared catalyst showed 21.4% CO_2 conversion and 55.5% DME selectivity after 100 h at 28 bar and 240 ^{0}C. Optimum temperature for DME synthesis was found as 240-260 ^{0}C on bifunctional catalyst depending on the condition.

Frusteri *et al.* [12] studied CO_2 hydrogenation to DME over CuZnZr-ferrierite hybrid catalysts prepared with two different methods, wet impregnation and gel-oxalate coprecipitation, combining metal oxide and acid sites on a single grain to investigate effect of metal loading and element dispersion on nature and morphology of the active sites. Reduction conditions were pure hydrogen flow at atmospheric pressure, 300 ^{0}C and 1 h. Reaction conditions were H_2:CO_2:N_2 ratio of 9:3:1, 220-260 ^{0}C, 50 bar and 8800 NL kg_{cat}^{-1} h^{-1}. Decreasing zeolite ratio caused an decrease in surface area. Increase in metal loading caused to formation of core and shell type structure, in which zeolite was core, when catalyst was prepared with wet impregnation, on the other hand, metal oxide clusters were distributed homogeneously when catalysts were prepared using gel-oxalate coprecipitation. Catalysts prepared with gel-oxalate coprecipitation shows increasing CO_2 conversion with incresing metal loading and for catalyst prepared with wet impregnation, case is the opposite. For catalytic activity and selectivity, CuZnZr:FER weight ratio greater than 1 was better. Key parameters determined for higher activity and selectivity were particle size, number of acidic dehydration sites and homogeneous distribution of metal-oxide and acid sites. At 260 ^{0}C, 23.6% CO_2 conversion, the highest conversion achieved, and 47% DME selectivity were obtained over catalyst prepared with gel-oxalate coprecipitation with metal oxide to acid ratio of 2. At lower space velocity, 2200 NL kg_{cat}^{-1} h^{-1}, with increasing CO_2 conversion, DME selectivity also increased opposed to decreasing DME selectivity with increasing CO_2 conversion at higher GHSV.

Atakan *et al.* [46] studied CO_2 hydrogenation over a hybrid catalyst consisting of Zr-doped mesoporous silica supports with intergrown Cu nanoparticles, copper-zirconium-SBA-15, to investigate effect of morphological and chemical properties on conversion and selectivity. Two different silica precursors used for synthesis of Zr-SBA-15 framework were tetraethyl orthosilicate and sodium metasilicate. Cu loading methods used were evaporation induced wetness impregnation and infiltration. Activation conditions were H_2 flow, 400 ^{0}C and 9 h. Reaction conditions were H_2:CO_2 ratio of 3, 250 ^{0}C and 33 bar. Silica precursor affected activity of the catalyst while Cu loading method affected the selectivity of the products. Zr dispersion and bonding to the silica matrix led to higher activity of tetraethyl orthosilicate materials compared to sodium metasilicate. Tetraethyl orthosilicate had larger pore size, microporosity, specific surface area and better adhesion between the Cu nanoparticles. Higher number of acid sites having higher acid strength were observed for tetraethyl orthosilicate compared to sodium metasilicate, which led to higher DME selectivity, together with an increased reoxidation state of Cu nanoparticles. Infiltration method as Cu loading allowed methanol conversion to DME because evaporation induced wetness impregnation led to lower Cu oxidation state due to higher Zr content. Catalyst prepared with tetraethyl orthosilicate as silicate source using infiltration method showed 15% conversion, which is highest among the combinations, together with $\sim$ 70% DME selectivity.

Zha *et al.* [47] studied CO_2 hydrogenation to DME over HZSM-5 packed CuO-ZnO-Al_2O_3 nanoparticles. Spherical carbons prepared using aqueous glucose were removed with calcination to yield CuO-ZnO-Al_2O_3 nano particles after aqueous Cu^{+2}, Zn^{+2}, Al^{+3} ions covered spherical carbons. CuO-ZnO-Al_2O_3 nanoparticles were packed hydrothermally onto HZSM-5 membrane. Activation conditions were 4 h pretreatment under 5% H_2/N_2 at 270 ^{0}C flow for 4 h and pure H_2 flow at 270 ^{0}C for 2 h. Reaction conditions were H_2/CO_2 ratio of 3, 30 bar, 270 ^{0}C and 1800 NL kg_{cat}^{-1} h^{-1}. CO_2 conversion and DME yield obtained were 48.3% and 23.4%, respectively for the catalyst having core and shell structure, in which HZSM-5 was the shell and CuO-ZnO-Al_2O_3 nanoparticles was the core. Increasing pressure above 30 bar was not helpful to increase CO_2 conversion further.

Table 2.5. Summary table of bifunctional and hybrid catalysts.

Ref #	**CO_x**	**H_2/CO_x**	**Synthesis Cat**	**Dehydration Cat**	**Hybrid**	**Core&Shell**	**GHSV**	**Pressure**	**Conversion**	**DME yield**
37	CO	2	Cu-ZnO-Al_2O_3	ZSM-5(30) Y(5.1) Ferrierite(20)	-	-	1500 ml g_{cat}^{-1} h^{-1}	50 bar	93%	65.9%
38	CO	2	Cu-ZnO-Al_2O_3	HZSM-5(80) NH_4ZSM-5	-	-	2400 ml g_{cat}^{-1} h^{-1}	20 bar	59.77%	$\sim$ 42%
39	CO	2	Cu-ZnO-Al_2O_3	HSY HZSM-5	-	-	1500 h^{-1}	40 bar	89%	78%
40	CO_2	3	CuZnZr	HZSM-5(25)	-	-	2500 h^{-1}	50 bar	23.6%	$\sim$ 12%
41	CO_2	3	Cu/ZnO	Al_2O_3	Hybrid	Sequential precipitation	1450 ml g_{cat}^{-1} h^{-1}	50 bar	25%	10%
42	CO_2	3	CuZnZr	HZSM-5	-	-	9000 ml g_{cat}^{-1} h^{-1}	30 bar	$\sim$ 10%	$\sim$ 5%
43	CO_2	3	Cu-ZnO	HZSM-5	-	-	1525 ml g_{cat}^{-1} h^{-1}	42 bar	30.5%	22%
44	CO_2	3	CuZnZr	Ferrierite	Hybrid	-	8800 ml g_{cat}^{-1} h^{-1}	50 bar	23.6%	11%
45	CO_2	3	Cu NPs	Zr-SBA-15	Hybrid	-	-	33 bar	15%	10.5%
46	CO_2	3	Cu-ZnO-Al_2O_3	HZSM-5	Hybrid	Core&Shell	1800 ml g_{cat}^{-1} h^{-1}	30 bar	48.3%	23.4%

2.4. Sorption Enhanced DME Synthesis

Methanol dehydration, water-gas shift reactions, (Equations 2.2, 2.3, respectively) involve water in equilibrium. Sorption enhanced means removal of the water inside the reactor to shift involved reactions forward to increase both CO_2 conversion and DME yield beyond thermodynamic limit. Sorption enhancement can be obtained with a membrane system, where water is continuously withdrawn from the system, and with a sorbent, which should be water specific. For membrane system, core and shell type catalysts can be one type of example. Disadvantage of core and shell type catalyst is deactivation of shell, where dehydration catalyst is present. Disadvantage of the sorbent usage is related with its capacity. After capacity of sorbent is filled, regeneration of the sorbent is conducted utilizing either pressure swing or temperature swing desorption techniques [48, 49].

Iliuta *et al.* [50] studied a model of DME production with CO_2 hydrogenation in the presence of *in-situ* H_2O removal by adsorption. H_2O removal was helpful to increase methanol and DME yields together with DME selectivity while methanol selectivity was decreased. Maximum CO_2 conversion was increased to triple of the initial while 1% of carbon feed was CO. DME yield was also increased to triple of the initial however 33% of the carbon feed was CO.

Rahimpour *et al.* [51] studied a model of methanol dehydration to DME in a gas-solid-solid trickle flow reactor while Zeolite 4A was present as adsorbent. Advantage of gas-solid-solid trickle flow reactor was continuous adsorbent regeneration. 11.17% enhancement in dimethyl ether production with gas-solid-solid trickle flow reactor with water adsorption was observed upon conventional reactor.

Recently, Kampen *et al.* [15] reviewed steam separation enhanced reactions. DME yield obtained for CO_2 feed could be increased to $\sim$ 80% with sorption enhancement while DME yield usually obtained was below 9% without sorption enhancement. Kampen *et al.* [52] mentioned that CO_2 yield with sorption enhancement can be low as much

as 2% allowing simplification of down stream seperation and recycle.

The literature review shows that in contrast with CO-to-DME conversion, CO_2 hydrogenation, which is technically more challenging due to *in-situ* steam formation, is studied to a much less extent. Moreover, the number of studies that address the benefits of *in-situ* steam adsorption under the conditions of CO_2 hydrogenation is scarce. Therefore, this study is primarily aimed to provide useful insight into the impacts of sorption enhancement and to synthesize a dehydration catalyst for increasing DME yield under the conditions of CO_2 hydrogenation.

3. EXPERIMENTAL WORK

3.1. Materials

3.1.1. Catalysts, Active Metal Precursors and Sorbent

Table 3.1 presents the catalysts supplied prepared, sorbent used in the experiments and active metal precursor to prepare more active dehydration catalyst.

Table 3.1. Catalysts, Active Metal Precursors and Sorbent.

Chemicals	**Formula**	**Supplier**	**Usage**
HiFUEL R120	$Cu/ZnO/Al_2O_3$ (CZA)	Alfa Aesar	Methanol Synthesis Catalyst
γ-Alumina	γ-Al_2O_3	Alfa Aesar	Methanol Dehydration Catalyst
Phosphotungstic Acid Hydrate	$12WO_3.H_3PO_4.xH_2O$	Sigma Aldrich	Impregnation of Methanol Dehydration Catalyst
Molecular Sieves 3Å	K_nNa_{12-n} $[(AlO_2)_{12}(SiO_2)_{12}.xH_2O]$	Sigma Aldrich	Sorbent

3.1.2. Gases

Table 3.2 presents reaction, calibration and carrier gases denoting application and specification. Composition of reaction gases in the feed stream was provided in the Section 3.2.3.

3.2. Pre-reaction

Pre-reaction section includes preparation of catalysts and sorbent used, loading of the reactor, reduction conditions, feed stream compositions and pressurization of the

Table 3.2. Reaction, Calibration and Carrier Gases.

Gas	**Purity(%)**	**Supplier**	**Application**
H_2	99.995	Linde	Reaction
CO	99.999	Linde	Reaction
CO_2	99.995	Linde	Reaction
N_2	99.998	Linde	Internal Standard
DME	≥99.9	Sigma Aldrich	Calibration
CH_4	99.995	Linde	Calibration
Ar	99.995	Linde	Carrier Gas
He	99.998	Linde	Carrier Gas
Dry air	78.4 N_2 21.5 O_2	Linde	Pneumatic Actuation

reactor before reaction was started. Crushing, sieving catalysts supplied prepared to desired mesh size and impregnation of dehydration catalyst was covered in preparation of catalysts. Loading of the reactor covers configuration of the catalysts inside the reactor, whether mixed or consecutive loading, methanol synthesis catalyst to methanol dehydration catalyst ratio and leak test to check if initiation of reaction is suitable. Feed stream compositions includes CO and CO_2 as different carbon sources beside H_2 and H_2/CO_2 ratios. Pressurization of the reactor is about increasing pressure of the reactor to desired pressure level with target feed stream composition.

3.2.1. Catalyst Preparation

In this study, HiFUEL R120 (CZA) catalyst, high surface area γ-Al_2O_3 catalyst and Molecular Sieve 3Å were crushed and sieved to 45-60 mesh size (corresponding to particle size range of 250-354 μm) using Retsch sieves. An example of crushed and sieved catalysts can be seen in Figure 3.1.

In an effort to obtain a more active dehydration catalyst when CO_2 was the carbon source present in the feed stream, γ-Al_2O_3, sieved to 45-60 mesh size, was

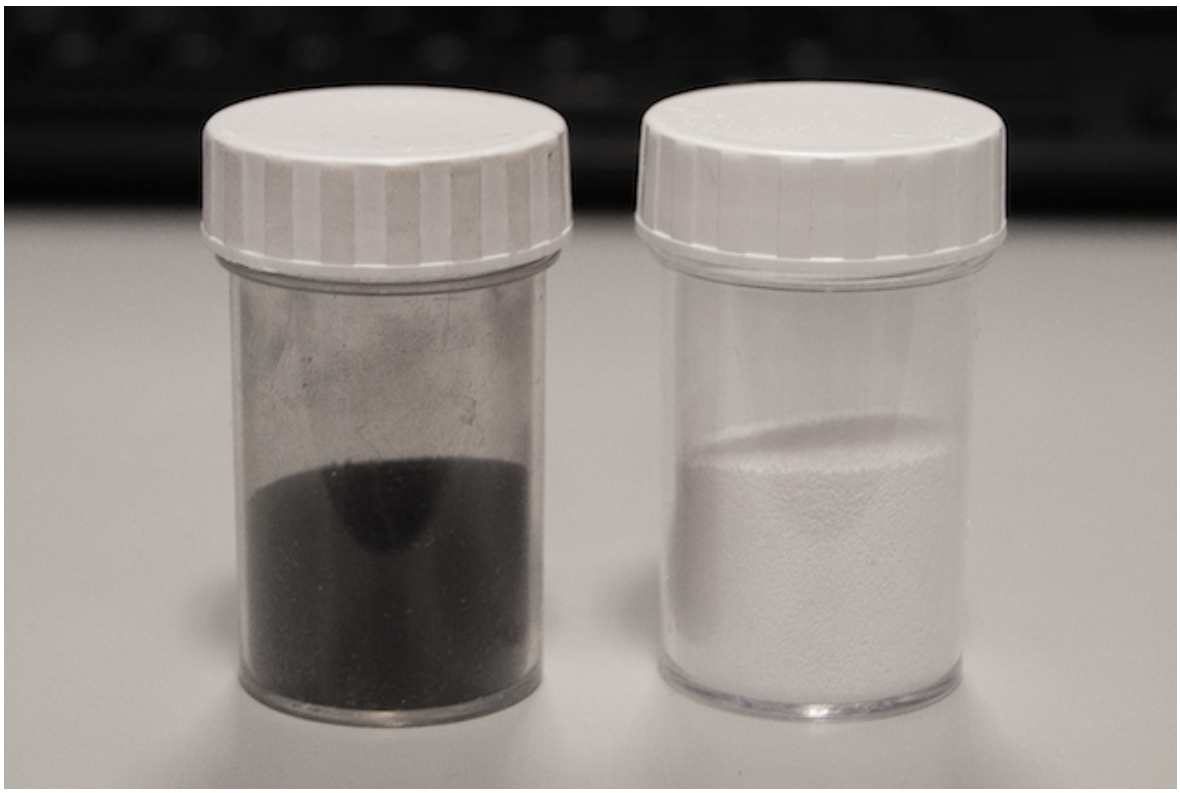

Figure 3.1. Crushed and sieved catalysts before loading to the reactor.

impregnated with phosphotungstic acid solution using incipient wetness impregnation method. KNF diaphragm vacuum pump evacuated air from the pores of the support, placed in a büchner flask. Zeneer Water Purification System was used to prepare deionized water with a conductivity less than 0.1 μS cm^{-1}. Precursor solution was added onto catalyst support using Masterflex peristaltic pump. Support-precursor solution was continuously mixed using Retsch UR1 ultrasonic mixer. To determine required amount of deionized water, support was wetted until excess water rest beside the support. Determined deionized water amount was 1 ml, taken with micropippette at four times, for 1 g γ-Al_2O_3 support. Batch size was taken as 3 g. For 30 wt.% PTA/γ-Al_2O_3, 2.1 g γ-Al_2O_3 and 0.9 g PTA were used. The latter was dissolved in 2.1 ml deionized water. Before addition of precursor solution to support, support was vacuumed for 30 min while ultrasonic mixer was on and bottom of the büchner funnel was inside distilled water placed in the ultrasonic mixer. After precursor solution was evenly added onto the support using peristaltic pump at a actual speed of 2 ml min^{-1},

büchner flask was left horizontally for 30 min, inclined to one side for 30 min and inclined to other side for another 30 min while vacuum pump and mixer were on. After impregnation was over, impregnated support was dried over night at 110 ^{0}C. Dried impregnated support was transferred to a crucible and temperature of furnace was increased to 500 ^{0}C in 46 min and leaved for 3 h at 500 ^{0}C before transfering crucible to desiccator [53].

3.2.2. Catalyst Loading and Reduction

A stainless steel, tubular down flow reactor having 17 cm length, 1.27 cm outer diameter and 1.02 cm inner diameter was used in the present study. Depending on the sorbent and dehydration catalyst amount, bed height changed between 5 and 11 cm. At the bottom of the bed, quartz wool layer having 2 cm height was placed while quartz layer at the top which was used to prevent falling of the bed while tightening nut of the reactor using clamp, was 1 cm in height. Particle size range of catalysts and sorbent loaded to the reactor were between 250 and 354 μm. Diffusive transport terms were neglected and plug flow assumption were made since when lowest bed height and largest particle diameter were considered, bed height to particle diameter ratio was $\sim$ 140 (>50 [54]) and tube diameter to particle diameter ratio was $\sim$ 29 (>15 [54]).

For feed streams containing CO as carbon source, sorbent was not loaded and two different configurations were tried. In the first configuration, methanol synthesis and dehydration catalysts were loaded consecutively as methanol synthesis catalyst at the top of the methanol dehydration catalyst. In the second configuration, the catalysts were mixed homogeneously before loading the mixture to the reactor. For feed streams containing CO_2 as carbon source, methanol synthesis and methanol dehydration catalysts were loaded to the reactor in a homogeneously mixed form. If sorbent was present, sorbent was also present in the mixture.

Leak tightness of the reactor was important since low GHSV was required in pressurized vessel and H_2 was one of the reactants. Unions, with which reactor was

connected to the system, were wrapped with PTFE band. After loaded reactor was connected to the system in a way flow was from top to bottom, the reactor was pressurized with N_2 to 32 bar and later, gas inlet and outlet were stopped while pressure of the system was monitored. If 0.1 bar decrease in the system pressure was observed in 75 min, leaking connection was found with bubble and tightened. Test was repeated until pressure decrease was not observed. Loaded reactor, installed into the system, can be seen in the Figure 3.2.

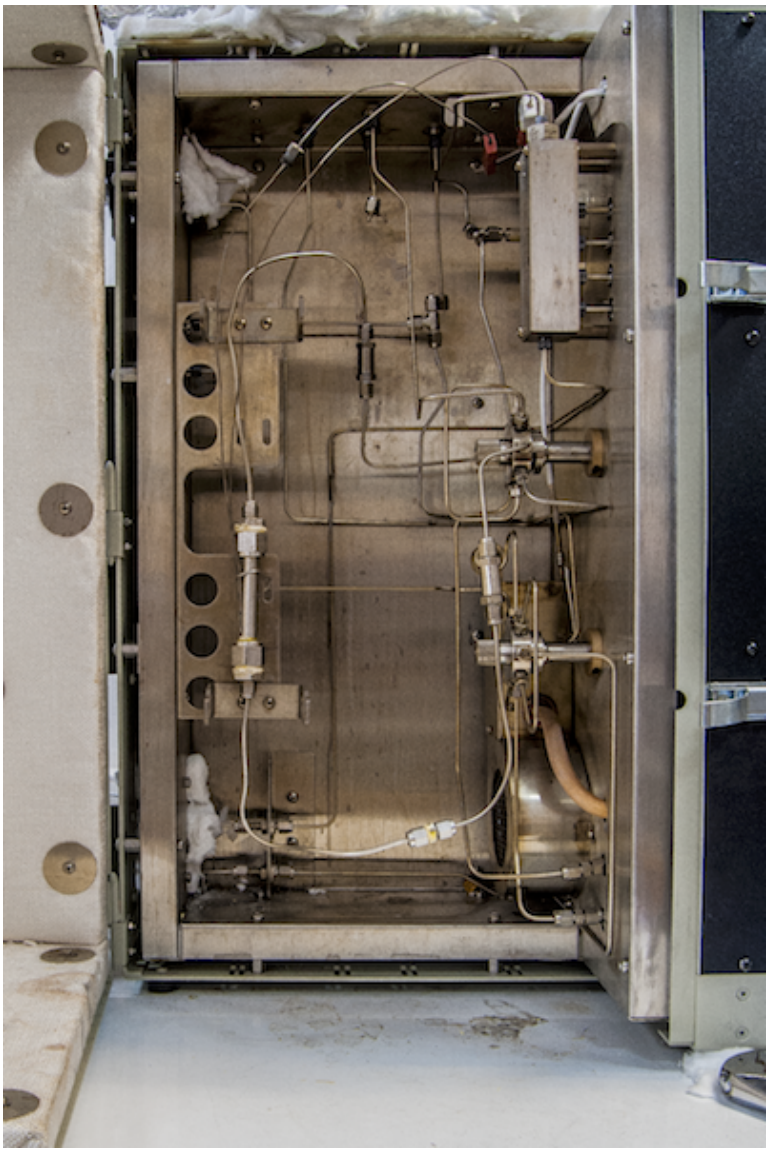

Figure 3.2. Loaded reactor installed into the system.

Before pressurization of the reactor, methanol synthesis catalyst had to be reduced. For reduction of the methanol synthesis catalyst, different strategies are present. Reduction duration, temperature, flow rate and H_2 composition in the reducing gas are typical pre-treatment parameters. The reduction conditions in this study are set to ensure reproducibility of the experiments and complete reduction of the CZA catalyst. Referenced article for this paragraph contains the closest reduction procedure applied in the experiments [55]. Reduction was conducted at atmospheric pressure and temperature of 230 ^{0}C for 2 h. Reduction temperature was above the reaction temperature, which is 225 ^{0}C. Reactor temperature was increased from room temperature to reduction temperature at a rate of 5 ^{0}C min^{-1} under 50 Nml min^{-1} N_2 flow. During the reduction, conducted at 230 ^{0}C, H_2 flow rate was 10 Nml min^{-1}. After 2 h of reduction, H_2 flow was switched to 50 Nml min^{-1} N_2 flow and temperature of the reactor was cooled to reaction temperature, 225 ^{0}C, as purge step which lasted for 1 h [55].

Table 3.3. Flow rates used in experiments during pressurization and reaction.

Flow Rate	**Pressurization (Nml min^{-1})**			**Reaction (Nml min^{-1})**		
Carbon Source	**H_2**	**CO_x**	**N_2**	**H_2**	**CO_x**	**N_2**
CO	68	36	26	12	6	5
CO	68	36	26	18	9	7
CO	68	36	26	23	12	9
CO	68	36	26	35	18	13
CO	68	36	26	57	30	22
CO	68	36	26	68	36	26
CO_2	-	-	-	9	7.1	5
CO_2	68	29.4	26	12	4.7	5
CO_2	77	22	26	13	3.4	5
CO_2	93	7.8	26	16	1.1	5

3.2.3. Mixture of Feed Streams and Pressurization

Table 3.3 shows options of flow rates used in the experiments as entered into mass flow controllers depending on the carbon source of the feed stream for both pressurization condition and reaction condition of the reactor. Given values in Table 3.3 can be converted to actual flow rates using the data given in Appendix Chapter B. During pressurization of the reactor, pressurization flow rate was supplied into the reactor using mass flow controllers and valve of back pressure regulator was in closed position. After switching to reaction flow rate, valve of the back pressure valve was turned into open position. For CO as carbon source, different reaction flow rate values were given for the corresponding GHSVs, which were calculated based on the CZA volume. For CO_2 as carbon source, different pressurization flow rate values and reaction flow rate values were given for the corresponding H_2/CO_2 ratios. Pressurization flow rate of the first line for CO_2 carbon source was not given since reactor was not pressurized with H_2/CO_2 ratio of 1 initially. For the ratio, only reaction flow rate was given. Data for the corresponding ratio was taken for the comparison purpose. After taking data for another ratio, flow rate was switched to flow rate for the corresponding ratio and waiting duration was longer since reaction flow rates were lower than the pressurization flow rates. Data for the corresponding ratio was taken after reactor reached equilibrium. Sorbent regeneration was carried out by swinging the pressure. In this context, regeneration was conducted for 1h at reaction temperature under 50 Nml min^{-1} N_2 flow and atmospheric pressure after reactor was depressurized. To complete regeneration cycle, reactor was pressurized back.

3.3. Reaction System

Figure 3.3 shows integration of reaction and analysis systems. In Figure 3.4, appearance of reaction system, which was called Parker Autoclave Engineers' BTRS-Jr PC, was shown. Controlled in-flow of pressurized reaction gases in feed stream, temperature control of the oven, pressure control of the reactor were all provided by BTRS-Jr PC and features of BTRS-Jr PC could be reached over connected computer.

Mass flow controllers inside BTRS-Jr PC, belonging to H_2, CO and N_2, were shown in Figure 3.5. Mass flow controllers of H_2, CO and N_2 gases were BROOKS Delta SLA5800. Mass flow controllers outside BTRS-Jr, belonging to CO_2, was shown in Figure 3.6. Mass flow controller of CO_2 was Bronkhorst El-Flow. Flow rate amount controlled gases were mixed upon entrance to the temperature controlled oven. For feed gas analysis, bypass of reactor was available. Pressure of the gas mixture was measured at the entrance of the reactor with a pressure transmitter and pressure of the system was controlled with a pneumatically actuated back pressure regulator, which was shown in Figure 3.7, by changing exit flow rate. Exit stream of BTRS was heated to 145 ^{0}C until the septum, with which samples were taken to qualitatively analyse presence of methanol and water, to prevent condensation of methanol and water before the cold trap.

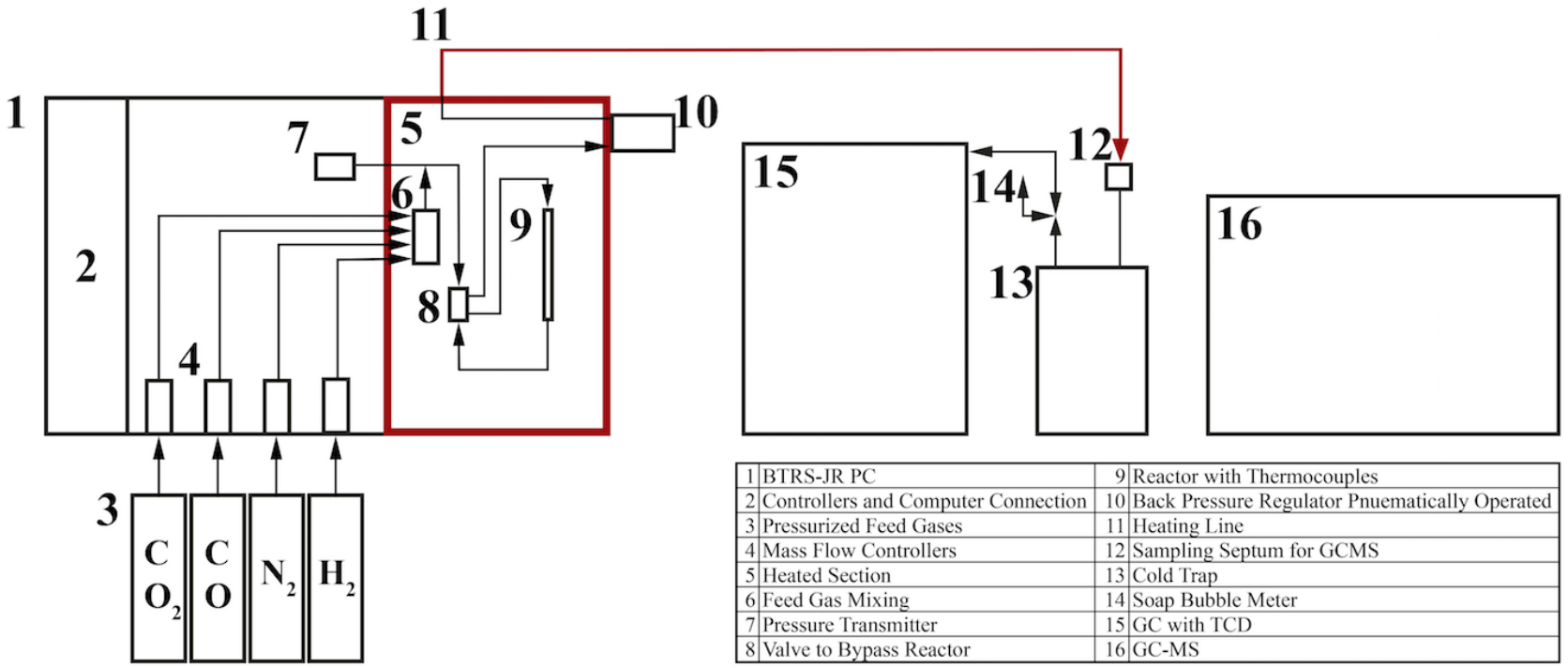

1	BTRS-JR PC	9	Reactor with Thermocouples
2	Controllers and Computer Connection	10	Back Pressure Regulator Pnuematically Operated
3	Pressurized Feed Gases	11	Heating Line
4	Mass Flow Controllers	12	Sampling Septum for GCMS
5	Heated Section	13	Cold Trap
6	Feed Gas Mixing	14	Soap Bubble Meter
7	Pressure Transmitter	15	GC with TCD
8	Valve to Bypass Reactor	16	GC-MS

Figure 3.3. Scheme of reaction and analysis systems.

Figure 3.4. Appearance of BTRS-Jr PC.

Figure 3.5. MFCs inside the BTRS.

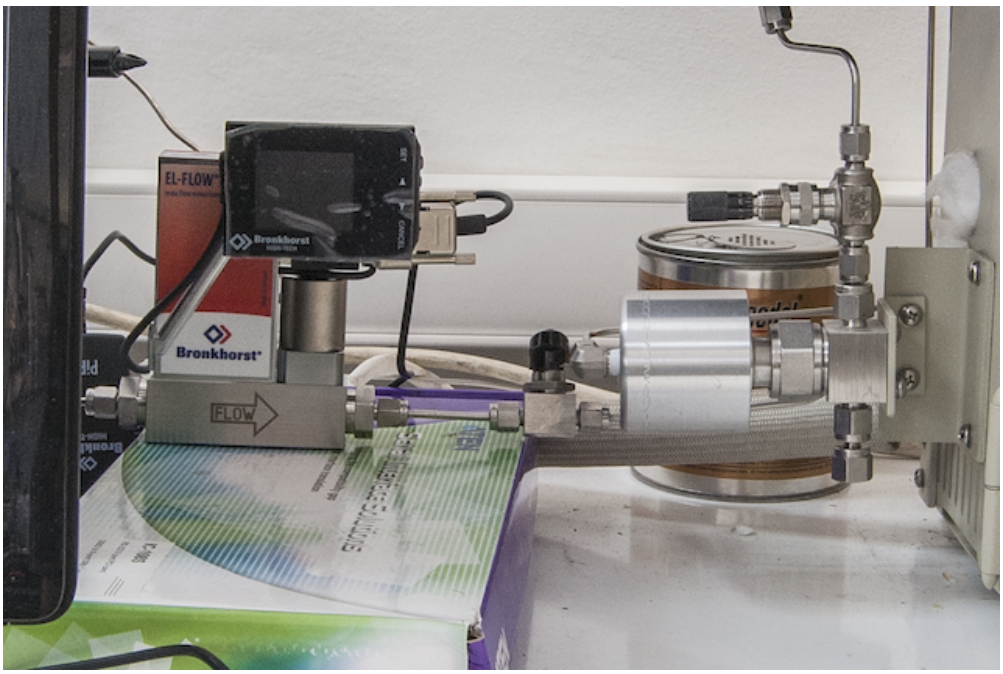

Figure 3.6. External MFC.

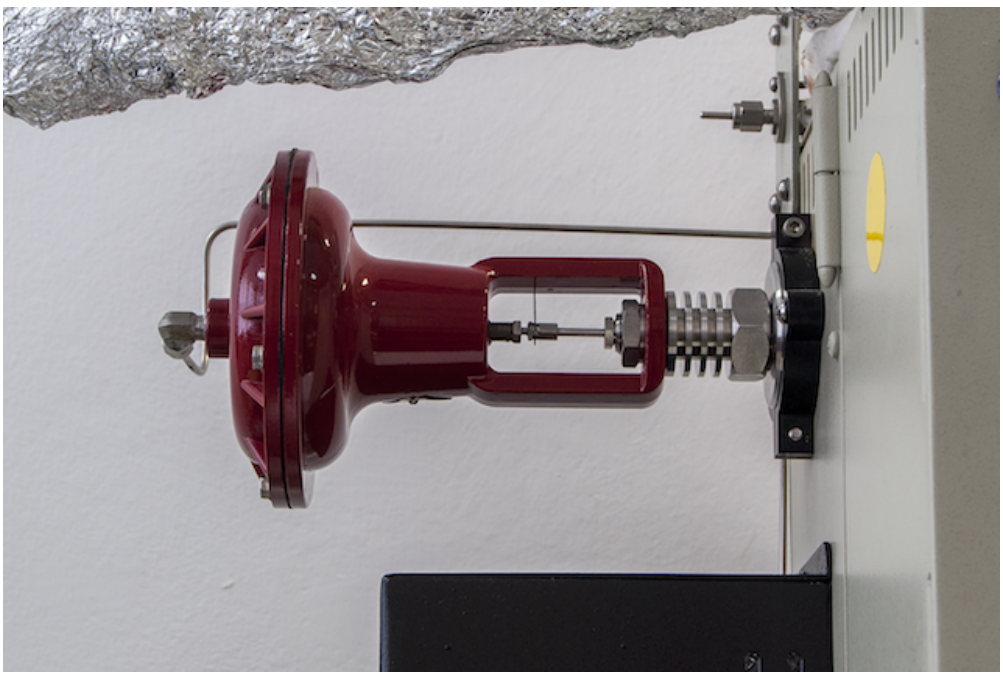

Figure 3.7. Back pressure regulator of BTRS.

3.4. Analysis Systems

Analysis systems were used to measure concentrations of compounds in the exit stream of the reactor. Using inert gas, N_2, as internal standard allowed to measure flow rate of the exit stream after cold trap. Exit flow rates of the compounds were calculated knowing total flow rate of exit stream and concentrations of compounds. GCMS, one of two separate analysis systems, was able to detect smaller compound concentrations so smaller sample injection sizes were preferred compared to other analysis system, GC, to prevent saturation of the MS detector and to analyse concentration of DME quantitatively. First analysis data of reactor exit stream was taken at 30^{th} min and for the following data data taking interval was 45 min.

3.4.1. Gas Chromatography with Thermal Conductivity Detector

Shimadzu GC-2014, shown in Figure 3.8, was calibrated to detect concentrations of H_2, N_2, CO, CH_4 and CO_2, written in the order of retention time. Knowing concentration of inert, N_2, at the exit stream, exit total flow rate was calculated. Sampling at the exit stream after cold trap was conducted with a valve connected to a sample loop having 1.1 ml of volume. Used analysis method was shown in Table 3.4. GC analysis method was independent of the carbon source in the feed stream.

Figure 3.8. Shimadzu GC-2014 System.

Table 3.4. Analysis Method of GC.

Parameters	
Carrier Gas	Argon
Carrier Gas Flow Rate	25 ml min^{-1}
Sample Loop Volume	1.1 ml
Injection Temperature	150 ^{0}C
Column Packing Material	Carboxen-1000
Column ID	2 mm
Column Length	6 m
Oven Temperature 1	60 ^{0}C
Oven Temperature 1 Duration	10.6 min
Oven Temperature 2	100 ^{0}C
Oven Temperature 2 Duration	9.1 min
Oven Temperature 3	150 ^{0}C
Oven Temperature 3 Duration	6.7 min
Oven Temperature Ramp Rate	25 ^{0}C min^{-1}
Detector Current	50 mA
Detector Temperature	175 ^{0}C

3.4.2. Gas Chromatography-Mass Spectrometer

GCMS-QP2010 Ultra, shown in Figure 3.9, was calibrated to quantitatively detect DME and to qualitatively detect methanol and water. Sampling method, being different than the one used for GC-2014, was conducted with septums and gas-tight

Figure 3.9. Shimadzu GCMS-QP2010 Ultra.

syringes. One of the septums used was before the cold trap and the second one was after the cold trap. Septum before the cold trap was used for qualitative determination of methanol and water in the exit stream. Septum after the cold trap was used for quantitative determination of DME in the exit stream. For different carbon sources, syringes different in size were used and different analysis methods were applied since DME concentration at the exit of the reactor changed depending on the carbon source in the feed stream. Features of different analysis methods including used syringes were given in Tables 3.5 and 3.6, respectively for CO and CO_2. Quantitative DME analysis were conducted after vacuum of the system was established.

Table 3.5. Analysis Method of GCMS for CO as Carbon Source.

Parameters	
Syringe Type	Gas Tight Syringe
Syringe Size	10 μl
Carrier Gas	Helium
Flow Control Mode	Linear Velocity
Linear Velocity	99.6 cm sec^{-1}
Split Ratio	19
Column Flow	7.05 ml min^{-1}
Total Flow	141.0 ml min^{-1}
Column	Rt-Q-Bond
Column Diameter	0.53 mm
Column Thickness	20 μm
Column Length	30 m
Injection Temperature	150 ^{0}C
Oven Temperature	120 ^{0}C
Analysis Duration	1.5 min
Ion Source Temperature	220 ^{0}C
Interface Temperature	250 ^{0}C
Detector Voltage	Relative To Tuning -0.4 kV
Acquisition Mode	Scan
Event Time	0.2 sec
Start m/z	10
End m/z	100

Table 3.6. Analysis Method of GCMS for CO_2 as Carbon Source.

Parameters	
Syringe Type	Gas Tight Syringe
Syringe Size	100 μl
Carrier Gas	Helium
Flow Control Mode	Linear Velocity
Linear Velocity	99.6 cm sec^{-1}
Split Ratio	9
Column Flow	7.05 ml min^{-1}
Total Flow	70.5 ml min^{-1}
Column	Rt-Q-Bond
Column Diameter	0.53 mm
Column Thickness	20 μm
Column Length	30 m
Injection Temperature	150 ^{0}C
Oven Temperature	120 ^{0}C
Analysis Duration	1.5 min
Ion Source Temperature	220 ^{0}C
Interface Temperature	250 ^{0}C
Detector Voltage	Relative To Tuning -0.4 kV
Acquisition Mode	Scan
Event Time	0.2 sec
Start m/z	10
End m/z	100

3.5. Complete Procedure as Flowchart

Flowchart for the complete procedure applied to conduct an experiment can be found in Figure 3.10.

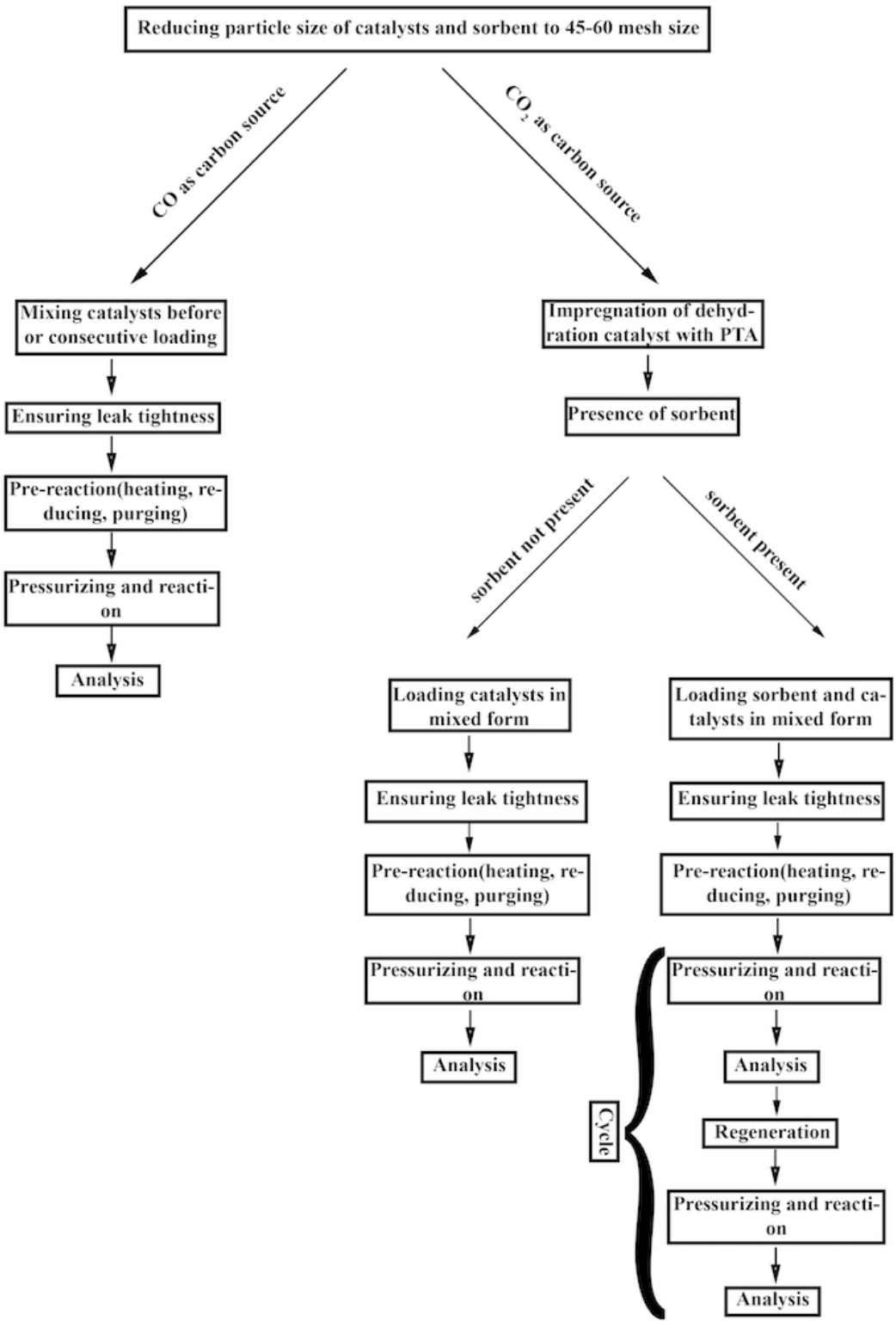

Figure 3.10. Flowchart Depending on Carbon Source and Presence of Sorbent.

3.6. Definitions

This section summarizes the definitions used throughout the study. Volumetric flow rate of each component in the inlet stream was found using compositions obtained with GC in the feed gas analysis and volumetric flow rate of the feed gas measured with soap bubble meter as follows:

$$Q_{in} \times x_{i,in} = Q_{i,in} \tag{3.1}$$

Volumetric flow rate of exit stream was calculated based on exit N_2 composition obtained with GC, inlet volumetric flow rate and inlet N_2 composition as follows:

$$\frac{Q_{in} \times x_{N_2,in}}{x_{N_2,out}} = Q_{out} \tag{3.2}$$

Volumetric flow rate of each component in the exit stream was found using compositions obtained with GC as follows:

$$Q_{out} \times x_{i,out} = Q_{i,out} \tag{3.3}$$

CO_x conversion was found comparing the exit CO_x volumetric flow rate with the CO_x inlet volumetric flow rate as follows [3, 40, 45]:

$$\frac{Q_{CO_x,in} - Q_{CO_x,out}}{Q_{CO_x,in}} \times 100 = X_{CO_x} \tag{3.4}$$

When H_2 to CO_x ratio was equal or above the stoichiometric ratio, valid for the experiments present, maximum DME volumetric flow rate in the exit stream can be calculated based on the number of carbon atoms present in the CO_x, 1, and DME, 2, molecules as follows:

$$\frac{Q_{CO_x,in}}{2} = Q_{DME,out,max} \tag{3.5}$$

Comparing DME exit volumetric flow rate with maximum achievable DME exit volumetric flow rate, DME yield can be calculated as follows [40, 45]:

$$\frac{Q_{DME,out}}{Q_{DME,out,max}} \times 100 = Y_{DME} \tag{3.6}$$

Maximum CO_2 volumetric flow rate and CO_2 yield were calculated using the same method for maximum DME volumetric flow rate and DME yield as follows [40, 45]:

$$\frac{Q_{CO_x,in}}{1} = Q_{CO_2,out,max} \tag{3.7}$$

$$\frac{Q_{CO_2,out}}{Q_{CO_2,out,max}} \times 100 = Y_{CO_2} \tag{3.8}$$

For calculation of GHSV, volume of 1 g CZA and feed gas volumetric flow rate, having unit ml h^{-1}, were used. Volume of 1 g CZA was obtained using height and diameter of 1 g CZA placed in the reactor. Feed gas volumetric flow rate, having unit ml h^{-1}, and GHSV were calculated as follows:

$$Q_{in} \times 60 = Q_{in,h^{-1}} \tag{3.9}$$

$$\frac{Q_{in,h^{-1}} \times \rho_{CZA,45\text{-}60}}{1} = GHSV_{CZA} \tag{3.10}$$

Sorption recovery percentage was calculated based on initial DME yield before sorbent was regenerated for the first time. DME yield obtained after each sorbent regeneration was compared with initial DME yield to obtain sorption recovery percentage as follows [56]:

$$\frac{Y_{DME,i}}{Y_{DME,1}} \times 100 = SR_i \tag{3.11}$$

4. RESULTS AND DISCUSSION

Results were divided into three section depending on the carbon source and sorption enhancement obtained when CO_2 was carbon source in the feed stream. Section 4.1 included the findings related with the effects of relative locations of the catalysts (i.e. catalyst configurations), reactor pressure and GHSV, when the carbon source in syngas was CO. These findings set path to the studies that involved the use of CO_2 as the carbon source in the feed whose results were presented in Section 4.2. Results of increasing H_2 ratio in the feed stream when CO_2 was carbon source in the feed stream were demonstrated in Section 4.2.1. More active dehydration catalyst requirement due to presence of water and lower concentration of methanol when CO_2 was the carbon source necessitated synthesizing more acidic dehydration catalysts and increasing their relative amounts in the packed bed. The related results were reported in Section 4.2.2. Effect of *in-situ* water removal with sorbent addition to the reactor on DME yield and CO_2 conversion were covered in Section 4.3.

Presence of exothermic reactions, except reverse water-gas shift reaction when carbon source in the feed is CO_2, sets a decreasing thermodynamic limit on the carbon source conversion and DME yield with increasing temperature. When CO_2 is carbon source in the feed stream, increasing temperature reduces equilibrium DME selectivity while equilibrium CO selectivity increases due to endothermic reverse water-gas shift reaction as seen in Figures 4.1 and 4.2. Reaction temperature was selected considering higher thermodynamic limit zone while satisfactory kinetics could also be obtained. Therefore 225 ^{0}C was used as the reaction temperature being independent of the section [3].

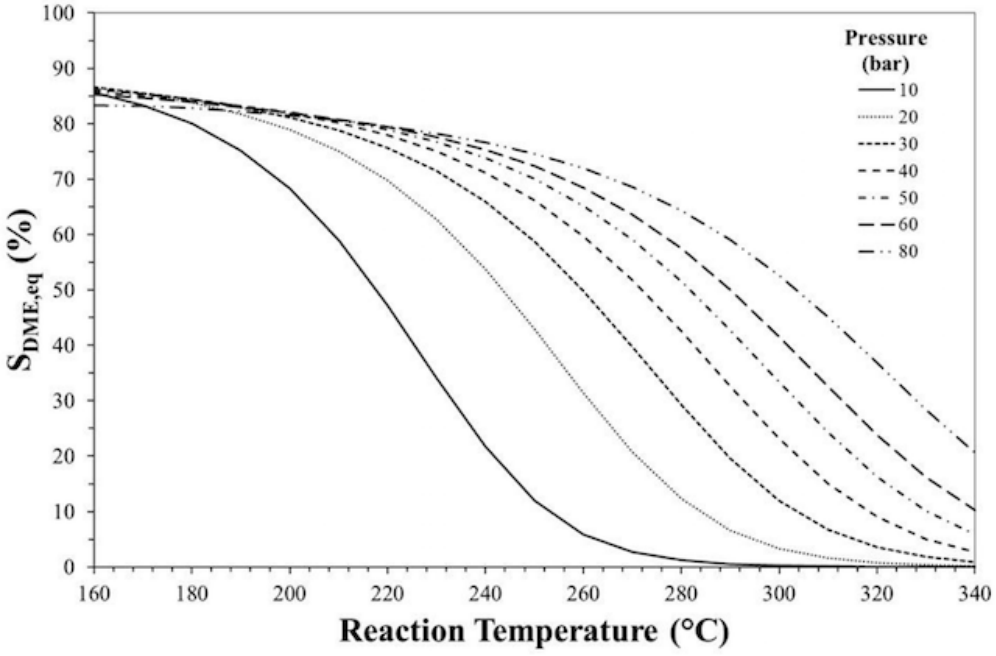

Figure 4.1. Effect of Temperature on DME Selectivity at Different Pressure Levels When H_2/CO_2 Ratio is 3 [3].

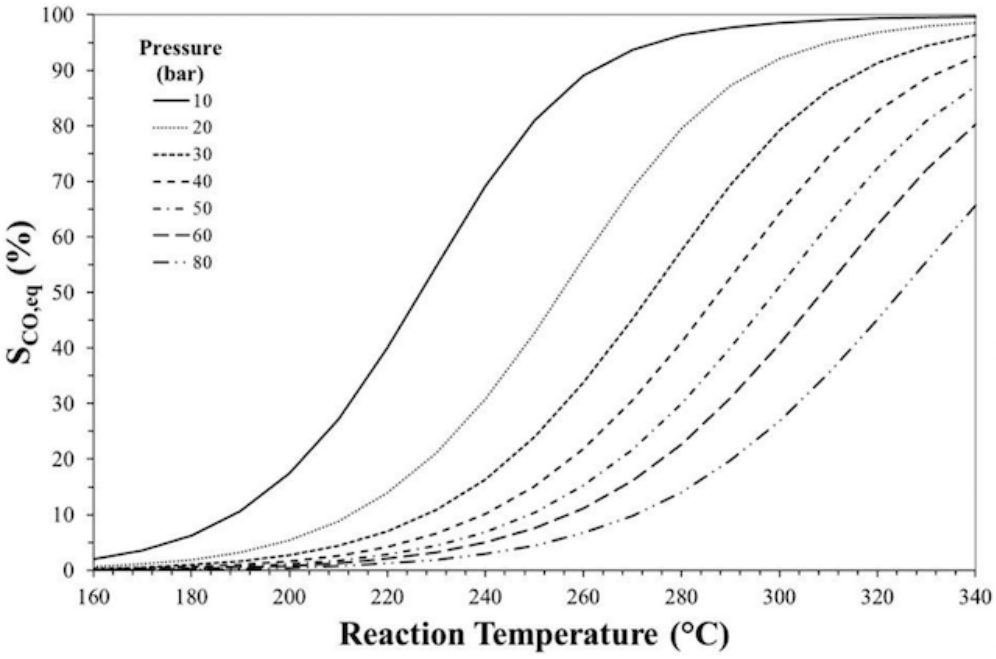

Figure 4.2. Effect of Temperature on CO Selectivity at Different Pressure Levels When H_2/CO_2 Ratio is 3 [3].

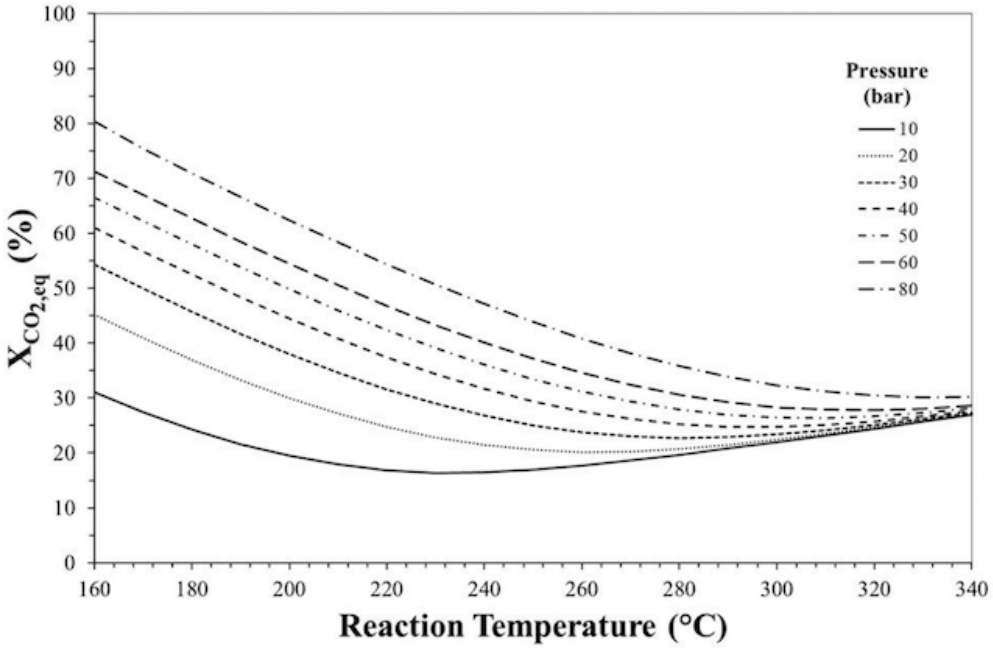

Figure 4.3. Effect of Temperature on CO_2 Conversion at Different Pressure Levels When H_2/CO_2 Ratio is 3 [3].

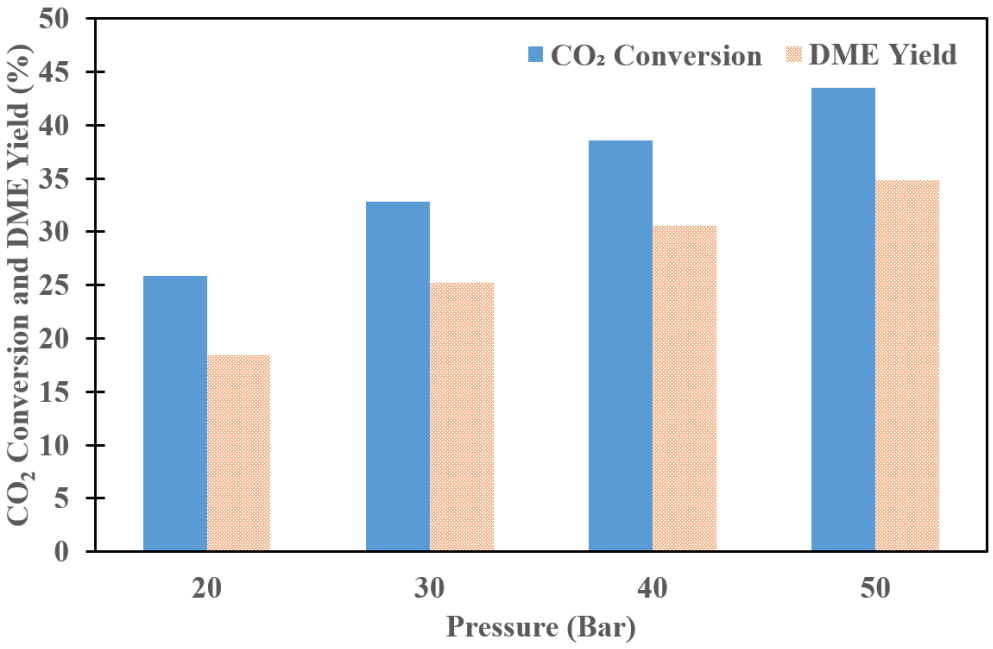

Figure 4.4. Effect of Pressure on Equilibrium CO_2 Conversion and DME Yield at 225 ^{0}C When H_2/CO_2 Ratio is 3.

For CO_2 as carbon source, increasing pressure from 30 bar to 50 bar produces an increase in CO_2 conversion and DME yield from $\sim$ 33 and $\sim$ 25, respectively, to $\sim$ 43 and $\sim$ 35 as shown in Figures 4.3 and 4.4 according to thermodynamic analysis conducted. Rate of CO_2 conversion and DME yield increase decreases with a small slope as pressure increases. Effect of sorbent addition was expected to be more pronounced than pressure increase above 30 bar. On the other hand when CO is carbon source, pressure increase does not produce desired CO conversion and DME yield increase above 30 bar because at $\sim$ 30 bar, as seen in Figure 4.6, obtained conversion value, which is $\sim$ 90% is already close to the thermodynamic value and complete conversion. Ruan *et al.* [39] at 50 bar obtained a similar conversion and yield value, 93% and 65.9%, respectively, as shown in Table 2.5.

Catizzone *et al.* [3] compared equilibrium CO_2 conversion values obtained for methanol synthesis and direct DME synthesis from CO_2 and H_2 for a temperature and pressure range as seen in Figure 4.5 and obtained a variable called CO_2 conversion gain. This variable, calculated using conversions obtained with both method, shows importance of one step DME synthesis from CO_2 and H_2 (i.e. higher the value better to use one step route). Maximum CO_2 conversion gain at each pressure level were gathered at lower temperatures until 60 bar.

4.1. CO as Carbon Source

In this section relative positions of methanol synthesis and methanol dehydration catalysts were investigated when CO was used as the carbon source. During this investigation, loading amount of methanol dehydration catalyst and methanol synthesis catalyst was 1 g for each. H_2 to CO ratio was 2, which is the stoichiometric ratio for methanol synthesis via CO hydrogenation. Higher H_2 to CO ratios reduced the exit volumetric flow rate of desired product because fed carbon amount was decreased while increase in CO conversion was not significant since near complete conversion was obtained for H_2 to CO ratio of 2. Another disadvantage of increasing the ratio is reduction of CO_2 selectivity, which means reduction of water removal from the system

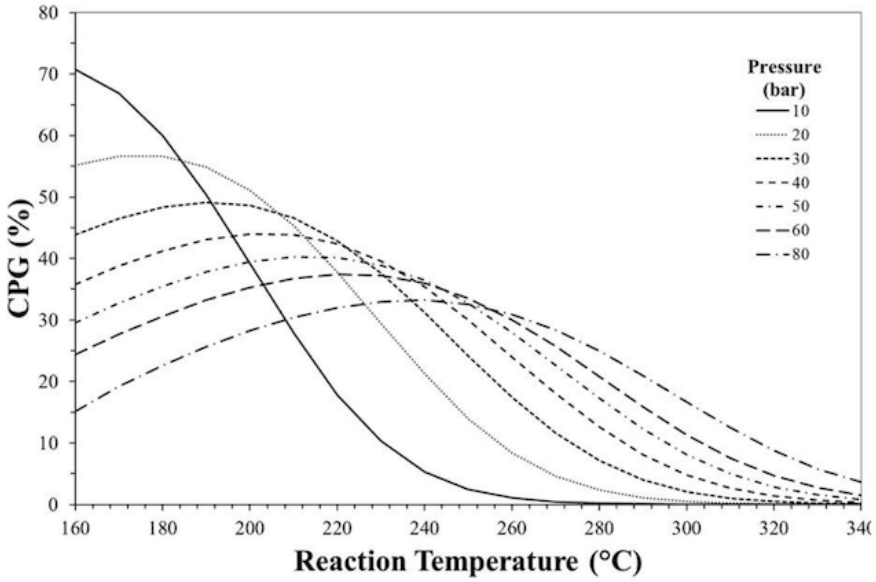

Figure 4.5. Effect of Temperature and Pressure on CO_2 Conversion Gain When H_2/CO_2 Ratio is 3 [3].

[4]. Default GHSV used for configuration and pressure tests was $\sim 1750\ h^{-1}$, calculated considering the volume of methanol synthesis catalyst, CZA, as shown in Section 3.10. Default pressure for the catalyst configuration and GHSV tests were set to 30 bar.

4.1.1. Catalyst Configurations

In this subsection, two different configurations for methanol synthesis and methanol dehydration catalysts, mixed and consecutive, were investigated according to CO conversion and DME yield obtained during experiments.

CO conversion and DME yield obtained on the mixed configuration were notably higher than those measured on the consecutive configuration (Figures 4.6 and 4.7). For consecutive loading of catalysts, DME yield was $\sim 0\%$ while for the mixed configuration DME yield was $\sim 50\%$. Advantage obtained in CO conversion and DME yield using mixed loading can be explained with simultaneous removal of water formed as result of methanol dehydration reaction, which drives equilibrium methanol dehydration reac-

tion forward, via water-gas shift reaction [24]. When carbon source in the feed stream is CO and catalysts are loaded consecutively, first methanol synthesis reaction takes place. However, water-gas shift reaction cannot occur because water is not present in the medium and is formed later during methanol dehydration. After certain amount of DME and water formation, dehydration reaction stops and as a result, water-gas shift reaction does not take place through out the reactor since methanol synthesis catalyst, on which water-gas shift reaction also takes place, is not present together with methanol dehydration catalyst. On the other hand, when mixed configuration was used, after first methanol molecule is formed and dehydrated to form DME, water-gas shift reaction, which leads to formation of CO_2, starts to take place simultaneously. In Figure 4.8, formation of CO_2 as a result of water-gas shift reaction can be seen. As a result, increase in CO conversion was both provided by water-gas shift reaction and DME formation. In this way using mixed configuration, via water-gas shift reaction, process intensification is achieved.

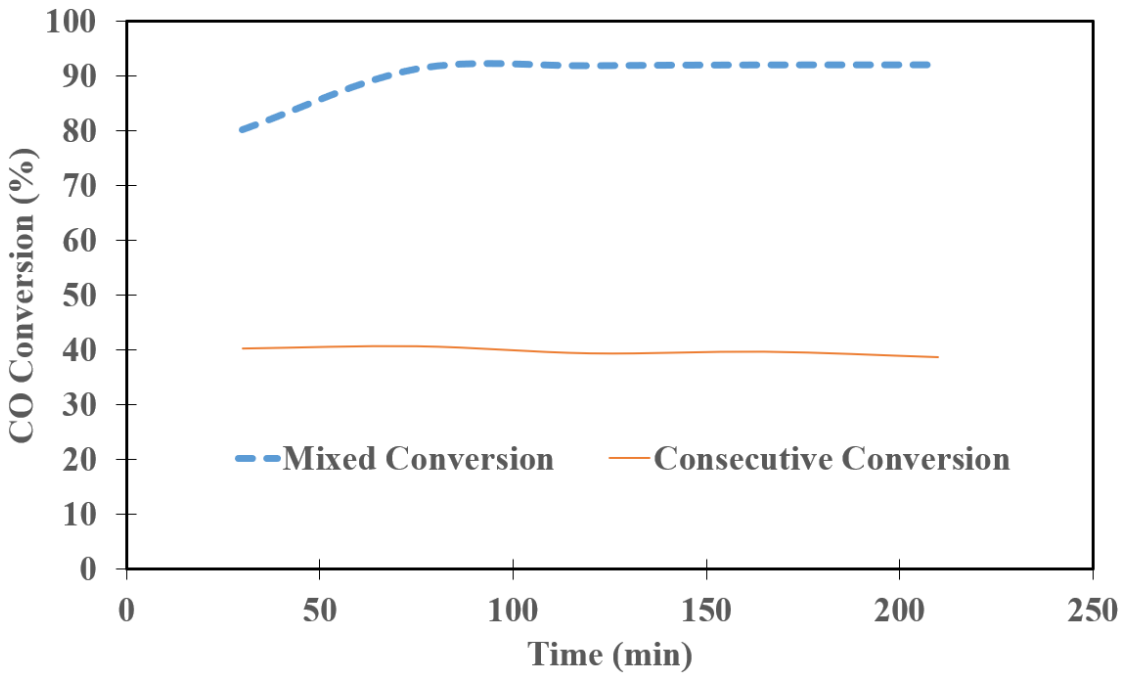

Figure 4.6. Effect of Catalyst Configuration on CO Conversion.

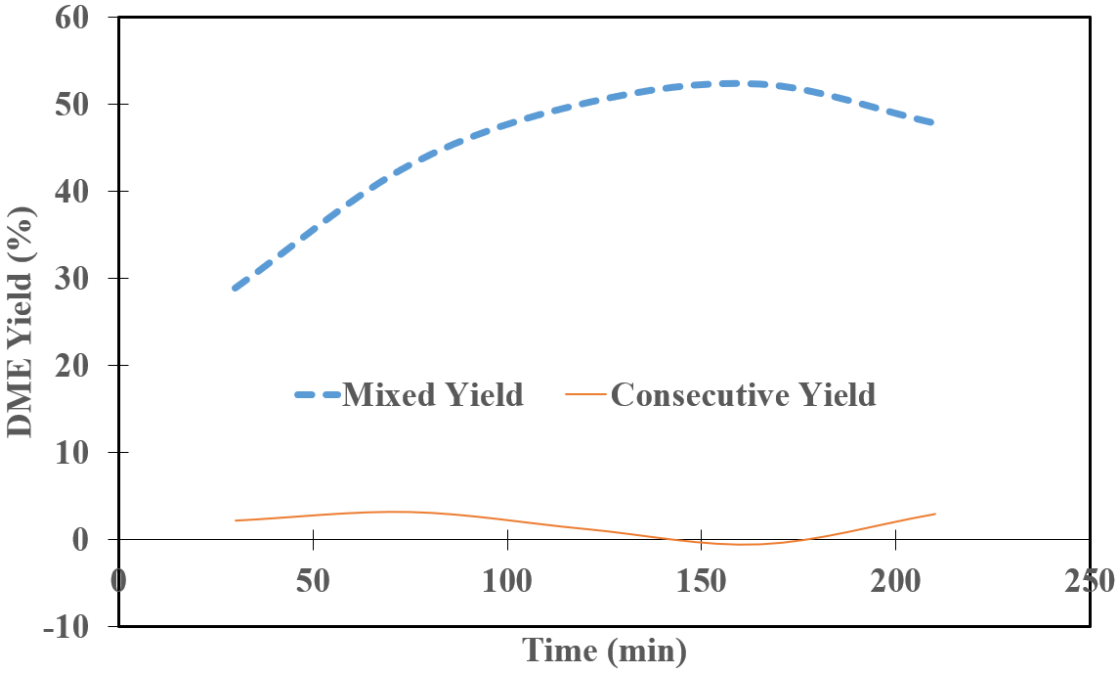

Figure 4.7. Effect of Catalyst Configuration on DME Yield.

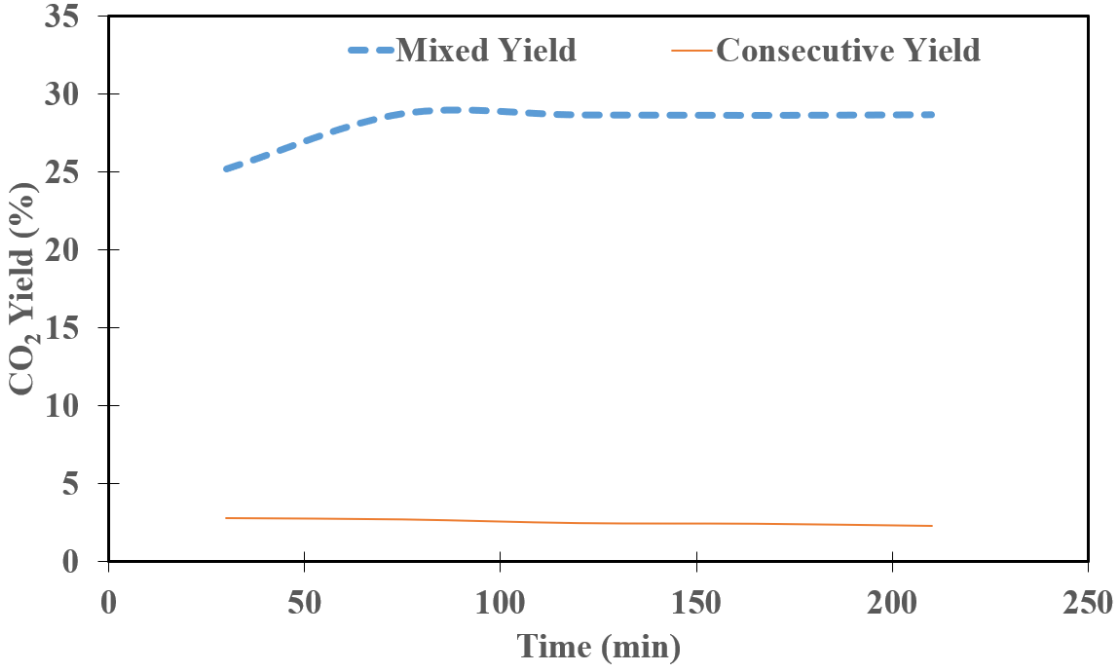

Figure 4.8. Effect of Catalyst Configuration on CO_2 Yield.

4.1.2. Reactor Pressure

According to Figure 4.9, increasing pressure was helpful to increase CO conversion and DME yield, obeying Le Chatelier's principle. The highest CO conversion and DME yield values were obtained at 30 bar pressure, the highest pressure used. The reason behind not to increase pressure above 30 bar is that CO conversion and DME yield increase above 30 bar is not significant when CO is carbon source because at $\sim$ 30 bar, as seen in Figure 4.6, obtained conversion value, which is $\sim$ 90% is already close to the thermodynamic value, presented in Table 2.4 and complete conversion. Moreover, Ruan *et al.* [39] at 50 bar obtained a similar conversion and yield value, 93% and 65.9%, respectively, as shown in Table 2.5. On the other hand, above 20 bar, decrease in significance of increasing pressure can be observed as shown in Figure 4.9. At higher GHSVs, significance of increasing pressure might be more apparent.

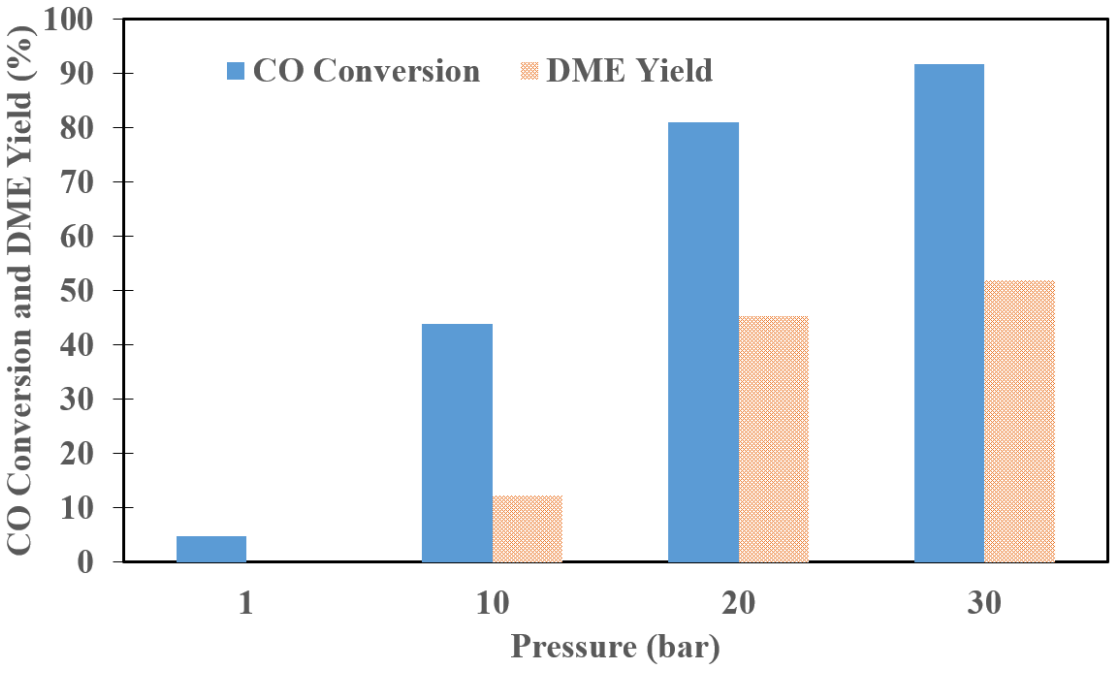

Figure 4.9. Effect of Pressure on CO Conversion and DME Yield.

4.1.3. Reactor GHSV

According to Figure 4.10, decreasing GHSV was helpful to increase CO conversion and DME yield. Above 2500 h^{-1}, $\sim$ 1.5 times the default GHSV, decrease in CO conversion and DME yield can be observed more clearly, which means there was a room to increase default GHSV. Above 8000 h^{-1}, decrease in CO conversion and DME yield became insignificant with increasing GHSV. As a conclusion, reactants can be assumed to like staying on the catalyst surface longer.

According to Figure 4.10 until 4800 h^{-1}, difference between CO conversion and DME yield remained the same. Considering that CO_2 was most of the side products, since difference was the same, water-gas shift reaction was not the limiting reaction. Methanol synthesis reaction should be limiting reaction since dehydration reaction stayed more active compared to water-gas shift reaction around 8000 h^{-1}.

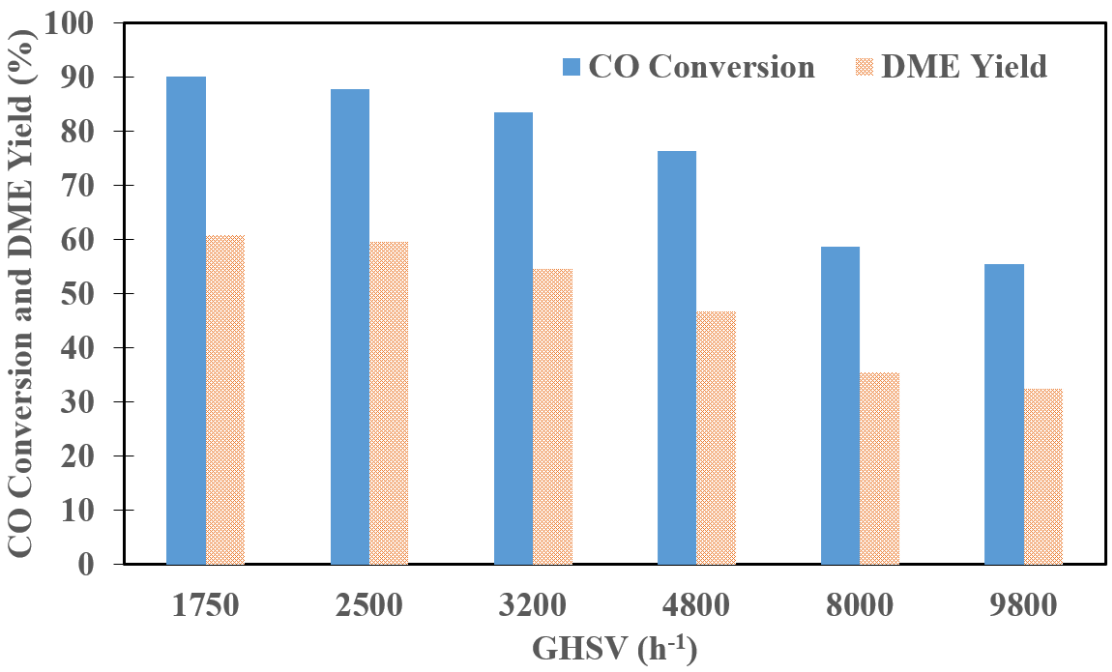

Figure 4.10. Effect of GHSV on CO Conversion and DME Yield.

4.2. CO_2 as Carbon Source

4.2.1. H_2/CO_2 Ratio in the Feed Stream

Increasing H_2 ratio in the feed stream as seen in Figure 4.11 caused CO_2 conversion to increase. Reason of this observed effect as a result of increased H_2 ratio in the feed stream was caused by moving forward of reverse water-gas shift and methanol synthesis reactions. On the other hand, impact of the increase in CO_2 conversion was not that significant since the inlet CO_2 molar flow rate decreased by increasing H_2/CO_2 ratio. Alternative to increasing the ratio, extent of CO_2 conversion can be increased by implementing an *in-situ* steam removal strategy. In this context, the use of a steam-selective adsorbent is investigated and the related findings are reported in Section 4.3.

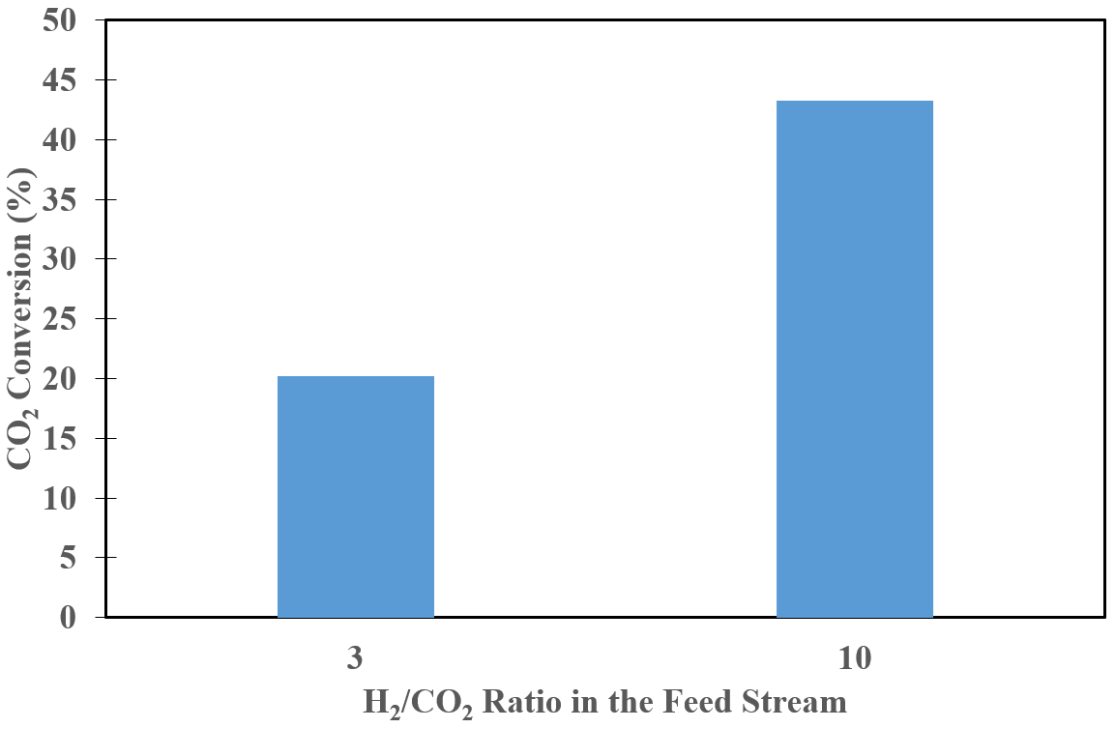

Figure 4.11. Effect of H_2/CO_2 Ratio on CO_2 Conversion.

4.2.2. Dehydration Catalysts and Dehydration Catalyst to CZA ratio

When carbon source is CO_2, water concentration inside the reactor increases due to reverse water-gas shift reaction and methanol concentration decreases due to lower thermodynamic limit of CO_2 hydrogenation, as shown in Table 2.4, compared to usage of CO as carbon source. These conditions enhances competitive adsorption of water onto the catalytically active Lewis acid sites of γ-Al_2O_3 when carbon source is CO_2. To form Brϕnsted acid sites, on which water has little effect, on γ-Al_2O_3 and to decrease number of Lewis acid sites, PTA impregnation is one of the options [31, 53]. Keggin structure of PTA leads to formation of stronger Brϕnsted acid sites; however, calcination above 450 ^{0}C transforms Keggin structure into moderate Brϕnsted acid sites, WO_3, which is more preferred since stronger Brϕnsted acid sites can lead to further (undesired) dehydration of DME [3, 31, 53, 57]. In fact, it was observed that addition of 20 wt.% of PTA to γ-Al_2O_3 increased DME yield from $\sim$ 4 to $\sim$ 9% as shown in Figure 4.12.

The effect of PTA loading on CO_2 conversion and DME yield is presented in Figure 4.13. For the following experiments, H_2/CO_2 ratio of 3, stoichiometric ratio for CO_2 hydrogenation, was used. Ratio of the mass of dehydration catalyst to that of the synthesis catalyst was set to 2. DME yield showed an increasing trend until 30 wt.% PTA loading above which the throughput of DME remained almost unchanged. Despite an increase in CO_2 conversion from $\sim$ 20 to $\sim$ 24% upon further PTA loading, 30 wt.% was selected as the optimum value based on the DME yield trend and was used in the rest of the experiments.

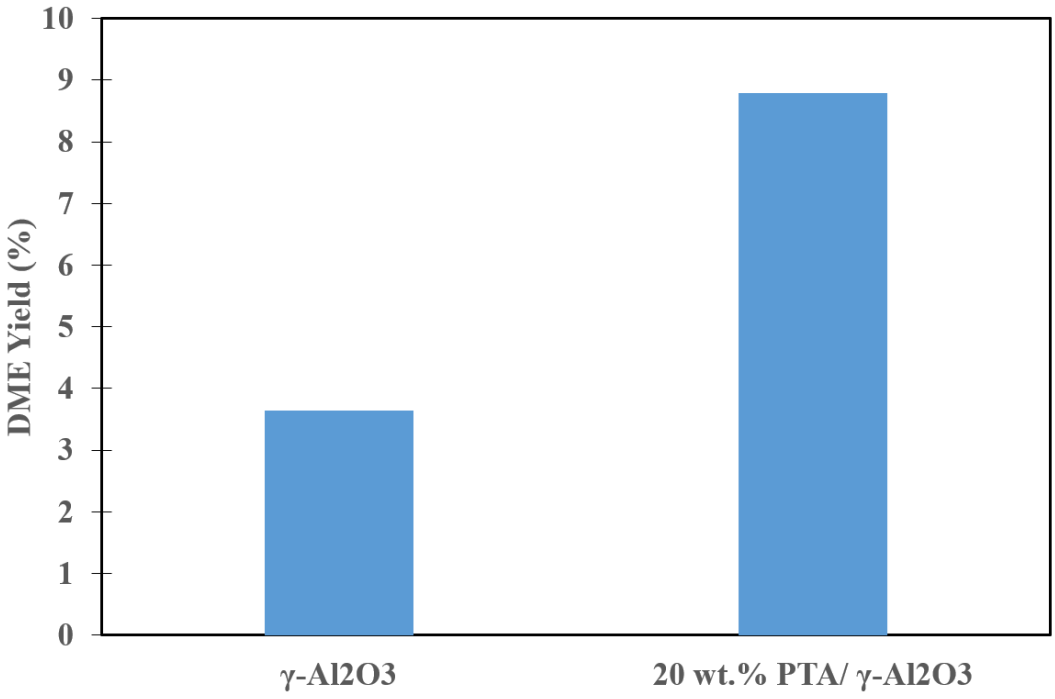

Figure 4.12. Effect of PTA Impregnation on DME Yield (H_2/CO_2 = 10, mass of dehydration catalyst = 0.75 g).

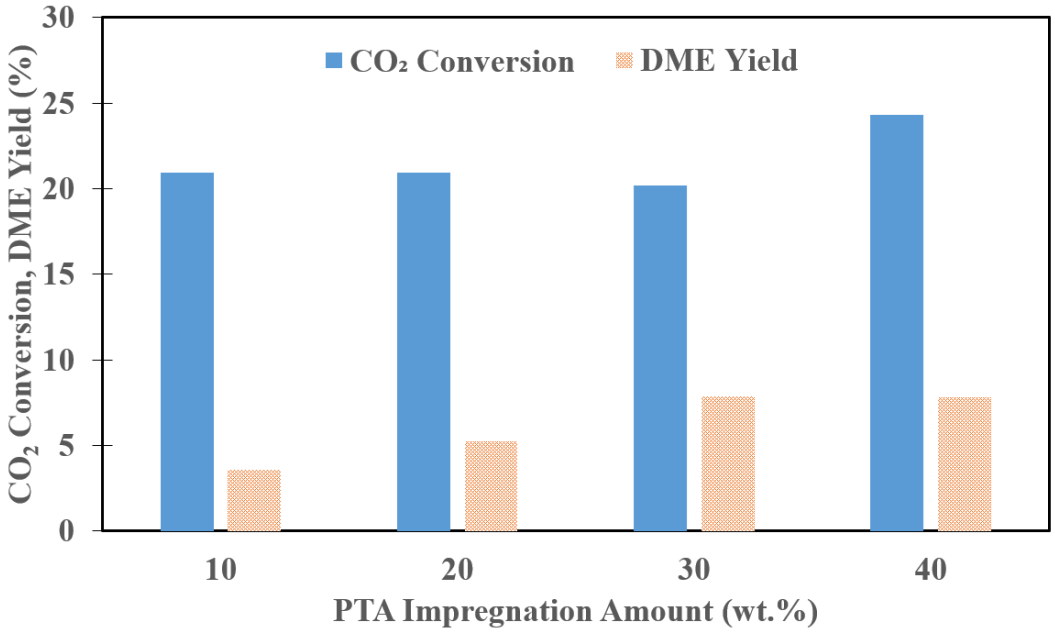

Figure 4.13. Effect of PTA Impregnation Amount on CO_2 Conversion and DME Yield.

The effect of the ratio of the mass of dehydration catalyst to that of synthesis catalyst was presented in Figure 4.14. Despite a small improvement in CO_2 conversion, DME yield remained unresponsive to the increased amount of 30 wt.% PTA/γ-Al_2O_3 in the packed-bed. This result shows that the 2 g of the dehydration catalyst provides sufficient number of acidic centers to dehydrate methanol to DME. Based on this finding, the mass ratio was fixed to 2 in the experiments involving the use of sorbent.

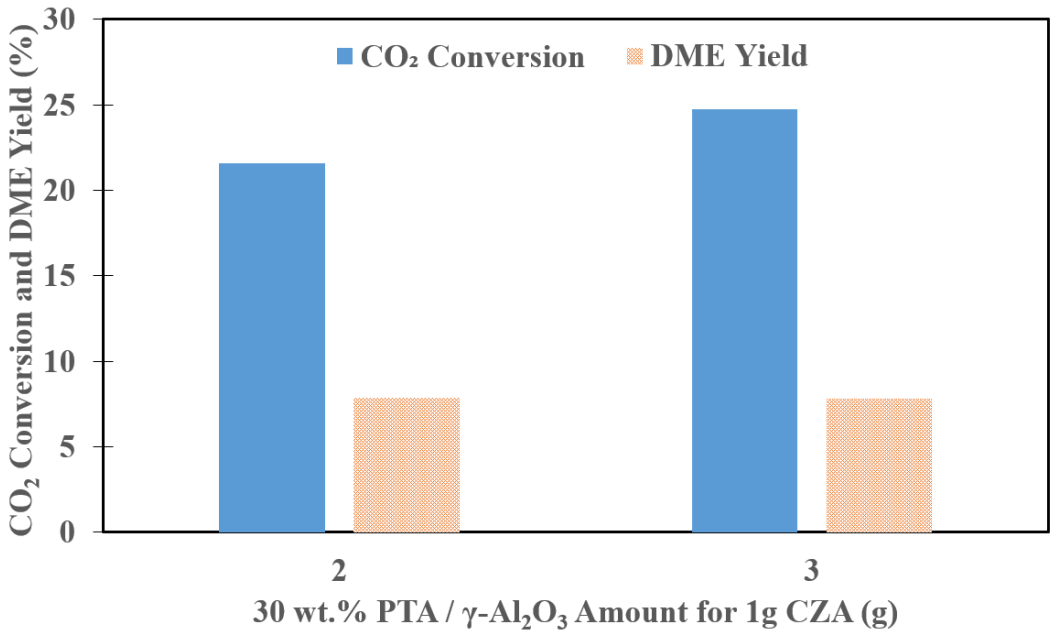

Figure 4.14. Effect of 30 wt.% PTA Impregnated γ-Al_2O_3 to CZA Ratio on CO_2 Conversion and DME Yield.

4.3. Sorption Enhanced DME production from CO_2

One of the methods available to promote forward reverse water-gas shift and methanol dehydration reactions was to add a steam selective solid sorbent to the packed-bed of catalysts. For this purpose, a commercial sorbent, Zeolite (or Molecular Sieve) 3A, was used. This material was selected due to its smaller pore diameter ($\sim$ 3Å) which accepts He, H_2O, NH_3 molecules having lower kinetic diameters [58]. This makes Zeolite 3A suitable for removal of steam preventing adsorption of larger molecules [15]. In order to determine effectiveness of sorbent addition, increase in CO_2

conversion and DME yield was monitored depending on the added sorbent amount and on time. Performance of the sorbent upon regeneration was also monitored.

Figure 4.15 gives the CO_2 conversion level measured in the presence and absence of the sorbent along with the pertinent thermodynamic value calculated via Gibbs Free Energy minimization technique (see Section 2.2.2.1). The results also include the responses obtained as a function of the mass of the sorbent packed with the catalysts. It is worth noting that the catalysts and sorbent were mixed uniformly. It was observed that 3 g sorbent addition showed the best performance in terms of showing highest CO_2 conversion prior to regeneration was required. CO_2 conversion levels were above the thermodynamic value for a certain amount of time depending on the sorbent amount. Compared to the case without sorbent, duration above the thermodynamic value increased with sorbent addition significantly. CO_2 conversions measured upon saturation of the sorbent were just below the pertinent thermodynamic limit. Moreover, the "saturation" CO_2 conversion obtained in the absence of the sorbent was below those of the sorption-enhanced cases. Other than constant benefit of sorbent addition, this deviation could be accepted as an error, since the impact of sorbent is expected to fade out upon its saturation. Deviation in the measured N_2 exit concentration used in the calculation of exit CO_2 molar flow rate of the system could be a potential root cause, since CO_2 concentrations of exit streams were close to each other.

In Figure 4.16, DME yield for each added sorbent amount were presented along with the theoretical predictions and the benchmark case that does not involve sorbent. It was observed that 3 g sorbent addition showed the best performance in terms of reaching the highest DME yield and showing the higher DME yield for longer time before regeneration was required. Being different than the findings in Figure 4.15, peak formation was not observed initially. Observing the peak in Figure 4.16 later than in Figure 4.15 should be related with the relative rates of reverse water-gas shift, methanol synthesis and dehydration reactions. Early consumption of CO_2 points out that reverse water-gas shift is faster than DME production. Peak formation in DME yield was not observed in the absence of the sorbent. For 3 g sorbent addition, reaching the

saturation value of DME yield took more than 160 min. Except 3 g sorbent addition, all of them reached the same saturation DME yield value before 160 min. The results also show that even 3 g of sorbent addition was not enough to reach thermodynamic DME yield value. In this respect, more sorbent addition seems necessary to overcome the theoretical DME yield. Formed water as a result of methanol dehydration might lead to formation of CO_2 if water sorption is not enough. This is not desired because of decreased CO_2 conversion. For higher DME yield and CO conversion to DME instead of CO_2, closer relative rates of reactions might be more beneficial. For Figures 4.17 and 4.18, maximum tested amount of sorbent, 3 g, was used.

In Figure 4.17, maximum DME yield values obtained in each cycle was shown. Decrease in the maximum DME yield was observed after each regeneration and it turned out to be slightly higher after twice regeneration. In Figure 4.18, regeneration capability of sorbent was shown in a more understandable way taking maximum DME yield obtained after each regeneration and comparing that with maximum DME yield obtained when sorbent was fresh. Regeneration capability of a once regenerated sorbent, above 99%, was higher compared to regeneration capability of a twice regenerated sorbent.

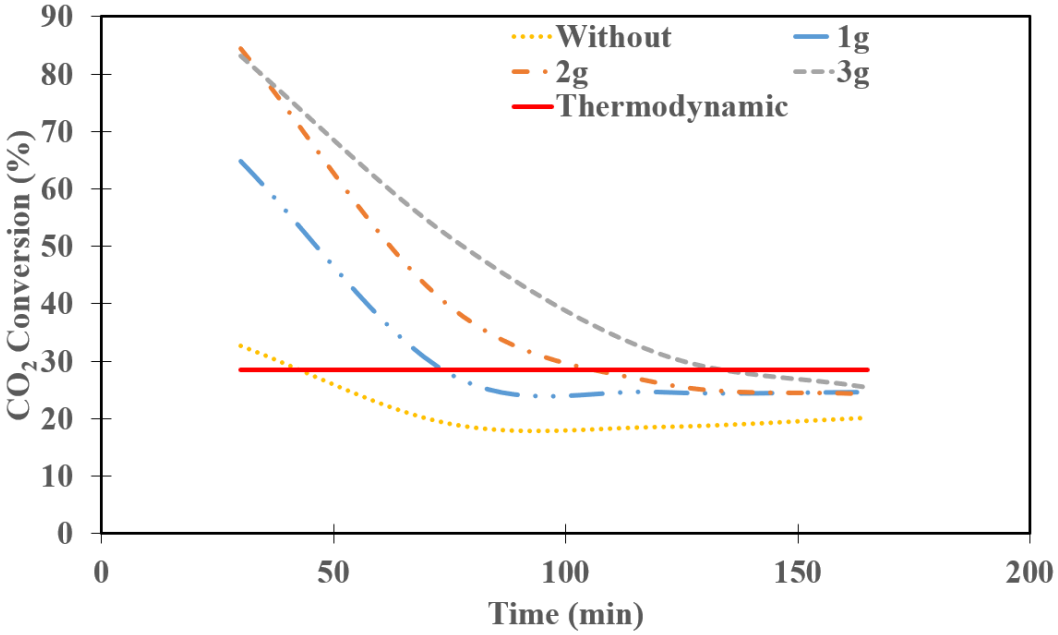

Figure 4.15. Effect of Sorbent Amount on CO_2 Conversion.

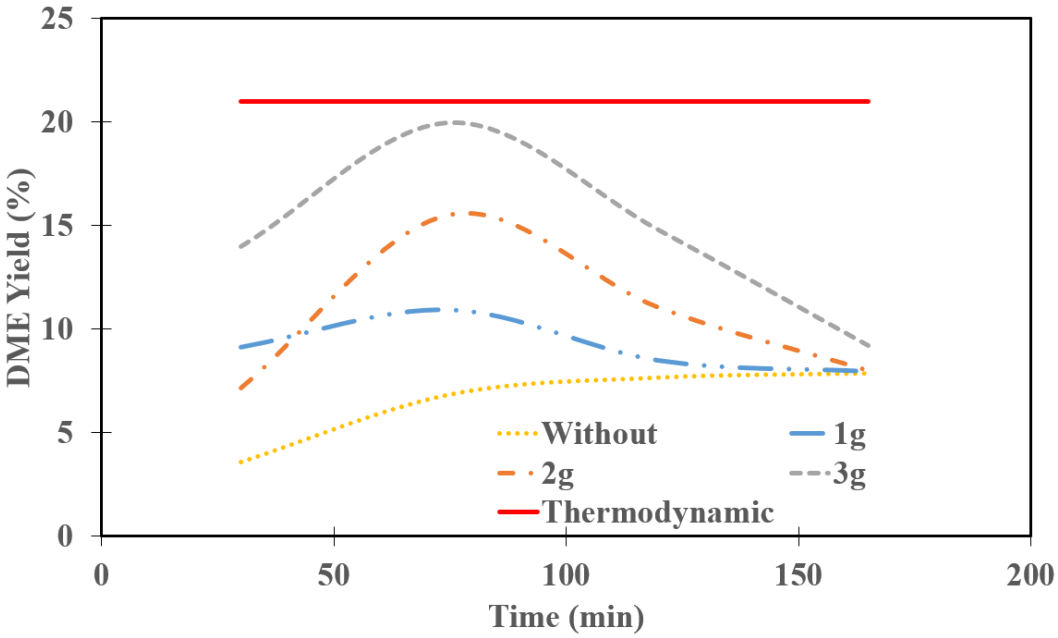

Figure 4.16. Effect of Sorbent Amount on DME Yield.

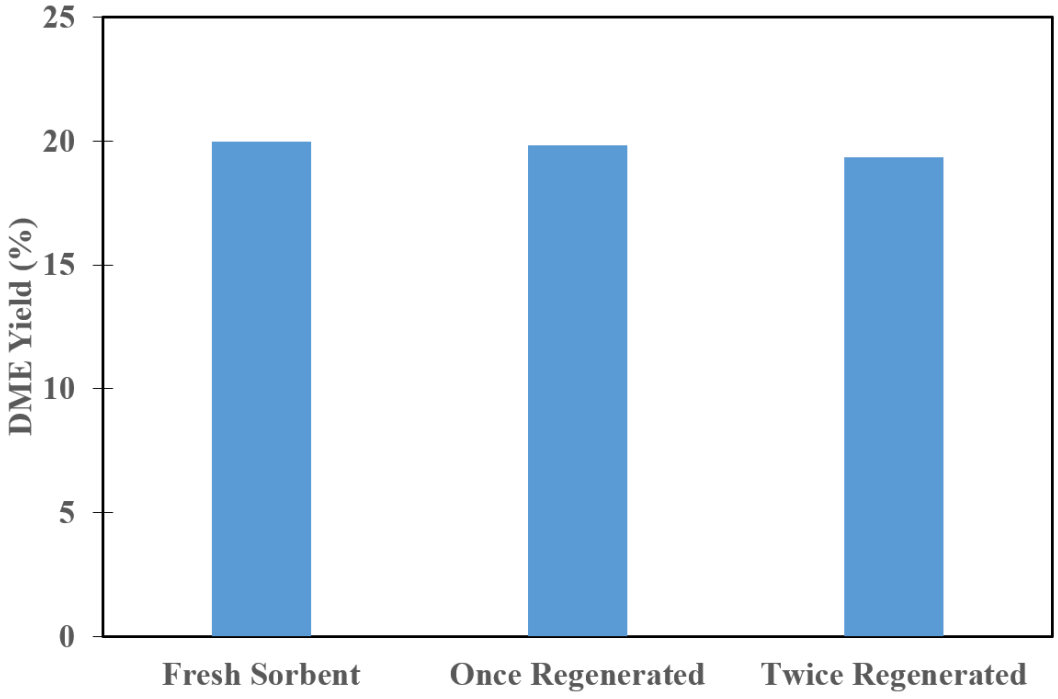

Figure 4.17. Regenerated Sorbent-DME Yield Relation for 3 g Sorbent Addition.

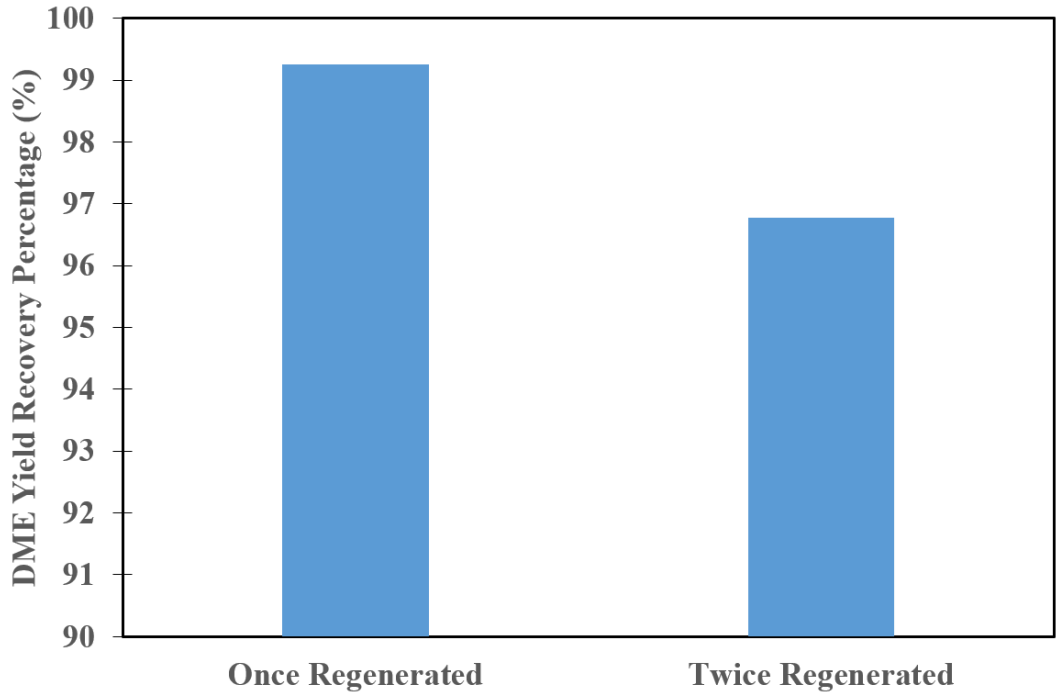

Figure 4.18. Sorption Recovery Percentage-Regeneration Times Relation for 3 g Sorbent Addition.

5. CONCLUSION

The aim of the study was to carry out a parametric investigation of CO and CO_2 hydrogenation, with more emphasis on the latter, and to elucidate the impacts of sorption enhancement on CO_2-to-DME conversion. Conclusions obtained to reach aim of this study was mentioned in three sections covering different steps of the study. For further improvements, recommendations section was included after conclusions sections.

5.1. Conclusions from CO as Carbon Source

- For mixed configuration of the methanol synthesis and dehydration catalysts, obtained CO conversion and DME yield values were higher compared to consecutive configuration. This advantage was provided by water-gas shift reaction that took place simultaneously with other reactions. With mixed configuration, near equilibrium values for CO conversion and DME yield were obtained.
- With increasing pressure, CO conversion and DME yield were increased. Highest values for CO conversion and DME yield were obtained at 30 bar, which was the highest pressure tested. Rate of increase in CO conversion and DME yield decreased with increasing pressure.
- Decreasing GHSV was helpful to increase CO conversion and DME yield. With increasing GHSV, rate of decrease in CO conversion and DME yield became more notable. GHSV of 2500 h^{-1} could be taken as threshold value for increasing rate of decrease in CO conversion and DME yield.

5.2. Conclusions from CO_2 as Carbon Source

- Increasing H_2/CO_2 ratio was helpful to increase CO_2 conversion. However, this benefit was masked by reduced percentage of DME in the exit stream.
- DME yield increased significantly upon PTA addition to γ-Al_2O_3.

- DME yield showed increasing trend until 30 wt.% PTA loading whose further increase did not improve DME yield.
- Increasing 30 wt.% PTA impregnated methanol dehydration catalyst to methanol synthesis catalyst mass ratio above 2 did not improve DME yield.

5.3. Conclusions from Sorbent Addition to The Reactor

- Addition of 3 g sorbent inside the reactor was more helpful than 1 and 2 g sorbent addition to sustain CO_2 conversions above the pertinent equilibrium value.
- Addition of 3 g sorbent inside the reactor was more helpful than 1 and 2 g sorbent addition to reach higher maximum DME yield value.
- Peak for CO_2 conversion level was observed before peak for DME yield level due to higher relative rate of reverse water-gas shift reaction compared to other reactions.
- Once regenerated sorbent retained sorption capacity more than twice regenerated sorbent and decrease in sorption capacity was more significant in second regeneration.
- With sorbent addition maximum CO_2 conversion values were higher than the pertinent thermodynamic equilibrium value while maximum DME yield value for 3 g sorbent addition was close to the pertinent thermodynamic equilibrium value.

5.4. Recommendations

- Even though results obtained with 30 wt.% PTA impregnated γ-Al_2O_3 as dehydration catalyst were good, dehydration catalyst having more density, occupying less volume inside the reactor and requiring less methanol dehydration to synthesis catalyst weight ratio could be investigated.
- Sorbent addition to the reactor was effective for water removal which increased CO_2 conversion and DME yield; however, regeneration of sorbent more than two times could be investigated to address cyclic stability of the sorbent.
- In order to increase DME yield value above the pertinent thermodynamic value,

increasing sorbent amount more than 3 g should be investigated.

- In order to observe durability of the catalysts, a time-on-stream experiment lasting for a longer time than the experiments included should be conducted.

REFERENCES

1. Semelsberger, T. A., R. L. Borup and H. L. Greene, "Dimethyl ether (DME) as an alternative fuel", *Journal of Power Sources*, Vol. 156, No. 2, p. 497–511, 2006.

2. Saravanan, K., H. Ham, N. Tsubaki and J. W. Bae, "Recent progress for direct synthesis of dimethyl ether from syngas on the heterogeneous bifunctional hybrid catalysts", *Applied Catalysis B: Environmental*, Vol. 217, p. 494–522, 2017.

3. Catizzone, E., G. Bonura, M. Migliori, F. Frusteri and G. Giordano, "CO_2 Recycling to Dimethyl Ether: State-of-the-Art and Perspectives", *Molecules*, Vol. 23, No. 1, p. 31, 2017.

4. Azizi, Z., M. Rezaeimanesh, T. Tohidian and M. R. Rahimpour, "Dimethyl ether: A review of technologies and production challenges", *Chemical Engineering and Processing: Process Intensification*, Vol. 82, p. 150–172, 2014.

5. Park, S. H. and C. S. Lee, "Combustion performance and emission reduction characteristics of automotive DME engine system", *Progress in Energy and Combustion Science*, Vol. 39, No. 1, p. 147–168, 2013.

6. Singh, A. P., R. A. Agarwal, A. K. Agarwal, A. Dhar and M. K. Shukla, *Prospects of alternative transportation fuels*, SPRINGER, 2018.

7. Curran, H. J., E. M. Fisher, P. A. Glaude, N. M. Marinov, W. J. Pitz, C. K. Westbrook, D. W. Layton, P. F. Flynn, R. P. Durrett, A. O. Z. Loye and et al., "Detailed Chemical Kinetic Modeling of Diesel Combustion with Oxygenated Fuels", *SAE Technical Paper Series*, 2001.

8. Song, R., K. Li, Y. Feng and S. Liu, "Performance and Emission Characteristics of DME Engine with High Ratio of EGR", *Energy and Fuels*, Vol. 23, No. 11, p. 5460–5466, 2009.

9. Ramadhas, A. S., *Alternative fuels for transportation*, CRC Press, 2011.

10. Sorenson, S. C., "Dimethyl Ether in Diesel Engines: Progress and Perspectives", *Journal of Engineering for Gas Turbines and Power*, Vol. 123, No. 3, p. 652–658, 2000.

11. Tsuchiya, T. and Y. Sato, "Development of DME Engine for Heavy-duty Truck", *SAE Technical Paper Series*, 2006.

12. Bonura, G., C. Cannilla, L. Frusteri, A. Mezzapica and F. Frusteri, "DME production by CO_2 hydrogenation: Key factors affecting the behaviour of CuZnZr/ferrierite catalysts", *Catalysis Today*, Vol. 281, p. 337–344, 2017.

13. Mondal, U. and G. D. Yadav, "Perspective of dimethyl ether as fuel: Part I. Catalysis", *Journal of CO_2 Utilization*, Vol. 32, p. 299–320, 2019.

14. Jia, C., J. Gao, Y. Dai, J. Zhang and Y. Yang, "The thermodynamics analysis and experimental validation for complicated systems in CO_2 hydrogenation process", *Journal of Energy Chemistry*, Vol. 25, No. 6, p. 1027–1037, 2016.

15. Kampen, J. V., J. Boon, F. V. Berkel, J. Vente and M. V. S. Annaland, "Steam separation enhanced reactions: Review and outlook", *Chemical Engineering Journal*, Vol. 374, p. 1286–1303, 2019.

16. Stiefel, M., R. Ahmad, U. Arnold and M. Doring, "Direct synthesis of dimethyl ether from carbon monoxide rich synthesis gas: Influence of dehydration catalysts and operating conditions", *Fuel Processing Technology*, Vol. 92, No. 8, p. 1466–1474, 2011.

17. Hu, Y., Y. Zhang, J. Du, C. Li, K. Wang, L. Liu, X. Yu, K. Wang and N. Liu, "The influence of composition on the functionality of hybrid CuO–ZnO–Al_2O_3/HZSM-5 for the synthesis of DME from CO_2 hydrogenation", *RSC Advances*, Vol. 8, No. 53, p. 30387–30395, 2018.

18. Ham, H., S. W. Baek, C.-H. Shin and J. W. Bae, "Roles of Structural Promoters for Direct CO_2 Hydrogenation to Dimethyl Ether over Ordered Mesoporous Bifunctional Cu/M–Al_2O_3 (M = Ga or Zn)", *ACS Catalysis*, Vol. 9, No. 1, p. 679–690, 2018.

19. Bahruji, H., R. D. Armstrong, J. R. Esquius, W. Jones, M. Bowker and G. J. Hutchings, "Hydrogenation of CO_2 to Dimethyl Ether over Brønsted Acidic PdZn Catalysts", *Industrial and Engineering Chemistry Research*, Vol. 57, No. 20, p. 6821–6829, 2018.

20. Witoon, T., P. Kidkhunthod, M. Chareonpanich and J. Limtrakul, "Direct synthesis of dimethyl ether from CO_2 and H_2 over novel bifunctional catalysts containing CuO-ZnO-ZrO_2 catalyst admixed with WO_x/ZrO_2 catalysts", *Chemical Engineering Journal*, Vol. 348, p. 713–722, 2018.

21. Marcos, F. C., J. M. Assaf and E. M. Assaf, "CuFe and CuCo supported on pillared clay as catalysts for CO_2 hydrogenation into value-added products in one-step", *Molecular Catalysis*, Vol. 458, p. 297–306, 2018.

22. Catizzone, E., G. Bonura, M. Migliori, G. Braccio, F. Frusteri and G. Giordano, "Direct CO_2-to-dimethyl Ether Hydrogenation over CuZnZr/zeolite Hybrid Catalyst: New Evidences on the Interaction Between Acid and Metal Sites", *Annales de Chimie - Science des Matériaux*, Vol. 43, No. 3, p. 141–149, 2019.

23. Sánchez-Contador, M., A. Ateka, P. Rodriguez-Vega, J. Bilbao and A. T. Aguayo, "Optimization of the Zr Content in the CuO-ZnO-ZrO_2/SAPO-11 Catalyst for the Selective Hydrogenation of CO+CO_2 Mixtures in the Direct Synthesis of Dimethyl Ether", *Industrial and Engineering Chemistry Research*, Vol. 57, No. 4, p. 1169–1178, 2018.

24. Ahmad, R., D. Schrempp, S. Behrens, J. Sauer, M. Döring and U. Arnold, "Zeolite-based bifunctional catalysts for the single step synthesis of dimethyl ether from

CO-rich synthesis gas", *Fuel Processing Technology*, Vol. 121, p. 38–46, 2014.

25. Arena, F., K. Barbera, G. Italiano, G. Bonura, L. Spadaro and F. Frusteri, "Synthesis, characterization and activity pattern of Cu–ZnO/ZrO_2 catalysts in the hydrogenation of carbon dioxide to methanol", *Journal of Catalysis*, Vol. 249, No. 2, p. 185–194, 2007.

26. Martin, O., A. J. Martín, C. Mondelli, S. Mitchell, T. F. Segawa, R. Hauert, C. Drouilly, D. Curulla-Ferré and J. Pérez-Ramírez, "Indium Oxide as a Superior Catalyst for Methanol Synthesis by CO_2 Hydrogenation", *Angewandte Chemie International Edition*, Vol. 55, No. 21, p. 6261–6265, 2016.

27. Jingfa, D., S. Qi, Z. Yulong, C. Songying and W. Dong, "A novel process for preparation of a Cu/ZnO/Al_2O_3 ultrafine catalyst for methanol synthesis from CO_2+H_2: comparison of various preparation methods", *Applied Catalysis A: General*, Vol. 139, No. 1-2, p. 75–85, 1996.

28. Ning, W., H. Shen and H. Liu, "Study of the effect of preparation method on CuO-ZnO-Al_2O_3 catalyst", *Applied Catalysis A: General*, Vol. 211, No. 2, p. 153–157, 2001.

29. Liu, J., J. Shi, D. He, Q. Zhang, X. Wu, Y. Liang and Q. Zhu, "Surface active structure of ultra-fine Cu/ZrO_2 catalysts used for the CO_2+H_2 to methanol reaction", *Applied Catalysis A: General*, Vol. 218, No. 1-2, p. 113–119, 2001.

30. Liao, F., X.-P. Wu, J. Zheng, M. M.-J. Li, A. Kroner, Z. Zeng, X. Hong, Y. Yuan, X.-Q. Gong, S. C. E. Tsang and et al., "A promising low pressure methanol synthesis route from CO_2 hydrogenation over Pd@Zn core–shell catalysts", *Green Chemistry*, Vol. 19, No. 1, p. 270–280, 2017.

31. Xu, M., J. H. Lunsford, D. Goodman and A. Bhattacharyya, "Synthesis of dimethyl ether (DME) from methanol over solid-acid catalysts", *Applied Catalysis A: Gen-*

eral, Vol. 149, No. 2, p. 289–301, 1997.

32. Fu, Y., T. Hong, J. Chen, A. Auroux and J. Shen, "Surface acidity and the dehydration of methanol to dimethyl ether", *Thermochimica Acta*, Vol. 434, No. 1-2, p. 22–26, 2005.

33. Jiang, S., J.-S. Hwang, T. Jin, W. Cho, Y. s. Baek and S.-E. Park, "Dehydration of Methanol to Dimethyl Ether over ZSM-5 Zeolite", *Bulletin of the Korean Chemical Society*, Vol. 25, No. 2, p. 185–189, 2004.

34. Catizzone, E., M. Migliori, A. Purita and G. Giordano, "Ferrierite vs. γ-Al_2O_3: The superiority of zeolites in terms of water-resistance in vapour-phase dehydration of methanol to dimethyl ether", *Journal of Energy Chemistry*, Vol. 30, p. 162–169, 2019.

35. Ladera, R., E. Finocchio, S. Rojas, J. Fierro and M. Ojeda, "Supported niobium catalysts for methanol dehydration to dimethyl ether: FTIR studies of acid properties", *Catalysis Today*, Vol. 192, No. 1, p. 136–143, 2012.

36. Masih, D., S. Rohani, J. N. Kondo and T. Tatsumi, "Low-temperature methanol dehydration to dimethyl ether over various small-pore zeolites", *Applied Catalysis B: Environmental*, Vol. 217, p. 247–255, 2017.

37. Chen, Z., X. Li, Y. Xu, Y. Dong, W. Lai, W. Fang and X. Yi, "Fabrication of nano-sized SAPO-11 crystals with enhanced dehydration of methanol to dimethyl ether", *Catalysis Communications*, Vol. 103, p. 1–4, 2018.

38. Sang, Y., H. Li, M. Zhu, K. Ma, Q. Jiao and Q. Wu, "Catalytic performance of metal ion doped MCM-41 for methanol dehydration to dimethyl ether", *Journal of Porous Materials*, Vol. 20, No. 6, p. 1509–1518, 2013.

39. Xie, Q., P. Chen, P. Peng, S. Liu, P. Peng, B. Zhang, Y. Cheng, Y. Wan, Y. Liu, R. Ruan and et al., "Single-step synthesis of DME from syngas on CuZnAl–zeolite

bifunctional catalysts: the influence of zeolite type", *RSC Advances*, Vol. 5, No. 33, p. 26301–26307, 2015.

40. Abu-Dahrieh, J., D. Rooney, A. Goguet and Y. Saih, "Activity and deactivation studies for direct dimethyl ether synthesis using CuO–ZnO–Al_2O_3 with NH_4ZSM-5, HZSM-5 or γ-Al_2O_3", *Chemical Engineering Journal*, Vol. 203, p. 201–211, 2012.

41. Ge, Q., Y. Huang, F. Qiu and S. Li, "Bifunctional catalysts for conversion of synthesis gas to dimethyl ether", *Applied Catalysis A: General*, Vol. 167, No. 1, p. 23–30, 1998.

42. Frusteri, F., G. Bonura, C. Cannilla, G. D. Ferrante, A. Aloise, E. Catizzone, M. Migliori and G. Giordano, "Stepwise tuning of metal-oxide and acid sites of CuZnZr-MFI hybrid catalysts for the direct DME synthesis by CO_2 hydrogenation", *Applied Catalysis B: Environmental*, Vol. 176-177, p. 522–531, 2015.

43. Jeong, C., J. Kim, J.-H. Kim, S. Lee, J. W. Bae and Y.-W. Suh, "Direct Conversion of CO_2 into Dimethyl Ether over Al_2O_3/Cu/ZnO Catalysts Prepared by Sequential Precipitation", *Catalysts*, Vol. 9, No. 6, p. 524, 2019.

44. Bonura, G., M. Cordaro, C. Cannilla, A. Mezzapica, L. Spadaro, F. Arena and F. Frusteri, "Catalytic behaviour of a bifunctional system for the one step synthesis of DME by CO_2 hydrogenation", *Catalysis Today*, Vol. 228, p. 51–57, 2014.

45. Ren, S., W. R. Shoemaker, X. Wang, Z. Shang, N. Klinghoffer, S. Li, M. Yu, X. He, T. A. White, X. Liang and et al., "Highly active and selective Cu-ZnO based catalyst for methanol and dimethyl ether synthesis via CO_2 hydrogenation", *Fuel*, Vol. 239, p. 1125–1133, 2019.

46. Atakan, A., J. Keraudy, P. Mäkie, C. Hulteberg, E. M. Björk and M. Odén, "Impact of the morphological and chemical properties of copper-zirconium-SBA-15 catalysts on the conversion and selectivity in carbon dioxide hydrogenation", *Journal of*

Colloid and Interface Science, Vol. 546, p. 163–173, 2019.

47. Liu, R., H. Tian, A. Yang, F. Zha, J. Ding and Y. Chang, "Preparation of HZSM-5 membrane packed CuO–ZnO–Al_2O_3 nanoparticles for catalysing carbon dioxide hydrogenation to dimethyl ether", *Applied Surface Science*, Vol. 345, p. 1–9, 2015.

48. Carvill, B. T., J. R. Hufton, M. Anand and S. Sircar, "Sorption-enhanced reaction process", *AIChE Journal*, Vol. 42, No. 10, p. 2765–2772, 1996.

49. Zha, F., J. Ding, Y. Chang, J. Ding, J. Wang and J. Ma, "Cu–Zn–Al Oxide Cores Packed by Metal-Doped Amorphous Silica–Alumina Membrane for Catalyzing the Hydrogenation of Carbon Dioxide to Dimethyl Ether", *Industrial & Engineering Chemistry Research*, Vol. 51, No. 1, p. 345–352, 2011.

50. Iliuta, I., M. C. Iliuta and F. Larachi, "Sorption-enhanced dimethyl ether synthesis—Multiscale reactor modeling", *Chemical Engineering Science*, Vol. 66, No. 10, p. 2241–2251, 2011.

51. Hamidi, M., F. Samimi and M. Rahimpour, "Dimethyl ether synthesis in a gas–solid–solid trickle flow reactor with continuous adsorbent regeneration", *Journal of the Taiwan Institute of Chemical Engineers*, Vol. 47, p. 105–112, 2015.

52. Kampen, J. v., J. P. v. Boon, F. v. Berkel, H. F. Dijk, J. v. S. Vente and M. u. Annaland, *The 25th International Symposium on Chemical Reaction Engineering*, `https://publications.tno.nl/publication/34631745/A1M83h/m17029.pdf`.

53. Said, A. E.-A. A., M. M. M. A. El-Wahab and M. M. Abdelhak, "The role of Brϕnsted acid site strength on the catalytic performance of phosphotungstic acid supported on nano γ-alumina catalysts for the dehydration of ethanol to diethyl ether", *Reaction Kinetics, Mechanisms and Catalysis*, Vol. 122, No. 1, p. 433–449, 2017.

54. Ilsen, O. Z. and A. K. Avci, *Microkinetic analysis of heterogeneous catalytic sys-*

tems, John Wiley & Sons, Inc., 2016.

55. Khzouz, M., J. Wood, B. Pollet and W. Bujalski, "Characterization and activity test of commercial Ni/Al_2O_3, $Cu/ZnO/Al_2O_3$ and prepared $Ni–Cu/Al_2O_3$ catalysts for hydrogen production from methane and methanol fuels", *International Journal of Hydrogen Energy*, Vol. 38, No. 3, p. 1664–1675, 2013.

56. Yang, Y., J. Liu, Z. Wang, Y. Long and J. Ding, "Interface reaction activity of recyclable and regenerable Cu-Mn spinel-type sorbent for Hg^0 capture from flue gas", *Chemical Engineering Journal*, Vol. 372, p. 697–707, 2019.

57. Raoof, F., M. Taghizadeh, A. Eliassi and F. Yaripour, "Effects of temperature and feed composition on catalytic dehydration of methanol to dimethyl ether over γ-alumina", *Fuel*, Vol. 87, No. 13-14, p. 2967–2971, 2008.

58. Auerbach, S. M., K. A. Carrado and P. K. Dutta, *Gas Separation by Zeolites*, Dekker, 2003.

APPENDIX A: CHROMATOGRAPH CALIBRATIONS

A.1. Gas Chromatograph Calibration

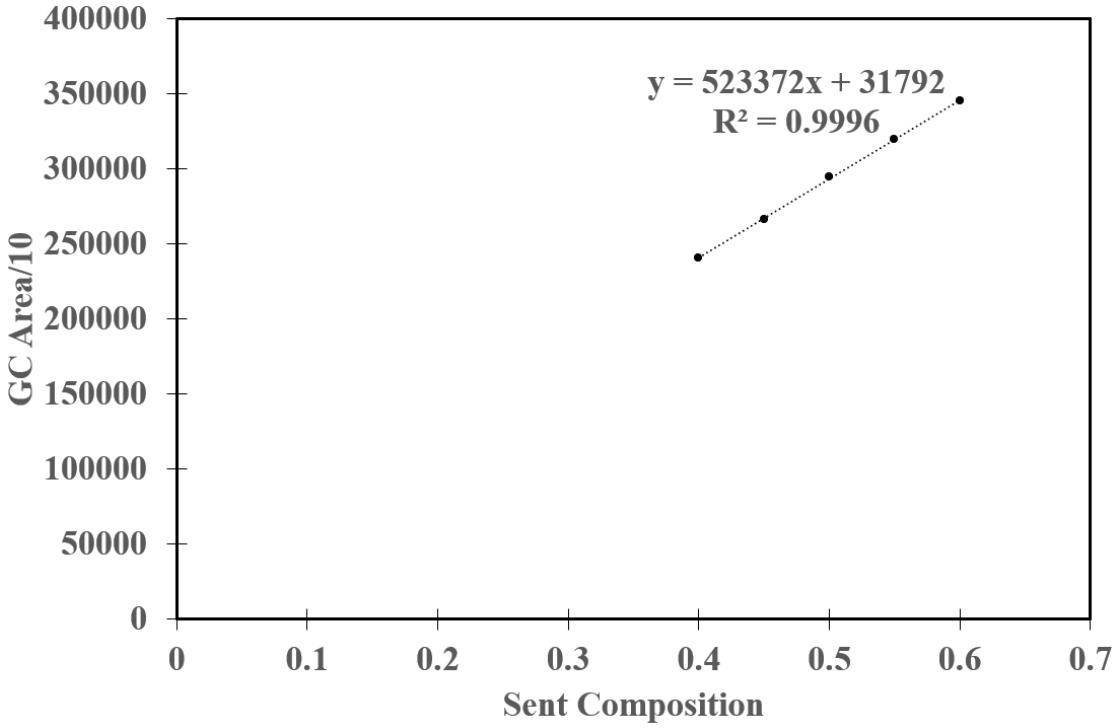

Figure A.1. Shimadzu GC-2014 H_2 Calibration.

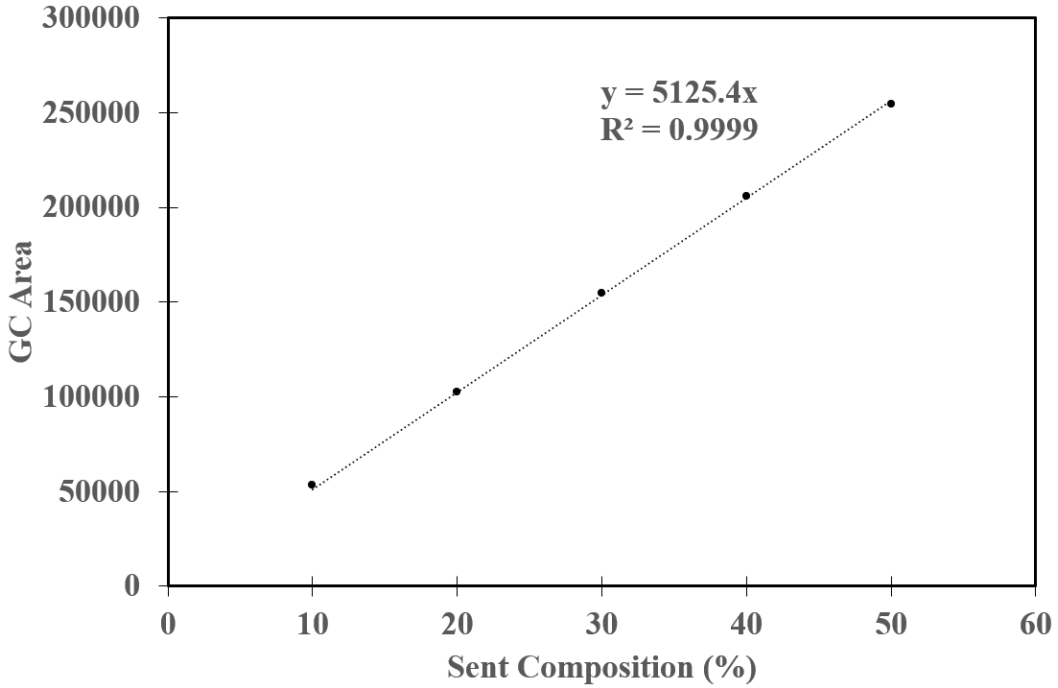

Figure A.2. Shimadzu GC-2014 CO Calibration.

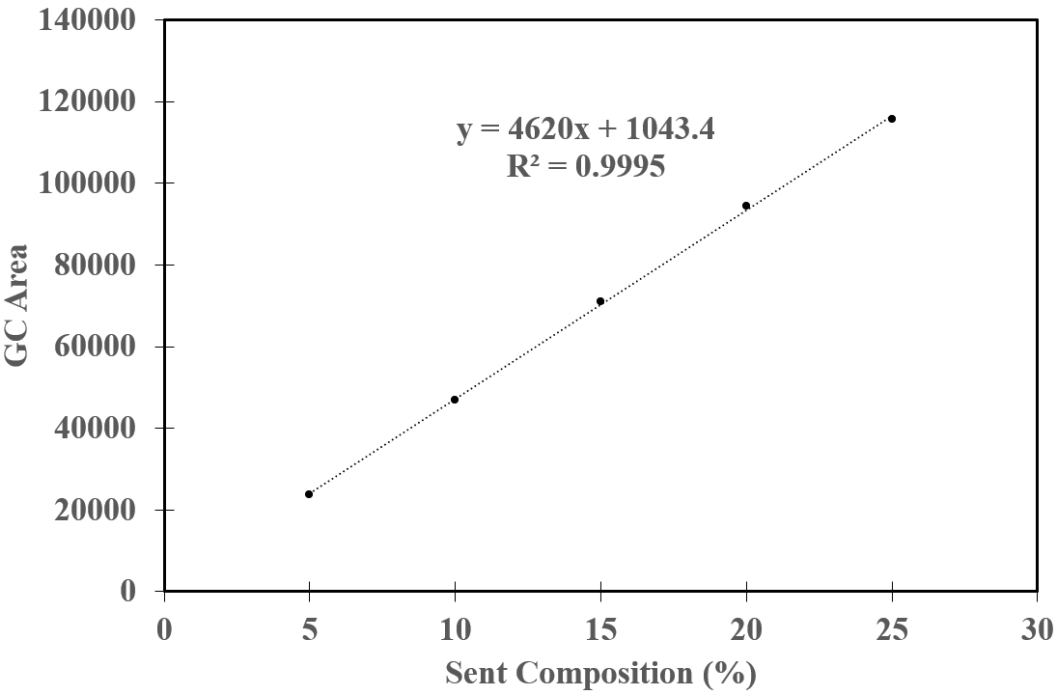

Figure A.3. Shimadzu GC-2014 CO_2 Calibration.

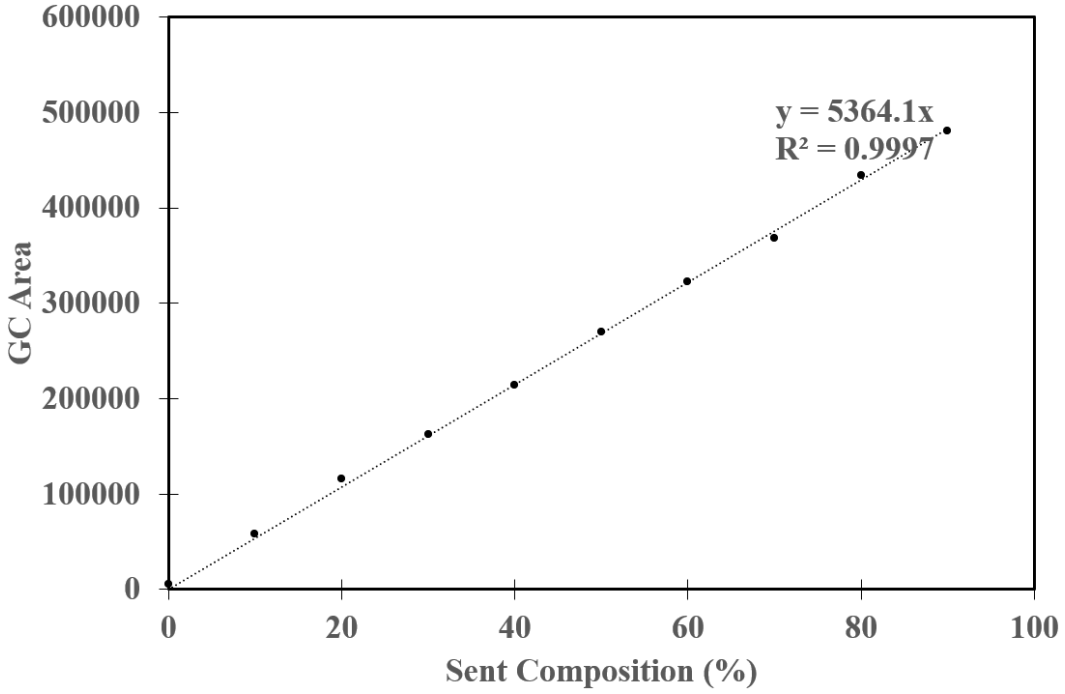

Figure A.4. Shimadzu GC-2014 N_2 Calibration.

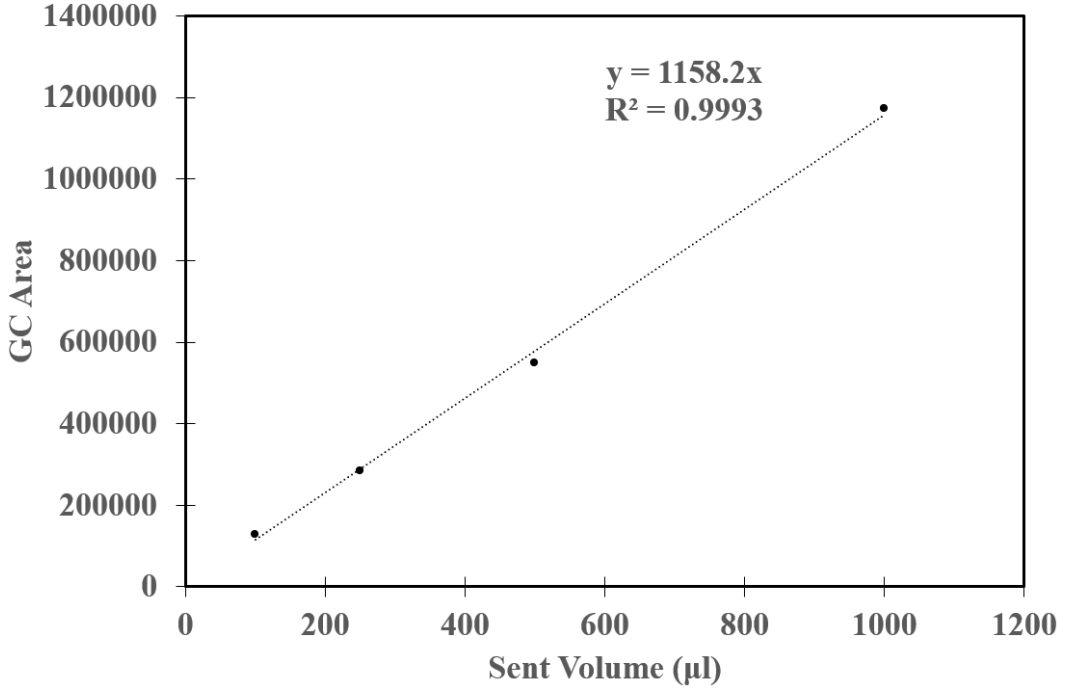

Figure A.5. Shimadzu GC-2014 CH_4 Calibration.

A.2. Gas Chromatograph-Mass Spectrometer Calibration

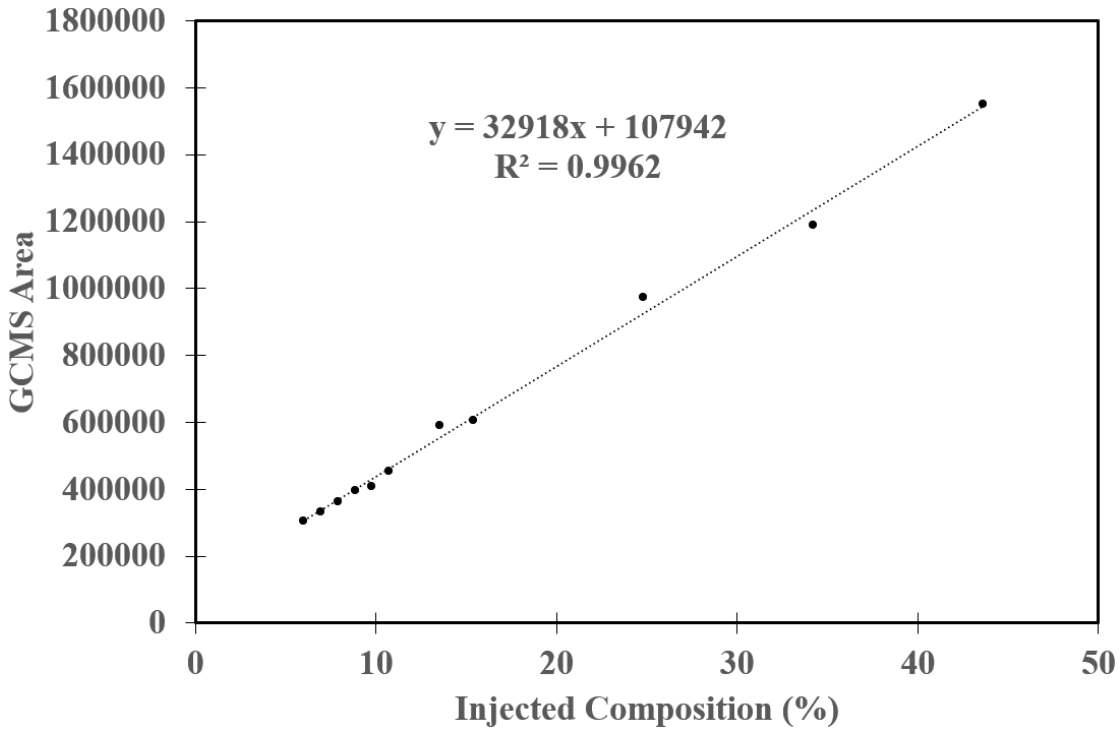

Figure A.6. Shimadzu GCMS Ultra QP2100 Ultra DME Calibration for CO as Carbon Source.

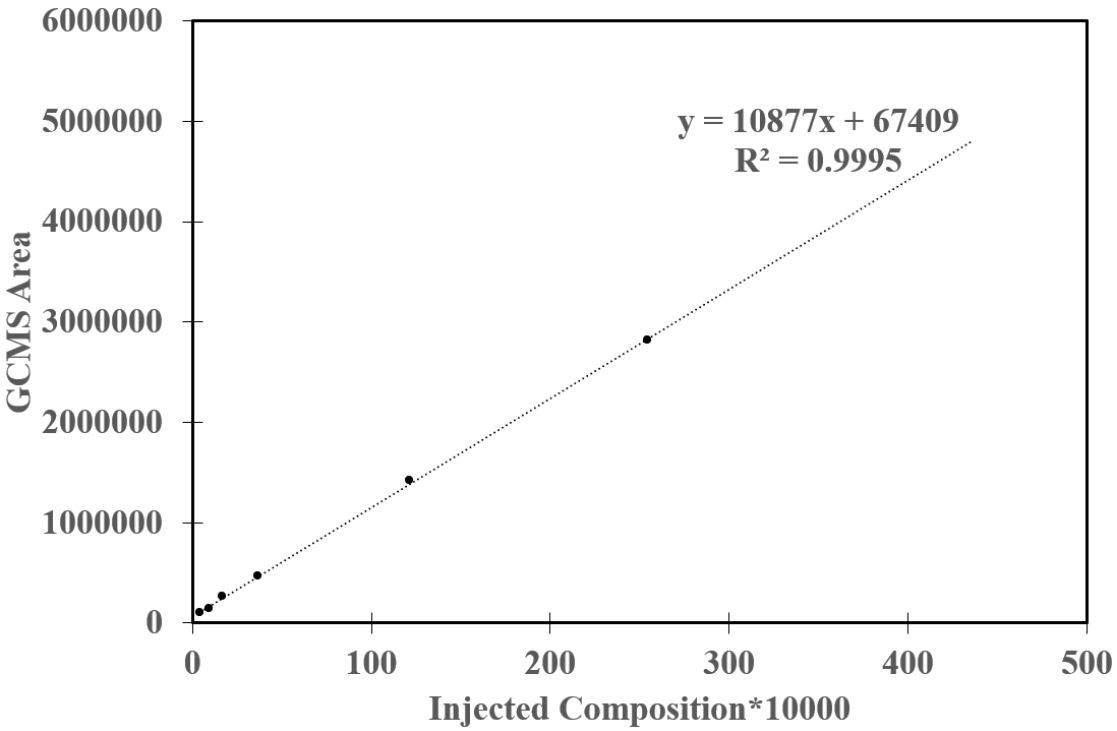

Figure A.7. Shimadzu GCMS Ultra QP2100 Ultra DME Calibration for CO_2 as Carbon Source.

APPENDIX B: MASS FLOW CONTROLLER CALIBRATIONS

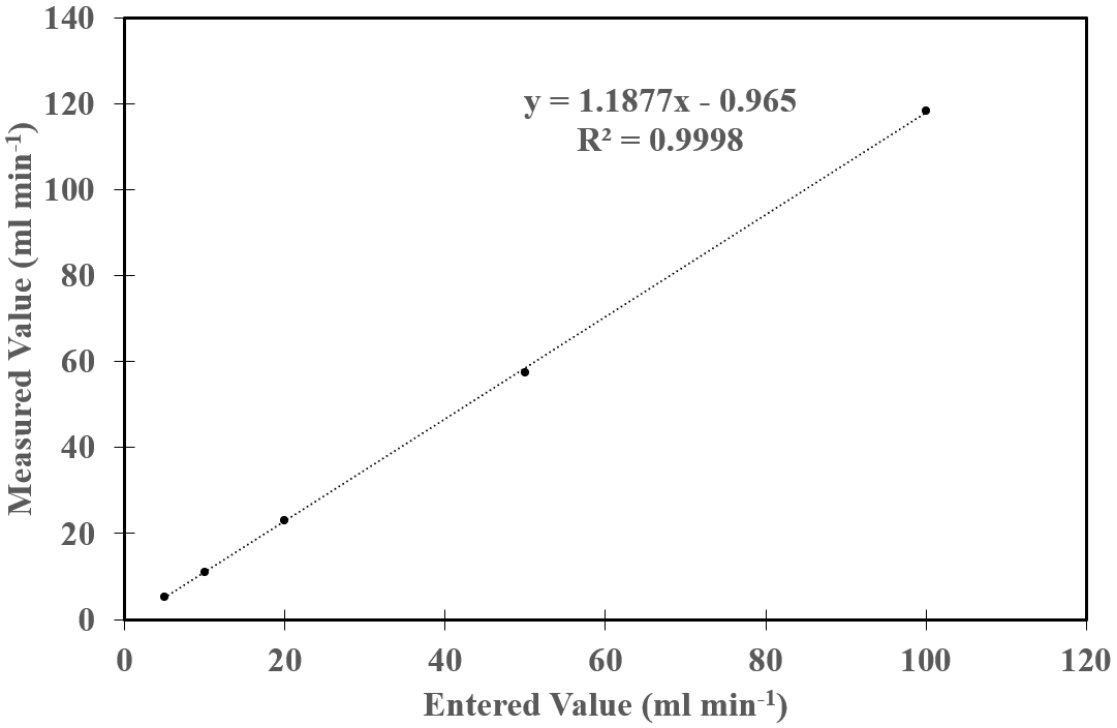

Figure B.1. H_2 MFC Calibration.

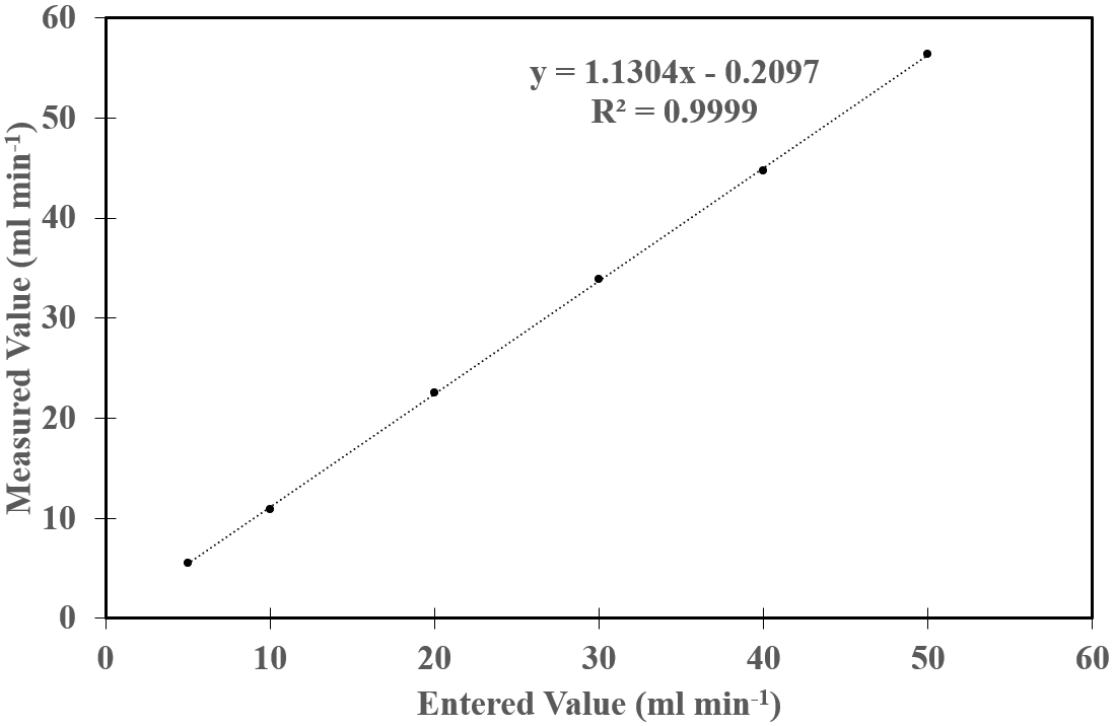

Figure B.2. CO MFC Calibration.

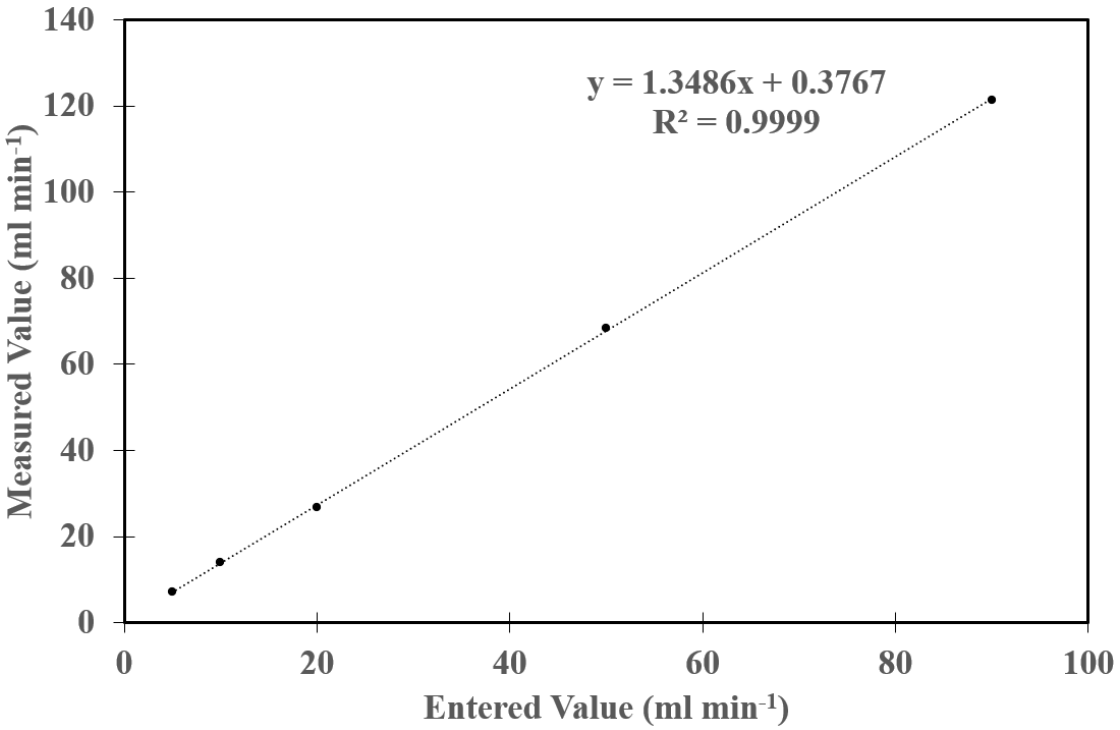

Figure B.3. CO_2 MFC Calibration.

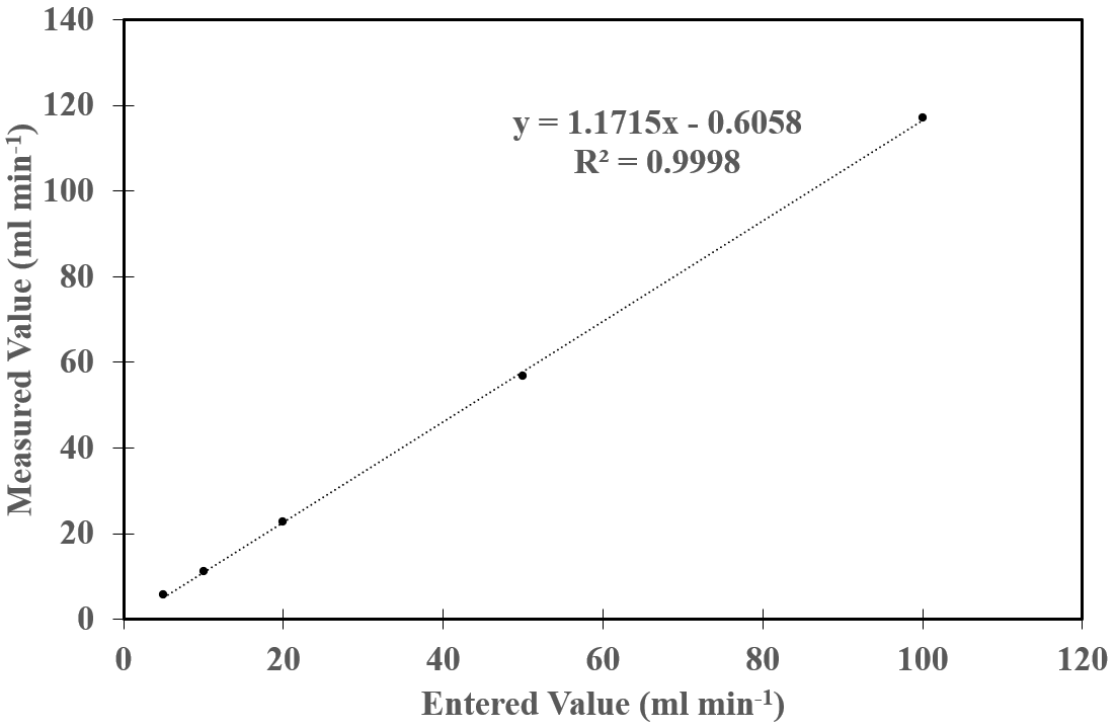

Figure B.4. N_2 MFC Calibration.